

POLITECNICO DI TORINO

Master's Degree in Mechanical Engineering



Master's Degree Thesis

Characterization of Inconel 718 fabricated by Selective Laser Melting (SLM) to achieve more productive parameters

Advisor:

Luca Iuliano

Co-Advisor:

Federica Bondioli
Abdollah Saboori

Candidate:

Guido Barale

Tutor:

Ing. Paolo Calefati

December 2019

Index

Abstract	1
1 State of art.....	3
1.1 Additive Manufacturing (AM)	3
1.1.1 Brief story and development of additive manufacturing.....	5
1.1.2 Additive Manufacturing techniques.....	8
1.1.3 Advantages.....	9
1.1.4 Disadvantages.....	11
1.2 AM Process.....	11
1.2.1 STL Format.....	13
1.2.1.1 STL Problem.....	16
1.2.2 Supports	17
1.2.3 Slicing.....	20
1.2.4 Part Orientation.....	21
1.2.5 Post Processing.....	22
1.3 Metal AM.....	25
1.3.1 Powder Bed Fusion Systems (PBF)	26
1.3.1.1 Laser Powder Bed Fusion (LPBF)	28
1.3.1.2 Electron Beam Melting (EBM)	31
1.3.2 Directed Energy Deposition (DED)	35
1.4 Inconel 718	37
1.5 LPBF of Inconel718	38
2 Materials and Methods	42
2.1 Starting material: Inconel 718.....	42
2.2 Design of Experiment	42
2.2.1 The first Design Of Experiment.....	44
2.2.2 Repeatability Test.....	48
2.2.3 The Second Design of Experiment.....	49
2.2.4 Tensile Properties.....	50
2.2.5 Characterization	53
2.2.5.1 Metallography	53
2.2.5.1.1 Cutting.....	53
2.2.5.1.2 Polishing	54
2.2.5.2 Image Analysis.....	56
2.2.5.3 Mechanical testing	58
2.2.5.3.1 Tensile Test.....	58

2.2.5.3.2	Microhardness.....	59
3	Results & Discussion.....	61
3.1	First DoE	61
3.2	Repeatability Test.....	66
3.3	Second DoE.....	69
3.4	Tensile Test.....	72
3.5	Microhardness.....	73
4	Case Of study.....	74
5	Conclusion & Future works	77
6	Acronyms.....	79
7	Bibliography.....	80
8	APPENDIX A	83
9	APPENDIX B	84

Abstract

This dissertation is the result of the internship that I took from April to October 2019 in Prima Industrie Spa. Prima Industrie heads a leading Group in developing, manufacturing and marketing of laser systems for industrial applications, sheet metal processing machinery, and industrial electronics and laser sources. In particular I worked as an intern in Prima Additive group, the part of the company that deals specifically with Additive Manufacturing.

During this period, I had the opportunity of dealing with the ordinary activities of the company. I also shared its dynamics by attending meetings with customers and suppliers under the supervision of my tutor and my colleagues. My work was focused on the Additive Manufacturing machines of Prima Additive, in particular the whole printing process concerning this innovative manufacturing system. Thanks to this experience I learned how to use an SLM machine and I printed all the samples useful to the activities carried out in this Master's thesis.

The aim of this project, as the title suggests, is to study and improve the parameters used to produce Inconel 718 with the "PrintSharp250". PrintSharp 250 is an SLM (Selective Laser Melting) machine, owned by Prima Additive, capable of transforming metal powder into 3d objects.

This thesis will be divided into 5 chapters. A general introduction to Additive Manufacturing is reported in the first one: "State of Art". In this chapter the cycle that characterizes this innovative process and the 3 main AM techniques used in the field of metals is presented. The chapter also includes a general review of the material Inconel 718 and the work done with it in the additive manufacturing field. From chapter 2, the experimental part of the thesis and the methods used for the characterization and study of the produced samples are described in detail. The experimental part can be divided into three phases. In the first phase 20 combinations of process parameters that characterize the L-PBF (Laser Powder Bed Fusion) techniques are defined. The choice of the parameters sets, called Design of the Experiment, was performed comparing the experience of Prima Additive in this field and the data found in literature about the Inconel718 fabricated by SLM. The purpose of this first phase was to identify the relation between the porosity percentage of the samples and the Volumetric Energy Density values used to print them. Once identified the most promising parameters sets the repeatability were tested. Same samples were printed again to see if the porosity percentage of this second job is consistent with the previous one. After checking the repeatability, the focus of the experiment moved on productivity. In the second phase, in fact, a second DoE was created with the purpose of decrease the building time of the process. The hatching distance, the laser power and the scanning velocity were modified with the aim to maintain the Volumetric Energy Density in the same range that showed the best results in terms of porosity during the first DoE. At the end of the analysis the two most promising sets of parameters in terms of productivity were selected. For the sake of simplicity, we defined a "optimized set of parameters 1" and " optimized set of parameters 2". The third phase of the thesis is dedicated to the mechanical properties of parts produced with these optimized parameters: three bars for each one were printed and tested. In addition, also 3 bars produced with the standard parameter in use in Prima Industrie were printed to have a comparison between the optimized parameters and the standard ones in terms of Ultimate Tensile Strength, Yield Strength and Microhardness.

At the end of the experiments, in the chapter 5, a case of study is presented in order to highlight the big advantages that the use of optimized parameters can lead to, both in terms of time and of costs. Finally, the chapter 6 summarizes the conclusion of the whole work and presents some possible future works that could be carried on in the future.

1 State of art

1.1 Additive Manufacturing (AM)

The Additive Manufacturing is a new innovative technology that makes possible the production of pieces with complex geometry directly from the CAD MODEL, in relatively low time and without the use of any kind of additional tools. ASTM (American Society for Testing and Materials) gave a good definition of this technology in 2012: “Additive manufacturing (AM) is a process of joining materials to make objects from 3D model data, usually layer upon layer, as opposed to subtractive manufacturing technologies” (ASTM International, 2012).

What is now known as additive manufacturing was originally born as Rapid Prototyping (RP). RP was developed in the mid-1980s. This term, as the name suggest, is used to describe the process that creates a prototype of a part or a system very quickly before the final release and commercialization. The outcome of this process was analyzed and tested to create more accurate models and eventually the final product. It was the first method that permits to create a three-dimensional objects layer by layer starting from a CAD model (computer-aided design) [1].

This was at the beginning the initial purpose of Additive Manufacturing. Since then Additive Manufacturing has evolved a lot. It is used for many purposes in different fields. The term Rapid Prototyping can no longer be used because it is insufficient to describe the concept of AM.

AM technology is still mostly used today for modelling, prototyping, tooling through a 3D printer or an appropriate machine. This technology helps the engineers during the conceptualization of new parts and tools. But the field where Additive Manufacturing can bring the greatest benefits is the small-scale series production. In fact, thanks to the characteristics of this technology, below a certain number of parts production and depending on their geometry complexity, AM can drastically reduce the cost and time of production as shown in the graph in figure 1.

Thanks to its features, the AM can greatly simplify the production of a 3D object with a complex geometry directly from the CAD model [2]. In fact, by using other manufacturing process to produce a complex 3D object, the engineer has to carefully analyze the geometry of the part to choose the more suitable tools to be used for each part. In addition, the correct sequence of operations in order to create the part correctly have to be carefully determined. In case of a complex geometry, this is a really hard task to be done. Instead AM does not need this kind of analysis, it only needs the dimensional details of the part that has to be created.

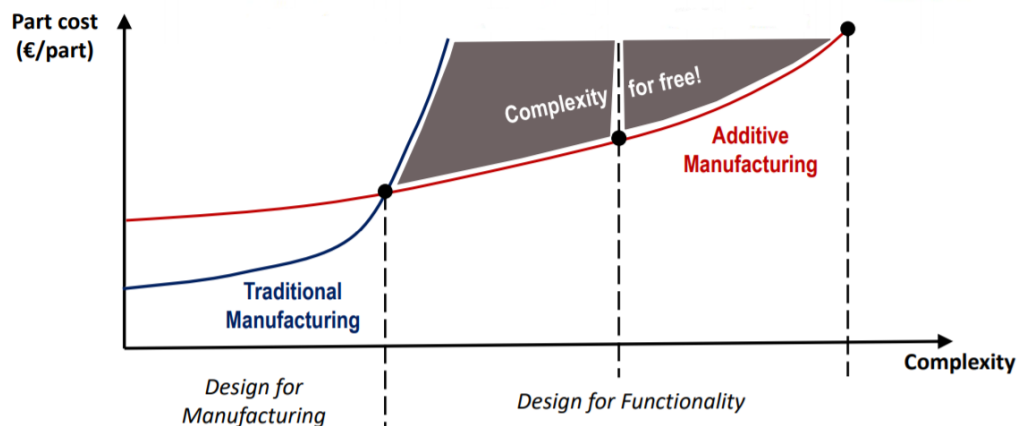


Figure 1) trend of part cost in terms of complexity for AM and traditional manufacturing [47]

The additive Manufacturing, as mentioned before, is very advantageous for pieces with complicated geometry not only in terms of costs. With AM, it is in fact possible to create particular shapes and internal channels that would not be possible with any other processing. An example is the internal channel of the part shown in figure 2.



Figure 2) cooling internal channels

The original and revolutionary idea behind AM is to think about the part divided into slices. The part is created adding material layer by layer. A layer is a thin cross-section of the model derived from the original CAD file. An example of a part divided into slice is shown in figure 3.



Figure 3) example of a model divided into layers [2]

More the layer is thin more the sliced part is close to the original CAD model. All the Additive Manufacturing machines available nowadays use a layer-based approach. The differences between the various techniques of AM depend on how the layers are created and bounded each other on the one hand, on the materials used on the other hand. Obviously, each technique gives a different part quality. Finally, the quantity of post process operations, the production time and costs are strongly correlated with the type of AM technique used.

1.1.1 Brief story and development of additive manufacturing

As highlighted in the above paragraph the first name of AM was rapid prototyping. The man who first applied for a patent for his rapid prototyping system was the Japanese Hideo Kodama of Nagoya Municipal Industrial Research Institute in 1980. Unfortunately, due to financial problems, the Japanese doctor was not able to fill the full patent specification within the one-year deadline after application. Few years later in 1985, Alain Méhauté, a French electrochemical engineer, creates stereolithography (SLA). He was conducting some studies on fractal geometry and developing some equations related to them. The problem was that he had to prove practically his equation. In order to do that he had to create a 'fractal object'. Because of the complex shape of the object, no machine permitted to create it. So with the help of Oliver de Witt and Jean-Claude André he creates the first 3D printer and they filed a patent for stereolithography process. But the CNRS (Centre National de la Recherche Scientifique) gave no importance to their idea and refused to invest on their project: as a consequence they gave up for founding problems.

Almost in the same period Chuck Hull, an engineer from Colorado, was working for a company who produces coatings using UV lamps. The problem of this company was the time required for the production of parts for prototyping, that could take up to two months. So, he started to think about a new method to use the UV light in order to save time creating prototypes. He wanted to create part adding a thin layer a time, to create at the end a 3D object thanks to the UV technology. He finally earned the patent, about 3 weeks after the French team got the patent, and he set up a 3D System in order to commercialize his new discovery: The Stereolithography (SLA). The first product was commercialized in 1988. The stereolithography technology uses as materials photopolymers, liquid resins that are turned into solid to create the parts thanks to an UV light. Chuck Hull is nowadays considered the father of the SLA [3]. Stereolithography gave then his name to the format file more common in the additive Manufacturing world: the "STL file".

Few years later Carl Deckard, a mechanical engineering from Texas, was working in a company in Huston that made part for oil fields. The process used by the company require a big amount of casting in the process. Carl, in order to reduce costs and time, began to work on creating a machine that could produce parts without any castings. In this way he created the Selective Laser Sintering (SLS) technology. In 1987 he filled a patent for SLS process.

In about the same period another mechanical engineer, Scott Crump, was trying to design a machine that could automatically print 3D objects. Using a hot glue gun, by mixing candle wax with plastic (polyethylene), he realized that he could print a 3D object. Scott's initial aim was to create a frog-shaped toy for his two-year-old daughter. After creating the froggy toy he realized that the process could be automated by attaching the hot glue gun to a robotic XYZ gantry system. So in 1989 with his wife, Lisa Crump, patented this new process called: "Fusion Deposition Modeling" (FDM). In 1992 they created the firs operational FDM 3D printer and they co-founded the company Stratasys [4].

It's very interesting to note that three of the most important additive technologies have been developed over a period of ten years.

Since then AM became a topic of great interest and attention: in Europe, the first companies producing SLS technology (for metal and plastic) and FDM began to appear in the nineties. Between 1992 and 1999 the market had a boom and al lot of companies emerged with various techniques such as binder jetting (BJ) and Selective Laser Melting (SLM). Moreover, thanks to this rapid grown, CAD tools for 3D printing began to be developed and readily available. The nineties were a very important period for

AM sector because some medical researchers started to combine medicine with 3D printing opening the way to endless opportunities in medical field.

The 2000's are also a key moment for additive manufacturing. Thanks to the numerous applications in the medical field, such as the working kidney printed in 2000 and implanted in a human patient in 2013 or the first 3Dprinted prosthetic limb, printed 'as is' without any required later assembly, the AM reached a great media presence[5]. This advertisement made the AM market grow out of all proportion especially for what concerns the polymeric materials. But it wasn't long before the metal field also developed.

Just to give an idea of the development of the Additive Manufacturing from the period in which RP was born until now two graphs are reported in figure 4 and In figure 5. They show the trend of the development in function of the years.

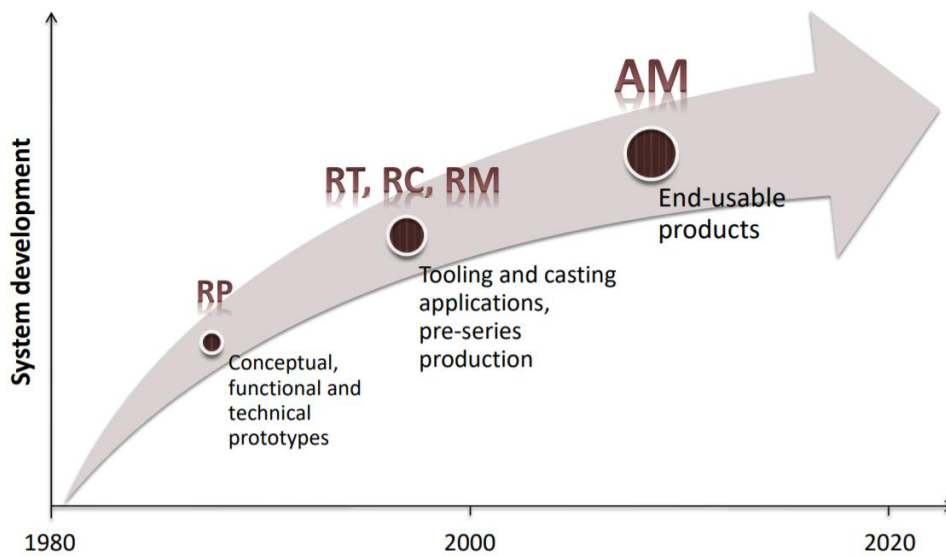


Figure 4) development of AM [47]

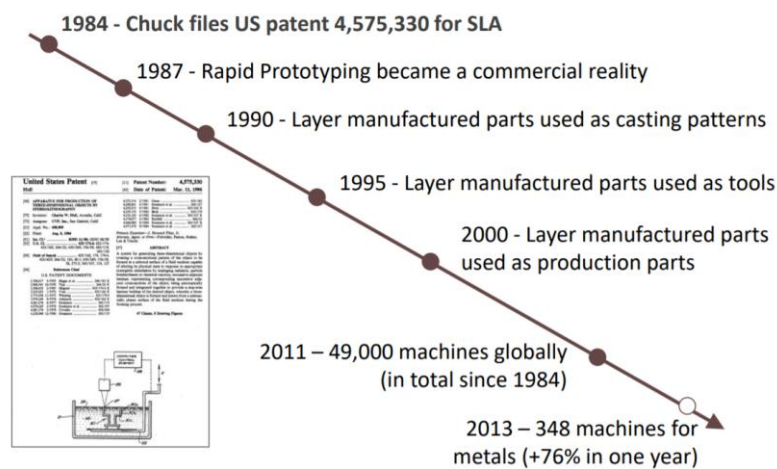


Figure 5) history of layer manufacturing [47]

Only in the early 2000s AM began to be used in the production of end-usable parts. AM is still a sector in rapid evolution. It is therefore very difficult to define a consolidated state of the art, unlike the others manufacturing sectors where a consolidated state of art can be defined.

The only aspect in which a certain “stability” can be observed is the “basic” approach of creating a part by adding layer by layer the material. On the contrary, almost daily variation can be observed with regard to applications and materials [6].

As we can see from the graph in figure 5, the market for AM metalworking machines between 2011 and 2013 has experienced an exponential development, reaching a growth rate of 76% . The main reason because AM can represent the future of the manufacturing process consists in the flexibility and level of customization that guarantees. The idea of AM technology goes perfectly with the new concept of “Industry 4.0”. Is therefore to be expected that additive Manufacturing will continue its expansion in the future, partly replacing other manufacturing processes.

Smart Tech, a company that can be defined one of the benchmarks for market analysis in the field of 3D Printing, published its year-end report (2018), which provide an overview of the entire industry. It shows that the additive global market worth over \$9.3 billion with a growth rate of 18%. Even more interesting, however, is that the new report presents a projection of the sector from 2018 to 2027 (figure 6). In 2018 the Additive production market really seems to have gained a percentage of constant growth [7].

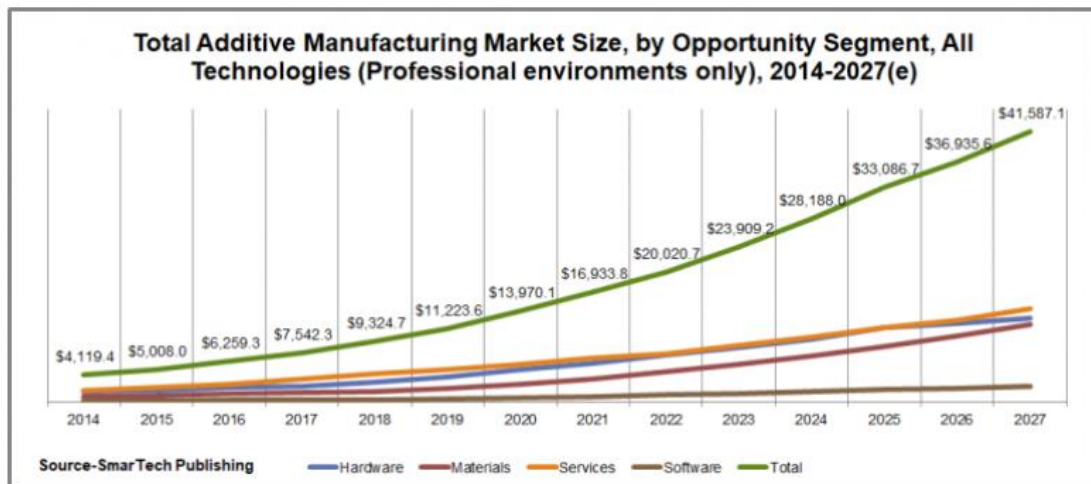


Figure 6) projection of AM from 2014 to 2027 for professional environment [7]

1.1.2 Additive Manufacturing techniques

Additive manufacturing techniques can be divided into 2 categories depending on the processed material: polymer (figure 7) or metal (figure 8). Each category can be divided again according to the state of the raw material used.

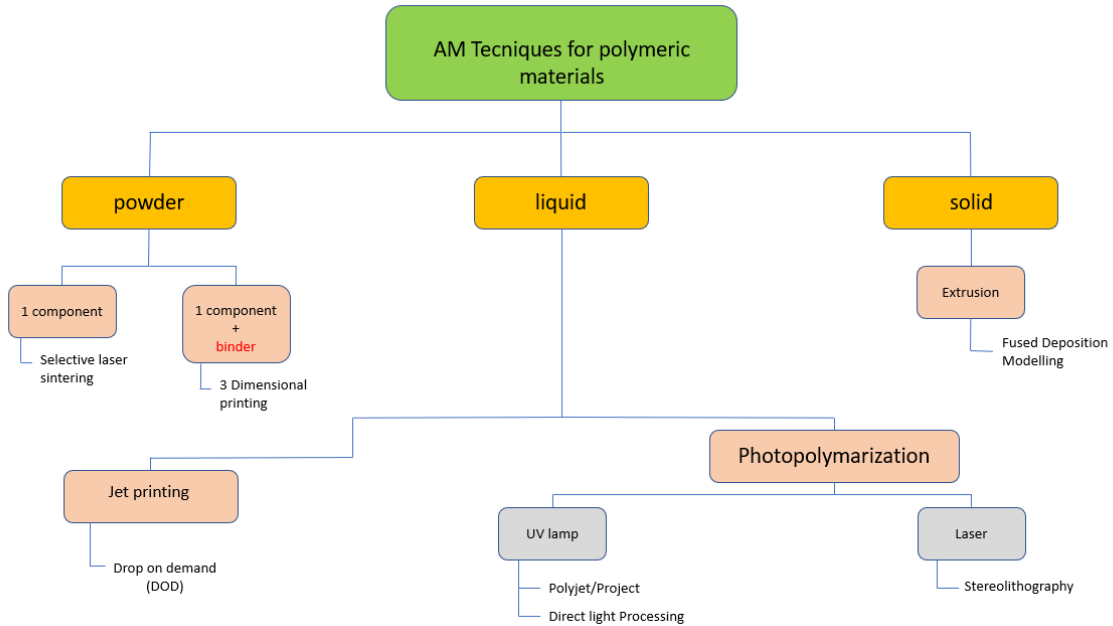


Figure 7) AM techniques for polymeric materials

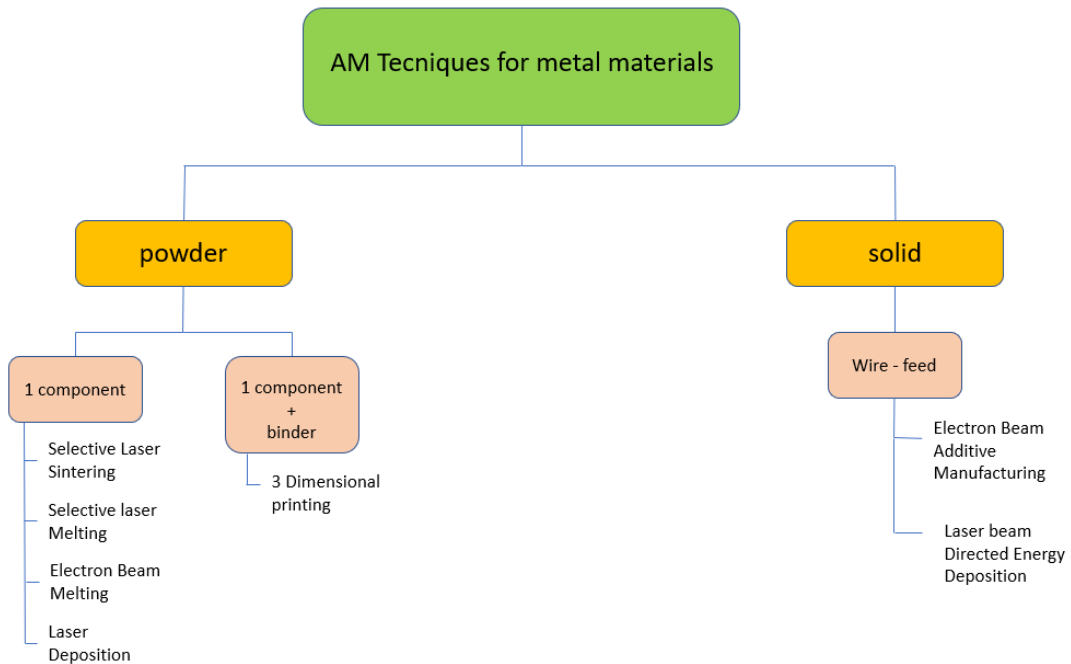


Figure 8) AM techniques for Metal Materials

1.1.3 Advantages

Many researchers have described AM as a revolutionary technology for product development and manufacturing. Some of them even say that we are experiencing a new industrial revolution. Surely AM has the potential to change the way we look at manufacturing industry [8]. AM, as mentioned in previous chapters, was born in the early 80's. Since then it has continued to develop, arriving today at a point where it can be compared with other traditional manufacturing processes in terms of cost, speed, reliability and accuracy. The word "rapid", in one of the several names this technology is known (Rapid Prototyping), is relative; the time required for the production of a job is in fact closely related to the type of machine used and the quantity, the size and number of parts printed simultaneously. The concept "rapid" is referred to the process philosophy of AM.

The most significant advantages of AM technologies can be listed as follow:

- Complexity

Thanks to the idea of AM to create a part with the layer-by-layer approach almost any kind of shape can be created. This method allows to turn a complex 3D problem into a much simpler set of 2D cross section of a certain thickness. With AM is possible to create almost any kind of shape and any kind of internal structure, i.e. it is possible to create complex channels inside a part to optimize the flow or to create porous structure in order to decrease weight and so on.

- Time saving

AM is a "rapid" process, not only in term of the time required to build up the part but also considering the whole product development. The starting point of the process is indeed the 3D CAD and the transfer to AM is relatively easy; there are less concerning about data conversion or interpretation of the design intent. The number of steps required during the process is lower than traditional manufacturing processes, this also reduce velocity. Others manufacturing process indeed, depending on the complexity of the parts, usually required multiple and iterative stage to get the final product. When more features are added in a design, the number of the required stages can drastically increase. In AM instead, regardless of the complexity of parts, the building process is performed in one single step and thanks to the development of the software you can also obtain an immediate estimation of the time required by the building process, considering as well changes may be implemented during the product development. There is no need for any kind of additional operation to change the part to be built. So, without need for any kind of molds and dies, the AM technologies allows to drastically decrease the time needed to create a new product.

- Optimization

The cost of the product in AM is no longer linked to the complexity but only to the size of the pieces to be produced. This allows the user to concentrate on optimizing the part design without having to worry about complexity. The part design can be optimized for the following requirements: maximum part weight, maximization of static strength, optimal dynamic behavior, optimal thermal performance, reduction of the number of parts (one-piece assembly) and integration of different

functions or graded material. For this purpose, a lot of topology optimization software tools are nowadays available on the market. An example of an optimized piece is reported in figure 9.



Figure 9) design optimization of a component

- Flexibility

Unlike other traditional processes, AM does not require an accurate study of the correct sequence of tools to be used in case the shape of the product has to be changed.

- Customization

One machine can potentially print unlimited shapes. This makes it possible for the user to customize the product.

- Autonomy

In almost all additive processes, no operator is required during the building process. The machine, once the file has been loaded and the process has started, is able to work in complete autonomy.

- Waste material

Another great advantage of the additive process is that the raw material is completely transformed into the finished product independently of the AM process used, reducing the amount of waste material. For example, in powder bed fusion process all powders that have not been melted in the final piece, once sieved to ensure the correct particle size, can be reused. This is also an advantage in terms of costs.

Another relevant point that can be mentioned is the consequences that an error in the programming stage can create. For example, in a CNC (computer numerical control) machine an error in programming the process can cause several damages to the machine and can be also risky for the operator. While in AM machine the only consequence for an error in the setting is that the part will not be properly built.

1.1.4 Disadvantages

Additive manufacturing has also some disadvantages due to the fact that the market is still on evolution. First of all, the work volume and the dimension of the parts are limited depending on the machine you are using.

The surface roughness is usually high without the post-processing operation if compared to the resolution that can be gain with a CNC machine (usually few tens of microns). The building rate velocity is still limited but many researchers are focusing in trying to increase the productivity of the process [9]. Comparing for example CNC machine with AM machine we can affirm that generally CNC removes material much faster than AM machine add a similar volume of material. The aim of this project will be indeed increasing the productivity by working on the parameters.

Another disadvantage of AM is that depending on the kind of AM process each machine can work with a limited number of materials and these materials are not yet very widespread on the market. Their cost is still very high. But it is likely that the price of these materials will drastically decrease with the diffusion of AM in the world market. The same trend is expected for the price of the machines, that is still very high.

1.2 AM Process

The cycle of Additive manufacturing is relatively easy (figure 10). It can be divided into 8 steps:

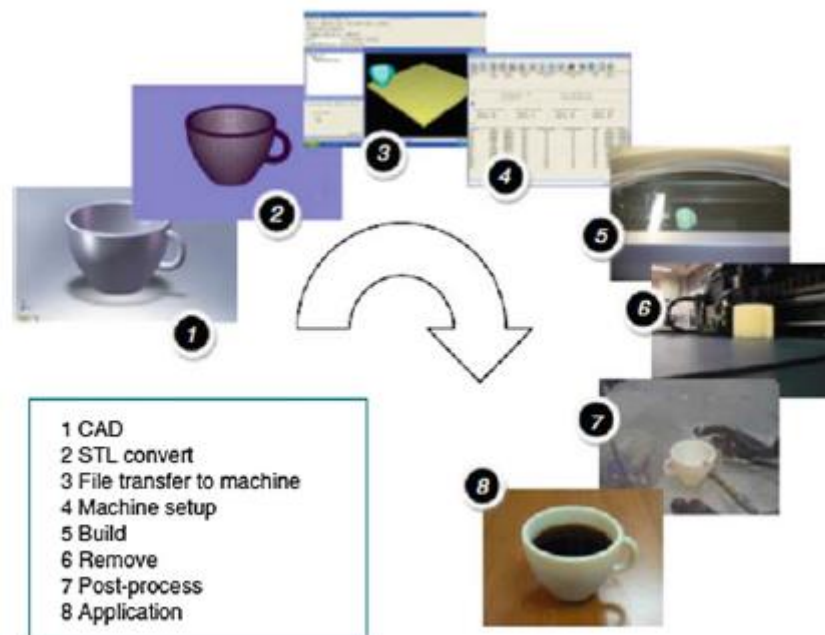


Figure 10) AM cycle [2]

1. CAD:

The starting point of all Additive Manufacturing process is a CAD model. A CAD model is a software model that can describe all the geometry of the part that has to be created. For this, almost any professional CAD solid modelling software such as SolidWorks, Katia, Solid Edge and many others can be used; the only important thing is that the used program must have as output a 3D solid representation.

2. Conversion to STL:

STL file format is the standard format used for almost all AM machines, as it will be well explained in the following section. Almost any professional CAD solid modelling has the possibility to save the model in STL format.

3. Transfer to AM machine and STL file manipulation:

The STL file describes the external closed surface of the original CAD model. This is the file that has to be transferred to the AM machine. In this step some manipulation of the file can be required such as the correct position and orientation for the building process and also, if it is needed, the creation of some support structures to ensure the correct distribution of thermal stresses. This step can be performed with a lot of professional software such as Materialise Magics [11].

4. Machine setup:

A properly setup of the machine is needed to ensure the correct build process. Material constraints, energy source, layer thickness, timing must be set correctly to ensure the desired property of the part. This step is made usually with the post-processor that can be either integrated in software like Materialise Magics. In some cases, the software can be in a separate software.

5. Build:

This is one of the most important point of the AM world. The building process is almost completely automated and does not require any supervision. Only in the first phase the process is semi-automated and the operator has to stay close to the machine in case some errors occur or for any further checks and interactions. After the first phase the control becomes fully automated and the only type of external control is to check that the raw material does not end before the job finished.

6. Removal:

Once the building process is completed, the part must be removed from the work area. The procedure of removal is strongly related to the kind of used AM technique. But regardless of the used technique, this step may require an interaction with the machine. For this reason, AM machines often have safety interlocks to ensure that the operating temperatures are sufficiently low or that there are no moving parts.

7. Post-Processing:

Once the part is removed from the work area, it can require some additional post-processing operations to be ready to use. These operations will be explained in the following chapters.

In the most cases, once the platform has been removed from the work area, some post processing operation had to be performed to detach the parts from the platform. This

is performed usually with a wire-cutting. In the case of presence of supports during the building process, the supports removal is necessary. Sometimes also sand-blasting can be useful to decrease the surface roughness (this only applies to metal parts).

8. Application:

This is the final step of the AM process. Once the post-processing operations have been performed the part is finally ready to be used.



Figure 11) CAD model converted into STL format [2]

1.2.1 STL Format

The STL file format has become the industry standard for data transmission for RP. STL format takes its name from the stereolithography process (SLA) and stands for Standard Triangulation Language. Converting the CAD solid model in STL file means convert it in a “shell kind” model where the external surface is approximated using triangles (called facets). An STL file consist of a list of this triangles data. Each triangle is identified by a normal unit vector (a line perpendicular to the triangle with a length of 1) and by 3 points (the vertices of the triangle).

The most important element is the orientation of the triangle because it defines the shape of the 3D object and is part of the boundary between the interior and the exterior of the part.

There are two redundantly ways to define the orientation of a triangle. The first is the direction of the normal (always outward). The second is the way the vertices are listed; in counterclockwise order when looking at the object from the outside figure 12.

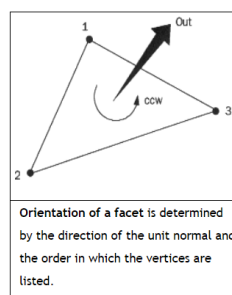


Figure 12) orientation of a triangle [12]

Each stored element (the normal and the 3 vertices) is specified by three coordinates, so a total number of 12 data per triangle is stored. Thanks to this data the slicing algorithm can be used to determine the cross sections of the three-dimensional shape to be built [12].

The rules used in the creation of this kind of file is the “Vertex to vertex” rule: “each triangle must share two vertices with each of its adjacent triangles”. More simply a vertex of a triangle cannot stand on the side of another so two adjacent triangles must always have in common two vertices and one side (figure 13).

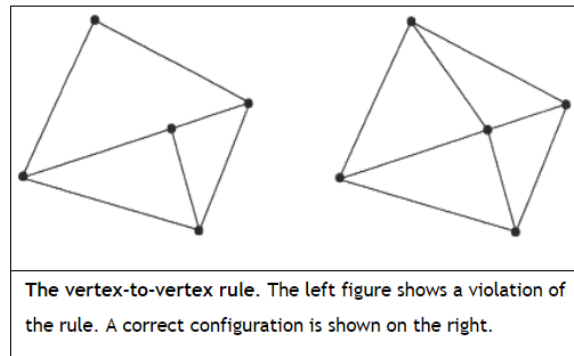


Figure 13) vertex to vertex rule [12]

It is also recommended, but not necessary, to order the triangles in ascending order of z-value to optimize the slice program performance. An STL file is saved with the extension “StL”. This standard includes two data formats: ASCII and binary.

The number of triangles in a model depends on the complexity of the geometry and on the accuracy that is needed. For example for an easy shape (characterized by a low number of curves), such as a cube (figure 14), only 12 triangles are sufficient to fully describe the model.

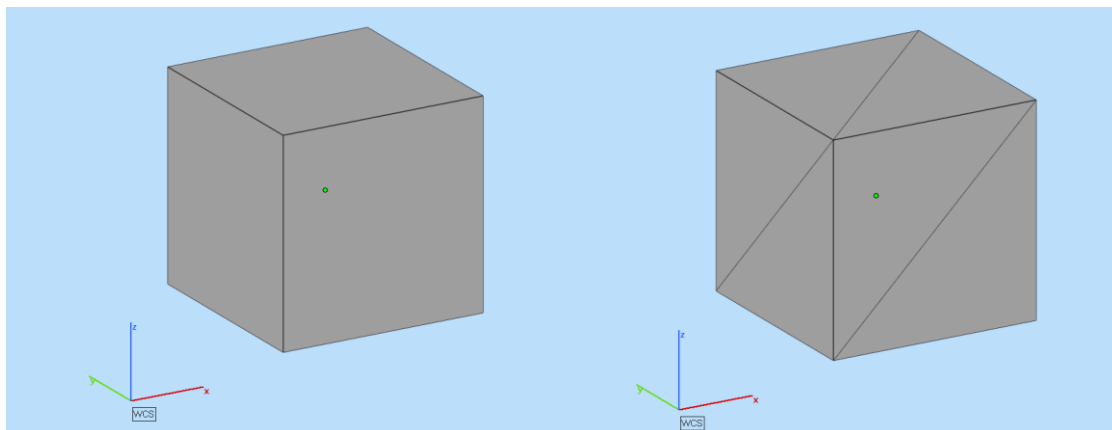


Figure 14) cube representation in STL format

If the geometry of the model is complex, to achieve the correct shapes, using the triangle approximation, a high number of triangles is required. As can be seen in the model of a extruded turbine (figure 15), there are a lot of curves. To get a better approximation of these curves a huge number of triangles is needed (figure 16).

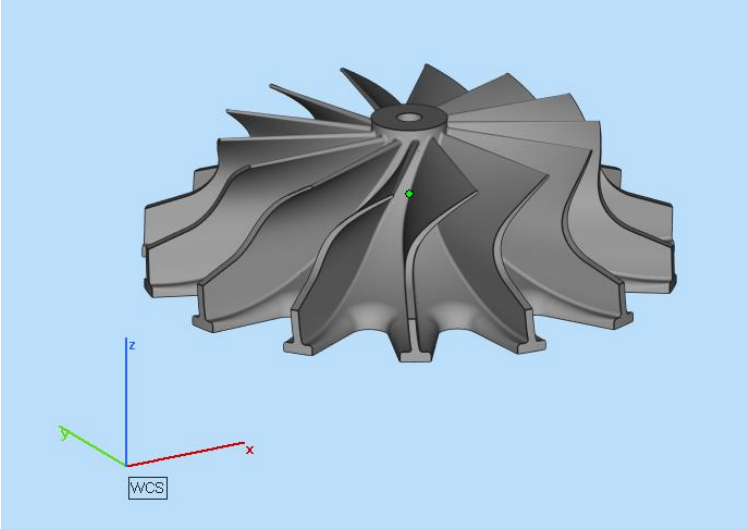


Figure 15) model of e turbine

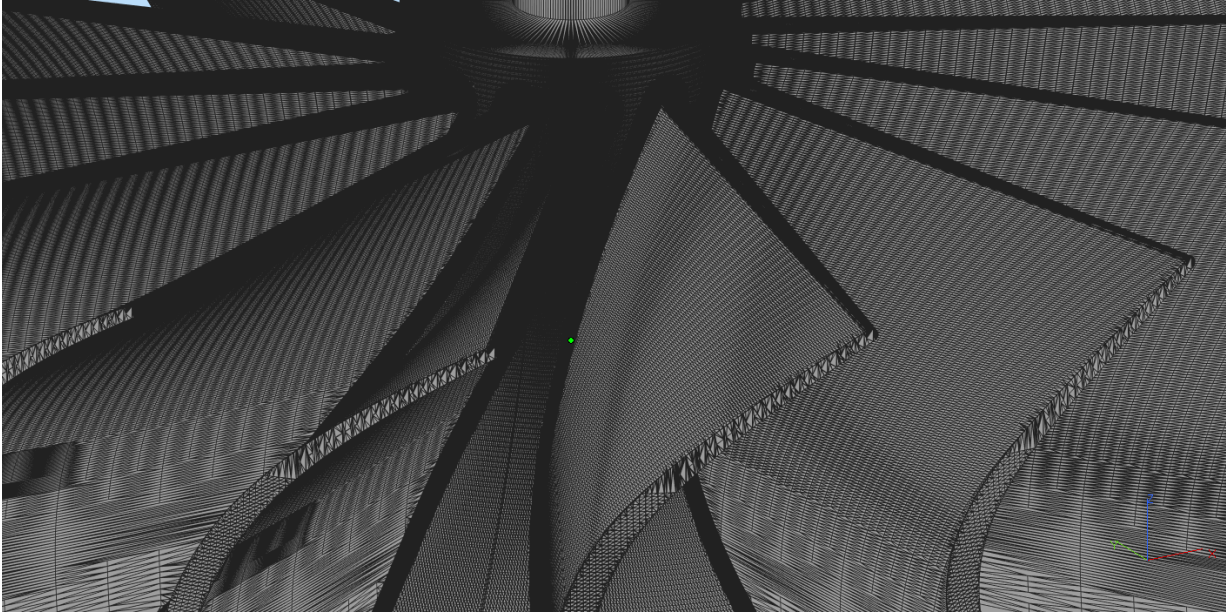


Figure 16) a zoom of the turbine reported in figure 15 approximated with triangles

Virtually all CAD systems today are capable of producing an STL file. For the user, the process is often very simple: select the file, save as with STL extension. In all cases, it exports the STL file as a binary file. This allows to economize both spent time and file size.

As mentioned above, the number of triangles depends on the complexity of the geometry. And the number of triangles influences the dimension of the STL file. For a simple geometry (i.e. characterized by a few curves), the file can have the size of a couple of hundred Kbytes. For complex models, files in

the 1-5 MB range will produce high-quality parts. For many geometries, files larger than 5 MB are not necessary and only increase the time needed to prepare quotations and deliver the part.

In addition, for most processes and materials, the minimum thickness is 0.020 mm. It is not possible to stay below this value, without risking a failure in the development of the part. An exception is the high-resolution SLA, which will create features up to 0.010 mm [13].

1.2.1.1 STL Problem

Converting a CAD file in an STL file may cause some problems. The most common are:

- Gap between cells
- Inverted normal
- Intersection of triangles
- Internal walls

Fortunately, there are programs that can easily solve this kind of problems. The one used during this thesis was Materialise Magics. Thanks to its numerous functions Materialise Magics is able to point out the problems and automatically fix it. The function used for this purpose is the diagnostic tool (figure 17). The program automatically gives advises to the user to fix the problems; if someone remains it can be fixed manually.

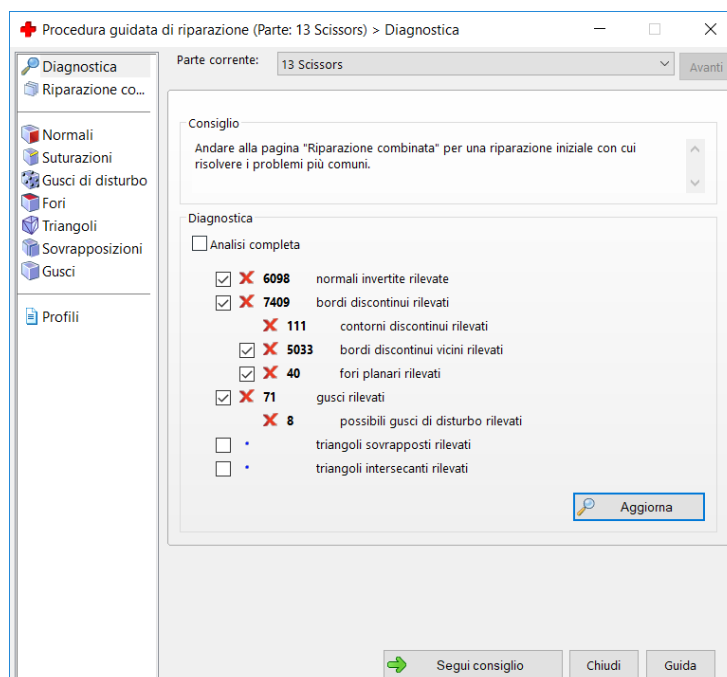


Figure 17) diagnostic tool in Materialise Magics

1.2.2 Supports

Very often in Additive Manufacturing production is necessary to use supports to guarantee the correct print of the pieces.

The main purpose of the supports are:

1. connect the model in construction to the work area allowing anyway the easy subsequently removal of the model;
2. protect the lateral wall from situations that can compromise the part;
3. support the protruding walls.

Figure 18 depicts some examples of structures that usually need supports regardless of the kind of used technique .

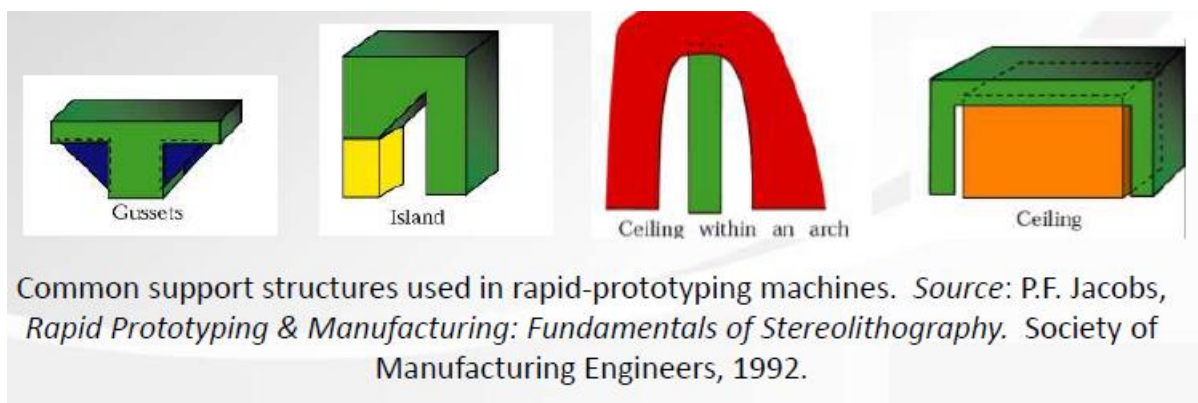


Figure 18) common support structures [32]

The supports can be added manually or automatically using system's software and they can be formed only with the same material of the part.

As it regards the powder bed fusion process for metallic materials, there are several reasons why it is necessary to insert the supports. The most important one is certainly to deal with thermal stresses.

Thermal stresses are in fact present both at macroscopic and microscopic level. On a microscopic level, during the dust bed processes, the small micron-size metal beads are basically melted together (01) creating a sort of metal liquid pool (02) and then cooling down and condensing to a solidified metal (03) (figure 19). This local and rapid heating (solidify-contraction-risolidify) leads to the creation of residual thermal stress on the layer.

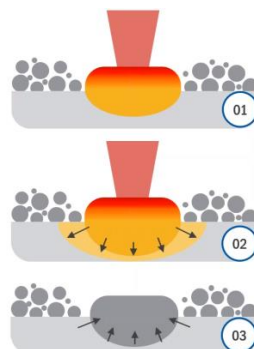


Figure 19) creation of thermal stresses [14]

On the other hand, looking at the macroscopic level, building the layers one on top of the other will create a difference in temperature between the layers. The upper layer will have a higher temperature with respect to the one below. This temperature gradient will bring to the shrinkage of top layers. In fact, in the creation of a part, the melting of the powders and the consequent re-solidification creates residual thermal stresses in the piece. This residual thermal stresses by looking at the macro-level can cause contraction during cooldown and the shrinkage of the top layer. For example, if a rectangular plate is printed without any kind of support structure the thermal stresses will pull the edges inwards and this will curl whole structure (Figure 20) [14]. Thanks to the use of support structure the thermal stresses can be dissipated.

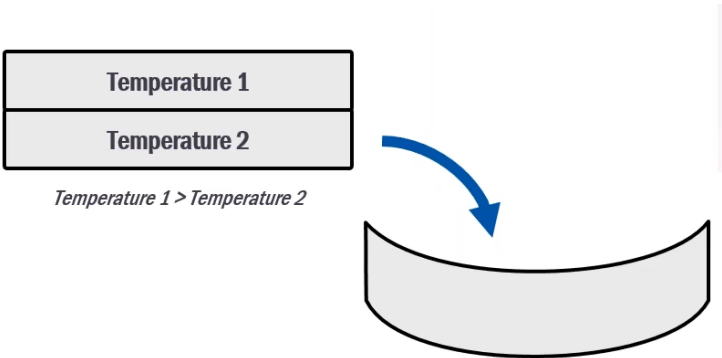


Figure 20) deformation of a rectangular plate [14]

In addition to dissipating residual thermal stresses, they are necessary to support certain part geometries. Below are reported the most common geometries that require the use of supports:

- Angle: under a certain angle (closely linked to the material used), a surface stops being self-supported. In this case, if it is not planned to use supports, the downward facing surface will become rough (figure 21) and require considerable post-finishing operation.

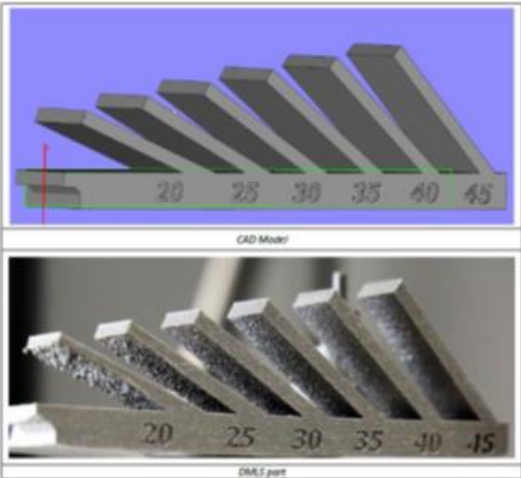


Figure 21) consequences of not supported acute angle [48]

- Vertical holes: large holes require support structures in the center (figure 22) otherwise the part will collapse or will become distorted during the building process (figure 23). Another way to avoid the collapse of the structure is the redesign of the hole by adding an angled or arched upper area (figure 24).



Figure 22



Figure 23



Figure 24

- Overhang : Any overhang greater than about 1mm in length needs support. In particular if it is bigger than 10 mm it requires a solid support (the measurements reported here are generally valid, the exact measurements are strictly correlated to the material used).
- Bridges: Bridges such as overhang are structures that require the insertion of supports above a certain length. The figure 25 shows a structure with bridges of different length. Thanks to this structure is possible to see the defect present in the bridge structures without the use of supports. For example, considering Inconel 718 (the material used during this thesis), it is possible to print bridges with a length of less than 6 mm.

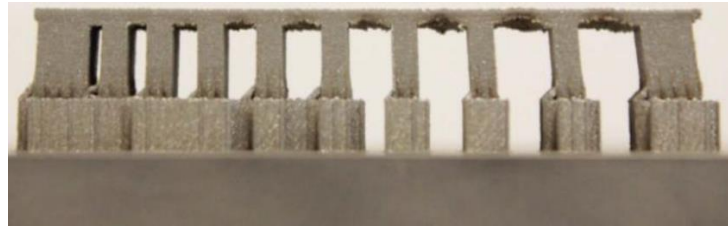


Figure 25) effects in unsupported bridges of different length [48]

- Part growing against the re-coater: The force applied by the re-coater blade can bend a structure inclined in the opposite direction with respect to the movement of the blade. For this reason, if the part cannot be oriented in some other way, a support structure is required to ensure the correct creation process.
- Thin wall: printing a thin wall could be a problem if they are alone but it is possible to support them with other walls. Circular/curved walls is better than flat walls (figure 26).



Figure 26) thin walls supported by other circular walls [48]

The support structure in powder-bed process is always made of the same material of the part. The cost of the raw material nowadays is still high, even if the cost is dropping every year, and remove the supports has a cost itself. There are two main reasons for which support structures are not composed of full dense material. The first is due to the fact that once the printing process is finished, the latter must then be removed. This operation is much easier if the supports are weaker. The second reason concerns the costs of the powders. In Additive Manufacturing process indeed the powders that are not been melted during printing can be reused. Therefore, supports are made in special structure in such a way as to be easily removable and at the same time use less powder. However, each application requires multiple analysis and tests to be created in the most efficient way. Once the printing is completed, the support structures are mechanically removed in a post-process operation.

1.2.3 Slicing

Another important step made by the software is the slicing. Before printing the part the slicing data must be acquired. The STL file is sectioned into parallel layer with a normal vector in the z direction of thickness Δz . In the case where the thickness of each layer is not so thin is very important to correctly orient the part. In fact, with the same thickness Δz and the same CAD model, it is possible to obtain pieces with a very different surface roughness. This is due to the "stair-stepping" created by the thickness of the layer. As shown in figure 27, this phenomenon can be reduced by choosing an appropriate orientation of the part.

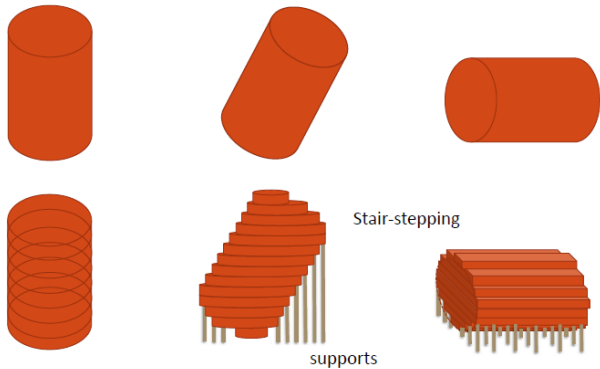


Figure 27) effects of orientation of the parts [32]

Usually the strategy used is the “Uniform slicing” that maintain a constant layer thickness. But an option to decrease the “stair-stepping” could be the so called “adaptive slicing”. Adaptive slicing methods consist in automatically adjust the build layer thickness to accommodate surface geometry as shown in figure 28 that compare direct slicing method with adaptive slicing one.

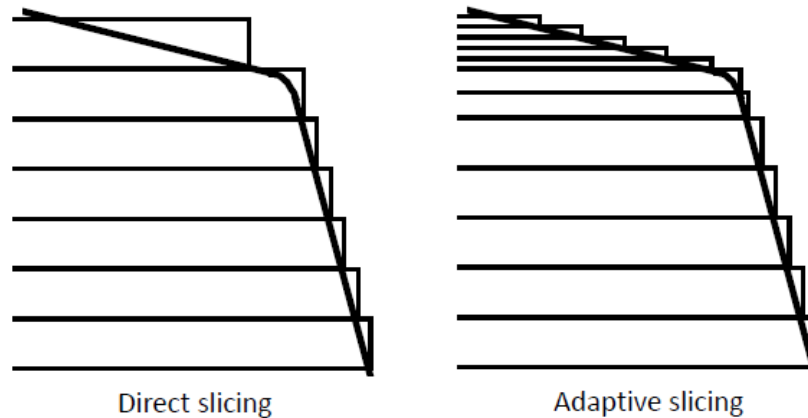


Figure 28) direct and adaptive slicing [32]

The reason because this kind of slicing method is not so used is because it is difficult to implement for most of the AM system. It does not integrate at best with current machines hardware.

Once the slicing data of the STL have been obtained and transferred to the AM machine the print can starts.

1.2.4 Part Orientation

“Part build orientation is a crucial process parameter which affects part quality, in particular GD&T (Geometric Dimensioning & Tolerances) errors on the part, the energy expended, and the extent of support structure require” [15].

The orientation of a part affects several aspects:

- Number of support structure: depending on how you decide to orient the part, the number and the area of surfaces that exceed the inclination limit (usually less than 45°) with respect to the working plane may vary. As a result, the number of supports required for the creation of that specific piece also varies [16].
- Building time: if the shortest dimension of the part is placed in the z direction reduces the number of layers required for the process. In fact, the workpiece size and the time required to melts the powders within it do not change but if the number of layer decrease, decrease also the number of recoating. This would reduce the whole building time.
- Surface quality: as mentioned in the chapter regarding the slicing, orient a part in the correct way can drastically reduce the surface quality of the parts. Indeed, in the case that a curved surface is oriented perpendicular to the z-axis, stair-step effect may occur. Obviously in most applications the geometry of the parts is quite complicated, so it is impossible to think of

orienting the part in such a way that no curved surface is perpendicular to the z-axis. But the task of the engineer is to find an optimal orientation considering all the advantages and the disadvantages of his choice.

- Mechanical properties of the component: usually the mechanical properties in AM process are strictly correlated to the orientation of the part with respect to the building direction. The parts have higher mechanical properties along the z axis then along x or y axis.
- Failures: each layer in a powder-bed fusion process is created by the re-coater blade. In this phase the re-coater blade may interact with the section of the part and can apply a force on this section. The force applied by the re-coater blade can bend a structure causing breakage or deformation. The worst case is a thin section parallel to the blade. To avoid problem a thin section must be oriented in such a way as to create an angle of at least 5 degrees with the re-coater blade (figure 29) [17].

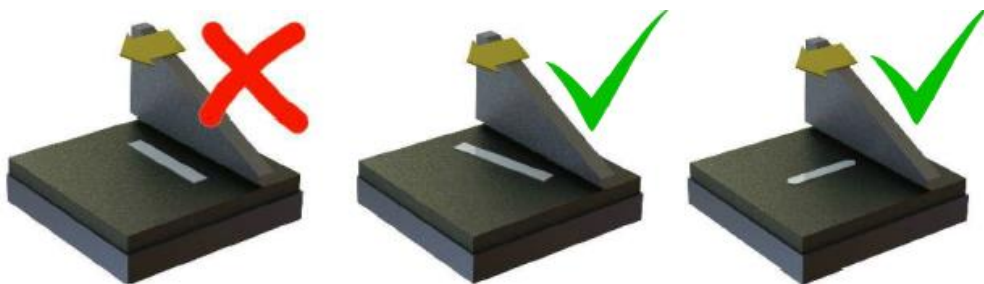


Figure 29) correct orientation to avoid deformation due to the movement of the re-coater blade [32]

Another configuration to avoid is a part that grows against the moving direction of the blade as mentioned in the previous chapter. Also in this case the force applied by the blade can bend and deform the structure.

1.2.5 Post Processing

In general, post-processing is a very important step in additive manufacturing process.

Post-processing in general is done for several reasons but the main purposes are to enhance components and overcome AM limitations. This includes [18]:

- support material removal
- surface texture improvements
- aesthetic improvements
- preparation for use as pattern
- property: enhancements using non-thermal techniques
- property: enhancements using thermal techniques
- accuracy improvements

In particular for PBF process post-processing has a crucial relevance. It consists of:

Cleaning of parts: once the process is completed the parts are completely covered by the powders. This situation required a cleaning of the part. More specifically all parts with internal channel has to be designed in such a way that the powder inside the part can escape. Otherwise, these powders particle will solidify during subsequent heat treatment. The powder can be removed both manually and with sand-blasting operation. One of the advantages of the additive technology, as mentioned in the chapter 2.3, is precisely the possibility of reusing the powders that have not been melted together for the creation of the part. Therefore, the powder that has not melted can be collected during the cleaning of the part and reused for a subsequent print.

Heat Treatment: the laser power in PBF (powder bed fusion) creates a temperature gradient in the part. This turns in a big amount of residual thermal stresses into the built part. These thermal stresses can lead to deformations in the part once it has been separated from the plate. To prevent deformation a heat treatment is required. The heat treatment is correlated to the kind of material used. There are standard treatments that can be done on the material to release thermal stress and to increase its mechanical properties. The typical heat treatment for Inconel 718 is reported in the graph in figure 30 with reference to AMS 5662 and AMS 5664.

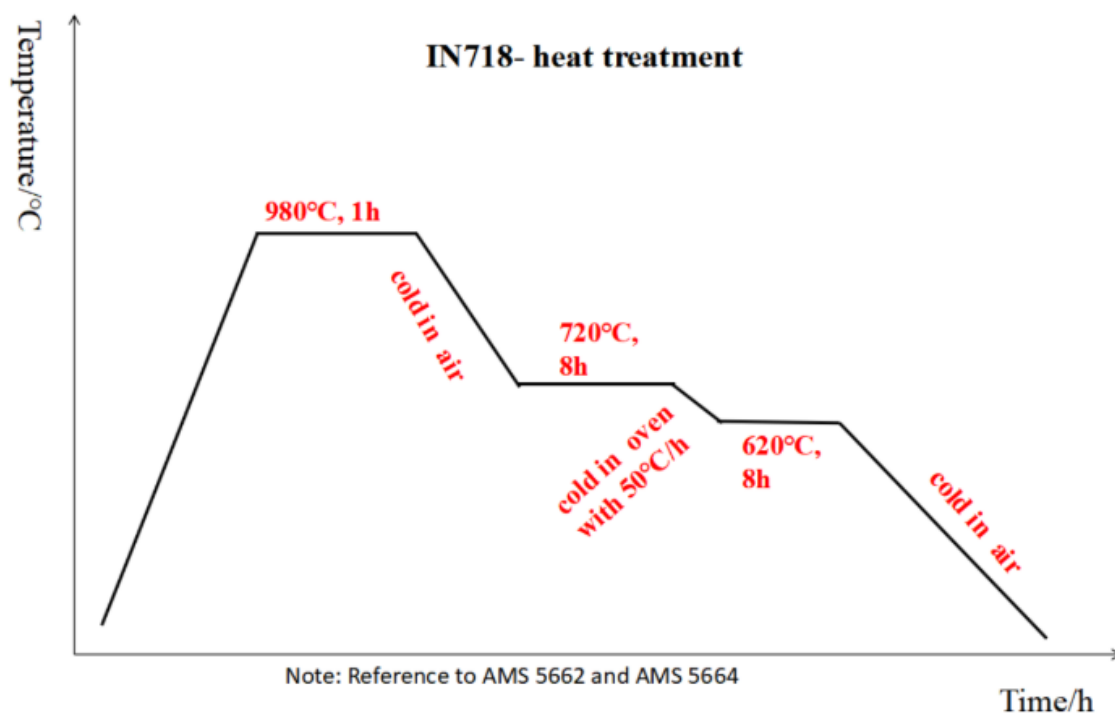


Figure 30) standard heat treatment for In718 [42]

Part separation from the platform: once the heat treatment has been completed the part has to be separated from the platform. This operation can be done by EDM (Electrical Discharge Machining). When the pieces have been separated the platform, the latter can be reused. The surface of the piece that has been cut from platform doesn't need to be polished or grinded.

Support removal: generally, the design of the part should allow easy support structure removal. This operation can be done manually, if the supports are not so hard, or using any

kind of metal cutting techniques such as milling, cut-off blades, wire-EDM and so on. The surface which the supports are attached may require subsequent post processing in order to decrease roughness and increase surface finish. So, the task of the designer is to minimize as much as possible the support structures.

Machining: The aim of machining operation is to improve part functionality, dimensional accuracy, surface finish, and the esthetics of the component. Thanks to these post-processing operations, AM products can also be used in applications that require very low tolerance thresholds.

1.3 Metal AM

AM of metals has begun to attract market attention only in the last ten years due to its immanent advantages, despite the fact that the techniques for Additive Manufacturing of Metals have been known for more than twenty years. That's because they were limited to the rapid manufacturing of porous structure and prototypes. Over time, however, the technology has improved becoming able to create almost fully dense parts [19].

SmarTech published its latest research report on the metal additive manufacturing market, which found that the industry's revenues from hardware, materials and software grew by 24% in 2017, topping \$1 billion for the first time and that there is an increasingly positive long-term outlook based on the current environment, which will reach \$9.3 billion by 2027. The perceived slowdown in the metal additive manufacturing industry observed at the end of 2016 until the first half of 2017 appears to have been an anomaly fueled by rapid changes in competition. SmarTech's research found that the market for metal additive production accelerated in the second half of 2017 and is now on the verge of further growth in the future, with the expectation of an overall growth peak in 2019 (35%) [20].

Thanks to this increase in the properties and characteristics of the product parts, AM of metals have found space in various applications, including:

- Medical (fig 31)
- Artistic (fig 32)
- Aerospace (fig 33)
- Automotive (fig 34)
- Industrial application (fig 35)



Figure 31) Titanium skull implant



Figure 32) 3Dprinted metal sculptur



Figure 33) Copper rocket nozzle



Figure 34) Race car steering produced by DMLS

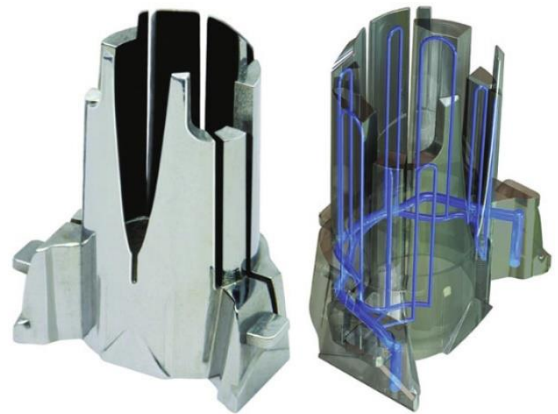


Figure 35) DMLS fabricated part and model showing internal conformal cooling channels

Usually AM technologies can be classified as shown in the second chapter by the nature and the aggregation state of the feedstock as well as by the binding mechanism between the joined layers of material [21]. AM of Metals uses as starting material powders or more rarely a wire. Independently on what kind of starting material being used it is fully melted by energy created with a laser or with an electron beam and transformed layer by layer into a solid part. The most common processes of AM of Metals are Directed Energy Deposition (DED) and the 2 powder bed fusion processes (PBF) divided according to the source of energy used: Laser beam melting (LBM) and Electron Beam Melting (EBM). For this reason, in the following chapter these three processes will be described in details.

1.3.1 Powder Bed Fusion Systems (PBF)

Powder bed technology, as the name suggests, uses powder as the starting material. Through the use of energy, created by laser or electron beam, it selectively melts the powder in the area defined by one slice of the 3D model. Each time a cross section is fully melted, a motor allows to lower the building platform in the z axis direction. The vertical movement of the building platform represents the thickness of each layer, so it is very important to have a high accuracy on the movement of the motor because the layer thickness is a parameter with a crucial relevance in the additive manufacturing process. Once the building platform has been lowered usually a roller lays a new layer of powder on the building platform to allow the melt of the next slice. Usually, all PBF systems share some basic set of characteristics. These are [23]:

- one or more thermal sources for inducing fusion between the dust particles;
- a method to control and limit the fusion of the particles only in the desired area;
- a method for adding powder layers.

In most of cases laser is used as a thermal source. With the use of PBF system it is possible to produce components with a high geometric complexity and with a better surface finish than other Additive Manufacturing techniques such as for example DED (Direct Energy Deposition).

In addition to the layer thickness, very important both from the process and the productivity point of view, there are a lot of parameters that can influence the process in PBF. Among this there are laser power, laser spot, laser focus, building temperature, humidity, vibration, powder size, powder density

and scanning strategy. Scanning strategy is the controlled path of the laser beam. Depending on the chosen path the time between 2 close passes changes and, as a consequence, changes the temperature reached during melting and consequent post-solidification shrinkage. This can lead to the formation of thermal stresses. So it is very important to find an optimal calibration of the parameters to reach the desired characteristic of the final part. This optimal solution can be reached through the so called "try and error" or "Design of Experiment (DoE)" methods.

Powder bed fusion process includes: Direct Metal Laser Sintering (DMLS), Electron Beam Melting (EBM), Selective Heat Sintering (SHS), Selective Laser Melting (SLM) and Selective Laser Sintering (SLS) [22]. In the following chapter LPBF and EBM systems will be explained in detail.

1.3.1.1 Laser Powder Bed Fusion (LPBF)

The term LPBF refers to 2 techniques: selective laser sintering (SLS) and selective laser melting (SLM). SLS was the first Powder Bed Fusion Process commercialized. It has been developed in the University of Texas at Austin, USA. Generally Selective laser Sintering (SLS) and Selective laser melting (SLM) are considered the same thing. The two names depend on historical reasons; they were used when the metal mixture did not reach the complete fusion under the effect of the laser radiation and the component presented high porosity after the process. Nowadays the complete fusion of the powders hit by the laser radiation can be achieved. As a consequence, a full density part can be obtained if the process is correctly controlled.

LPBF systems, as the name suggests, use laser as thermal source to selectively melt the powder. Different type of laser can be used, including CO₂, Nd: fiber lasers, YAG, disc lasers etc. depending on the desired results [25]. Each laser has indeed his wavelength that influences the laser absorptivity of material. In addition also the operative metallurgical mechanism for powder densification depend on the input laser energy density.

A general sketch of how the LPBF works is reported in figure 36. The laser beam generated by the source (top left in the figure) is directed by moving mirrors, located in the scanner system, directly to the bed of powders where the part is being printed. It melts the cross sectional area defined by the sliced 3D Cad model [24]. After the slice has been completed the powder bed is lowered by the desired thickness of each slice thanks to the fabrication piston. At the same time the powder delivery system is raised by the powder delivery piston. Afterwards the roller (or a blade) spread a new layer of powder on the fabrication powder bed. The laser can now melt the subsequent slice of the part model. This cycle is repeated until the last section of the model is reached.

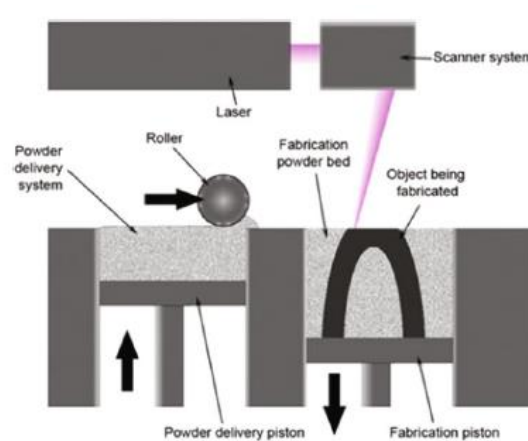


Figure 36) general LPBF process [24]

The figure 37 shows a zoom of the laser beam while it melts a new layer of powder. The fused deposit layer thickness is always thinner than the powder layer thickness. And is important that the melt penetration depth is greater than the thickness of a layer. Often the molten pool can penetrate 3 or more layers. The reason behind this feature is to more fully fuse the deposit (figure 38) and ensure the attachment between the layers. Over the years, LPBF systems evolved to such an extent that they are able to create a near 100% fully dense metal part.

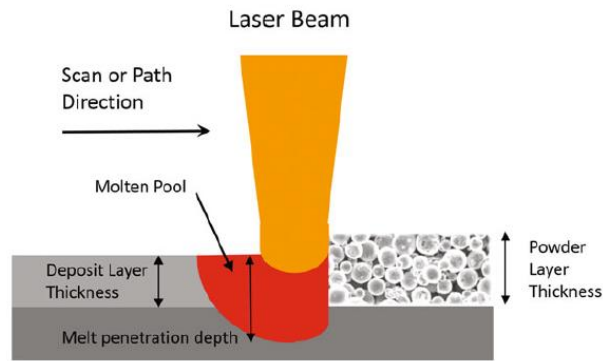


Figure 37) melting of powder [24]

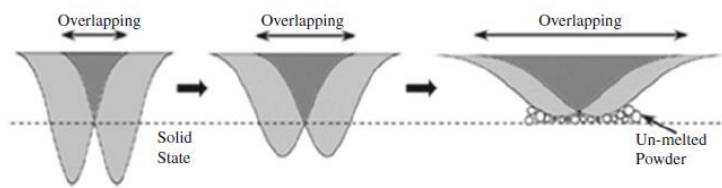


Figure 38) Adjacent melt tracks must penetrate into the layers below to achieve full fusion [24]

LPBF systems require a working area in an inert atmosphere to avoid oxidation of powder during the process and guarantee the optimal condition for melting. For this reason the working chamber is usually filled with an inert gas, this gas usually is nitrogen or argon to lower the oxygen level below 500 ppm (part per million). In most of cases nitrogen is enough but for some reactive materials such as titanium, argon is recommended.

However, the direction of the gas flow with respect to the scan direction can influence the final properties of the part. If they are in the same direction, it is possible that the fumes produced by the fusion of powder may interfere with the laser by creating some gas porosity (figure 39).

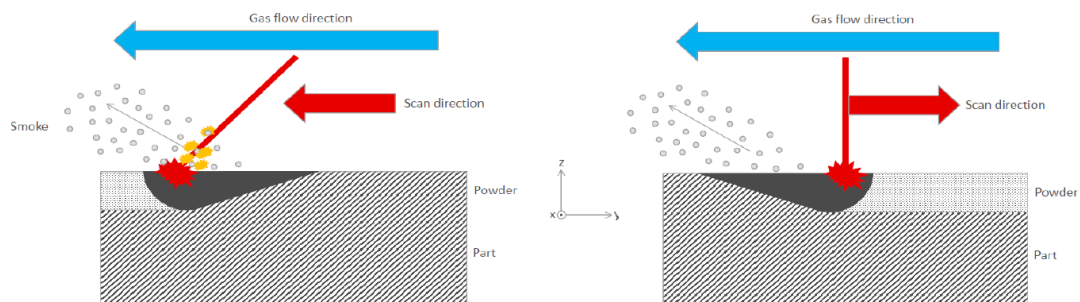


Figure 39) possible interaction between smoke and laser

With the spread of this technology also the number of materials used is increasing. At present the materials used are: Titanium and associated alloys (Ti6Al4V), where a high strength to weight ratio is

required, Inconel alloy (In718 and In 625), Aluminum alloy (AlSi10Mg), Cobalt Chrome, Maraging Steel and Stainless Steel.

The laser scanning optics works thanks to magnetically driven mirrors that use galvanometers. This solution enables rapid movement of the laser beam on the working area, in addition there is no need to articulate the mass of a laser head's final focusing optics to achieve accurate X and Y axis beam positioning. Having a scanning optics that works moving only the mirrors is hence a big advantages in terms of cost and velocity.

LPBF has the possibility to print multiple part at the same time and very complex structure and geometry can be created. For example, structure with complex shells, internal cooling channel, lattice structures. Thanks to the possibility to have this kind of structure is hence possible to optimize the part by decreasing the weight maintaining the desired characteristics.

This kind of AM techniques guarantee a high accuracy on the surface allowing in some cases to produce directly end-usable parts.

The big limitation, as in all AM methods, is the process complexity in terms of process parameters [27]. Is very difficult to find the best process parameter combination to fully exploit the potential of this process. The problem is that the best combination of parameters does not exist, indeed in the most of cases the goal of 100% density, in all deposition condition, for all material conflicts with the productivity goals.

The working area of the commercially available professional LPBF systems has a maximum size on about 400-500mm. So, the part that can be created with this technology are limited to that size. Is possible to increase the working chamber but it will lead to other disadvantages; if a small part has to be built within a larger build volume, this part is will take longer to be print. In fact, the recoating time for a bigger build chamber surely will increase lengthening the process time.

A large volume of powder is required for each job, even if the part is small the powder needed must be at least the quantity to fill up the entire work volume for the height of the desired part. A large amount of powder in fact does not become part of the object. Although the powder un-melted can be reuse by sieving them. Research is ongoing to find the number of times the powder can be reused before some changes to the powder properties render it unusable.

Thanks to the fusion and subsequent very fast solidification, the mechanical/metallurgical characteristics of AM parts prove to be better than those obtained with traditional methods; an important problem is the phenomenon of the so-called Balling, which consists in the formation of small spheres with a diameter approximately equal to the size of the beam. These spheres can cause a discontinuous melted trace resulting in poor surface finish.

Last but not least the cost of both machine and material is still very high.

1.3.1.2 Electron Beam Melting (EBM)

EBM is a powder-based AM technology. It was born in the early 90s and was commercialized in 1997 by Arcam AB corporation, a Sweden company.[28]

The process is very similar to the LPBF; both starts from 3D CAD model and by slicing the STL file the heat source selectively melts layer by layer each cross section of the part. The real difference between these 2 techniques is the heat source. EBM use a stationary electron beam to melt the powder together instead of the laser. The beam is electromagnetically deflected in X-Y plane to scan and fuse the dust in each section of the part. This ability to scan the electron beam by the use of electromagnetic coils allows faster scanning (up to 8000 m/s) and the electron beam positioning accuracy of ± 0.0025 mm. The build rate is so higher than the similar L-PBF systems. The layer thickness is in the range of 0.05-0.2 mm [29].

The principle behind the electron beam is shown in figure 40. “A high voltage supply is placed across a grid cup and anode. A negatively charged cathode is heated to boil off electrons in a process referred to as thermionic emission. Those electrons are accelerated at high voltage (60 kV) and focused by the grid cup toward the anode passing through a hole and into a work chamber. In the chamber the charged electron beam is focused using electromagnetic coils and may be directed to locations on the workpiece using magnetic deflection coils to steer the beam. EB equipment can generate beam voltages of 60–150 kV and beam powers of 3–30 kW or more and focus to beam spot sizes of fractions of a millimeter”.[30]

This technology exploits the kinetic energy of the accelerated electrons that, when they hit the powder bed is transformed into heat that melts together the powder particles.

In EBM the interaction between the beam and the powder is characterized by a deeper penetration of the beam with respect of the laser beam. The electrons indeed require a big amount of collisions with the atoms of the material so that all their kinetic energy is absorbed by the material. The EB has, therefore, a very high efficiency and a higher energy density than the LPBF process.

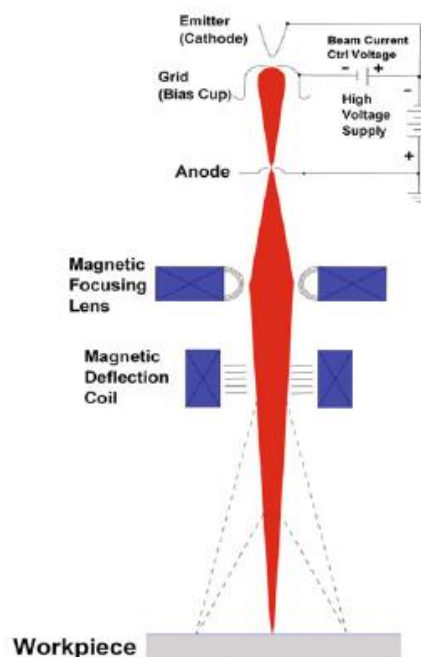


Figure 40) Electron Beam Melting [30]

The EBM system (figure 41) is made up of a powder distribution mechanism, an electron beam gun, a build tank and a vacuum chamber. Using vacuum chamber the material does not oxidize, and this ensure high mechanical performance. This kind of technologies exploits the electron beam to preheat the powder up to a temperature about 700°C. The preheating is made by the EB defocused using low power and high scanning speed. This is done to regularize the powder bed and decrease the powder diffusion in the chamber. The powder diffusion is caused by 2 reason: the impact of the electron beam on the powder bed and the electrostatic force repulsion. In addition to deal with this electrostatic charging the electrical grounding of the build plate is required. Also the build chamber is heated up to ~700 and thanks to the maintenance of this temperature the residual thermal stresses in the part decrease considerably. The preheating is strictly correlated to the materials used and the build chamber can take tens of hours to cooling down the temperature. This slow cooling down allows grain growth and relaxation of the microstructure. To decrease the time between 2 consecutive job, the modular build volume can be removed and left to cool down, while a new build chamber is installed for the next job.

Very often in this kind of system a camera based monitoring and a modular powder recovery system is provided as for example in the one made by Arcam. The smallest reachable spot size of electron beam is about 100 μm, allowing a good resolution of finer details.

As in LPBF system multiple parts can be produced during one job in order to guarantee high utilization of the building volume that has usually an area of 350x380mm. The rapid scanning velocity of EBM systems, up to 8000m/s, allows also multiple melt pools at the same time.

One of the limitations of this kind of technology is that the material must be electrically conductive to allows interaction between the electron beam and the powder. For this reason, fewer material options are available on the market. The manufacturing of polymeric or ceramic materials is indeed impossible with EBM technology.

The EBM systems require larger powder diameter size with respect to LPBF systems and this is a disadvantage because the bigger grain size decrease the part accuracy.

This technology offers freedom in design combined with attractive material properties and high productivity.

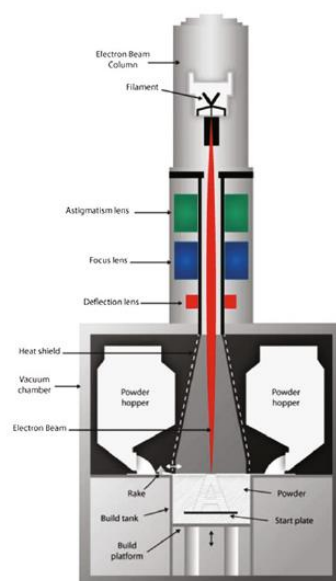


Figure 41) Electron beam system [30]

As mentioned above, after the process, a cooling down of the chamber is required. This cooling is performed usually insufflating helium into the chamber that increasing the pressures to $\sim 10^{-2}$ Pa. Helium is useful also to reduce electrostatic charging of the powder particles [31].

The EBM system require a vacuum chamber because when the electrons pass through a gas interact with it and are deflected. This doesn't happen with the laser source at least as long as the gas is transparent to the wavelength of the laser itself.

One of the most important parameters in EBM systems, considering his high scanning velocity ability, is surely the scanning strategy. The scanning strategy has a strong influence on:

- the impacts of electrons beam on the powder;
- the reached temperature;
- the system of withdrawal of the part after the solidification.

The scanning strategy is divided into two subsequent phases plus an optional one. The first phase is called stabilization phase (preheating). During this phase the electron beam defocused with low power and high scanning velocity preheat the powder to regularize the powder bed and decrease the diffusion effect. The second phase is the so called "fusion phase": the beam completely melts the powder with a high power and a low scanning speed. And the third optional phase that consist of a complete scansion of the whole zone with high power and high velocity. The purpose of this last phase is to obtain a greater dimensional accuracy and a better surface finish. In figure 42 and figure 43 the most used scanning strategy are reported [32].

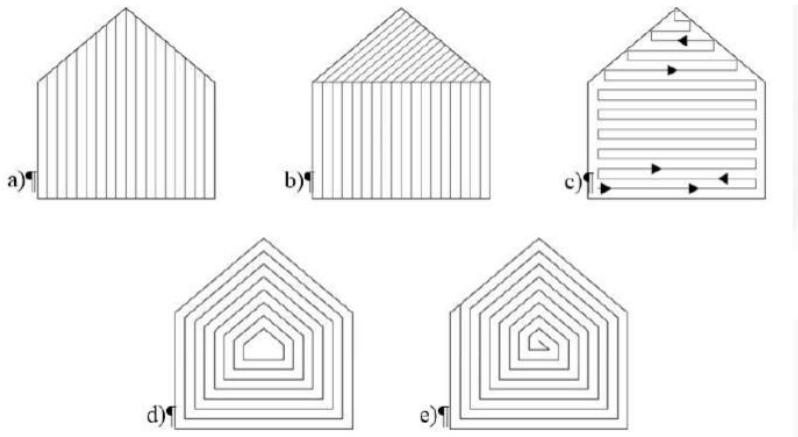


Figure 42) Scanning strategy: a) Unidirectional raster, b) Multi-directional raster, c) zig-zag, d) concentric scanning, e) spiral scanning [32]

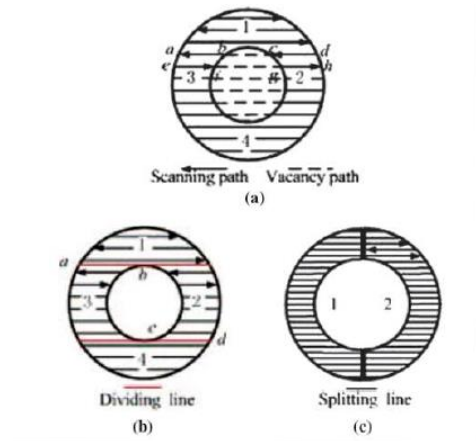


Figure 43) Scanning strategy of hollow section: a) jump strategy, b) subdivision into zones, c) split strategy [32]

EBM downward surfaces, as in LPBF, must be supported but unlike in LPBF the support structure can start directly from the powder and not only from the building platform. This characteristic allows to better exploit the volume of work increasing the productivity of the process.

A table comparing EBM System with LPBF systems is reported in table 1.

	EBM systems	L-PBF systems
Thermal source	3-4 kW EB	100-1000 W Fiber Laser
Atmosphere	Vacuum	Inert gas (nitrogen or argon) or vacuum
Build rate	55-80 cm ³ /h	13-50 cm ³ /h
Tolerance	± 0.5 mm	± 0.1 mm
Powder bed temperature	700-1000 °C using Electron Beam	30-200 °C
Layer thickness	50 – 200 µm	20-50 µm
Scanning	Deflection coils	Galvanometers
Scan speeds	up to 8000 m/s	up to 8 m/s
Surface finish	Ra= 15 – 25 µm	Ra= 5-10 µm
Materials	Metal (conductors)	Polymers, ceramics and metal
Metal Materials used	<ul style="list-style-type: none"> • Ti6Al4V • TiAl • Co-Cr <p>Limited by conductivity</p>	<ul style="list-style-type: none"> • Inconel 625/718 • Co-Cr • AlSi10Mg • Stainless/Maraging Steel • Au Alloy <p>Limited by reflectivity</p>
Powder particle size	medium	fine
Energy costs	moderate	high

Table 1

1.3.2 Directed Energy Deposition (DED)

Directed Energy Deposition, also known as LENS (Laser Engineered Net Shaping) or DMD (direct Metal Deposition), differs from the techniques mentioned above mainly by the fact that creates parts by melting the material as it is being deposited. There are different types of DED, which are similar in working principles but differ from each other in the type of raw material used and the type of focused heat source. The raw material may be in wire form or in powder form while the energy source may be a laser or an electron beam. The most common DED technique is the L-DED (Laser Directed Energy Deposition) that use powder as raw material. The deposition, as shown in the figure 44, takes place by means of a nozzle mounted on the head that creates a flow of powder directed to the point where the melting takes place. The number of nozzles can usually vary between one and four. The use of multiple nozzle allows also the machine to create a metal alloy directly on the part thanks to the possibility to feed different nozzles with different powders. In order to avoid oxidation and others interaction between the atmosphere and the melt pool during the process, the printhead is usually equipped with a system that creates a shielding gas flow around the points where the melting takes place. This gas flow has also the function of helping the deposition of powder. Is important using this system to find the correct value of the pressure of gas to keep away the ambient air and at the same time avoid disturbance within the melt pool. Some L-DED machines, however, have the possibility to make the deposition in an inert chamber thanks to the use of Argon or Nitrogen depending on the reactivity of the materials.

With this kind of process, almost any type of material or mixture of powders which are sufficiently stable to form a melt pool can be used. Materials that are very difficult to process are those with high thermal conductivity and high reflectivity such as some aluminium alloys, gold and copper. This materials, because of their characteristics, can reflect the laser beam and in some cases even cause internal damage to the machine itself.

Unlike powder bed techniques, L-DED does not originate from plastic prototyping technology. Laser-Directed Energy Deposition systems can be considered an evolution of the laser cladding techniques for welding, where, instead of adding material only in the welding areas, the material is deposited to built the entire 3D object. Differently from wire deposition, not all the raw material is melted on the final piece. Part of the powder fired from the nozzles inevitably ends up scattered in the work chamber. It is therefore necessary to provide a mechanism to collect it both for safety reason and also to be able to use it again [46].

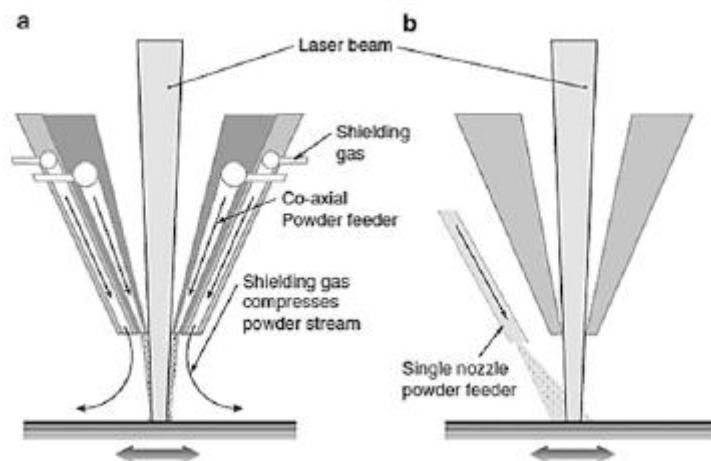


Figure 44) illustration of powder nozzle configurations: (a) coaxial nozzle feeding, (b) single nozzle feeding [46]

In the 3-axis systems the laser beam is usually delivered along the z-axis. To control the focus of the laser and the powder the lens and the powder nozzles can be moved always along the z-axis. What allows the creation of the desired cross sectional area is the work-holding platform that can move along the xy plane by a computer controlled drive system. Then the other layers are additively deposited to form a three dimensional object. In recent years, more innovative systems with 5-axis and 6-axis machine have also been developed by using rotating table and fixing the printhead on robotic arms. For machines using more than 5 axes there is usually a closed-loop control of the process; this is to ensure the correct deposition and melting of the powder at the desired point. The parameters controlled are 3: Geometry (height of deposited layer), temperature of the melted pool and the composition (microstructure of the deposited material). Thanks to this closed-loop system is possible to adjust the parameter during the process and ensure optimal results. The microstructures obtained with Laser Directed Energy Deposition are very similar to the ones obtained for L-PBF processes. In both cases the material solidifies very rapidly (10^3 - 10^5 °C/s) causing thermal gradient and formation of microstructures impossible to achieve with other forming methods. Furthermore, thanks to the control system the microstructure can be checked and modified during the process in case of problems.

The working chamber (more than 1m^3 in size) of DED process are greater than the working chambers of others Additive Manufacturing techniques. This allows the creation of much larger objects and makes this technology really suitable for part repairing, coating and features addition. With the clamping systems of the machine is in fact possible to clamp a real piece and start adding features or repair the damaged parts or even deposit some layers of dense, wear and corrosion resistant metals directly on it.

In conclusion, DED processes are able to produce parts with very low porosity percentage. They offer the possibility to control, at least in part, the microstructure of the components thanks to the close-loop control and the subsequent modification of the process parameters during the job. The biggest disadvantage however, is the low resolution and surface finish achievable, lower than the one achievable with Powder Bed Fusion processes. The resolution is in fact about the 0,25 mm and the surface roughness is about 25 μm . In addition, the construction time for DED systems is also quite long. The deposition rate is between 25 and 40 g/h and any action aimed at increasing its productivity would result in a reduction of resolution. For this reason is important to find a correct balance between all the process parameters involved to achieve a good compromise for the cut off between resolution and productivity. However, the presence of several parameters that can affect the final properties of the piece, makes it more complicated. Unlike the two processes described above, the final result of which is mainly influenced by the characteristics of the powder used and the parameters of the laser (speed, power, etc.), in L-DED process have to be taken into account also the parameters of the flow of powder fired from the nozzles.

1.4 Inconel 718

The material considered for this study is Inconel 718. It is a nickel-based alloy with characteristics of strength and resistance to corrosion, that can be used at very high temperatures, in a range from -204 to 704°C. These levels of thermo resistance derive from the material's ability to develop a thick layer of passivating oxide that performs a protective function. Thanks to the characteristics mentioned above, the use of these nickel-based alloys is widespread in the aerospace sector and nuclear industries. In particular the Inconel 718 is present in many parts of jet engines, gas turbines, rocket motors, nuclear reactors, cryogenic tanks and so on. The composition of this material is reported in the table 2 [33].

Element	Inconel 718	
	min Weight %	max Weight %
Nickel (plus Cobalt)	50	55
Chromium	17	21
Iron	balance	
Niobium	4,75	5,5
Molybdenum	2,8	3,3
Titanium	0,65	1,15
Aluminum	0,2	0,8
Cobalt	N/A	1
Carbon	N/A	0,08
Manganese	N/A	0,35
Silicon	N/A	0,35
Phosphorus	N/A	0,015
Sulfur	N/A	0,015
Boron	N/A	0,006
Copper	N/A	0,3

Table 2

The phase composition of Inconel 718 mainly consists of a γ matrix with the precipitates of γ' , γ'' , δ and, additionally, some carbides. These precipitates, particularly γ'' , provide the desired mechanical properties to Inconel 718. On the other hand, it's not easy to work Inconel 718 with the traditional machines however it is suitable for additive manufacturing processes, ensuring that the parts produced have the properties required for the application.

1.5 LPBF of Inconel718

Before the start of this work, a literature search was carried out on the Inconel718 produced in SLM. The most interesting articles are listed and briefly summarized in this paragraph.

- in 2016 Xiaoqing Wang studied the effect of build height on the mechanical properties and microstructure of Inconel 718 parts fabricated by Selective Laser Melting. The samples of this test were cut from the as-deposited In718 parts and prepared for microstructure observation and nanoindentation test. From these tests emerged that the Young's modulus and hardness are comparable with the values found in traditional methods or literature. Furthermore, no changes in the behavior along the build height of the parts were observed and the parts did not showed anisotropic characteristics between the side surface (Y-plane) and scanning surface (Z-plane) (figure 45) [38].

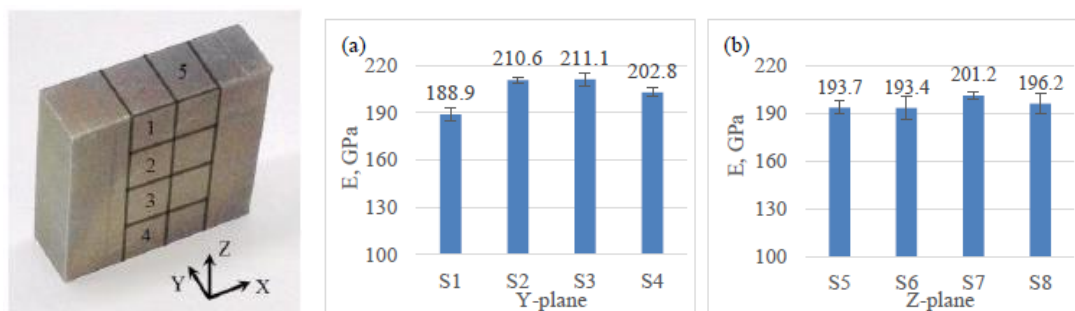


Figure 45) Young modulus on Y-plane and Z-plane [38]

- On February 2019 Yang Gao studied the effect of δ -phase on high temperature mechanical performance of Inconel 718 fabricated with SLM process in as-build, SHT 980, SHT1080, SHT 980+1080 heat treated conditions. It's known that the excessive δ phases in grains and along grain boundaries leads to dislocation piling up in the process of tensile test at elevated T, causing microcrack generation and local stress concentration in the matrix and resulting in premature failure of parts. Conversely, lack of δ phase reduces the high temperature strength of grain boundaries and that influences the high temperature mechanical properties. What was observed during the experiments is that because of the precipitation of δ , γ' and γ'' phases hinder the dislocation slip due to the pre-designed heat treatment schemes, so that the tensile strengths at elevated temperature are higher than that in the as-built condition while the elongation becomes lower [39].
- In 2019 Luke Scime studied the melt pool geometry and morphology variability for several process parameter combinations for the Inconel 718 alloy in a laser powder bed fusion additive manufacturing process. A study of a statistical distribution of melt pool dimensions was performed for each combination of parameters. This analysis proved that cross-sectional melt pool widths, depths and areas follow a normal distribution with the exception of a handful outliers that clearly diverge from a normal distribution (figure 46). [40]

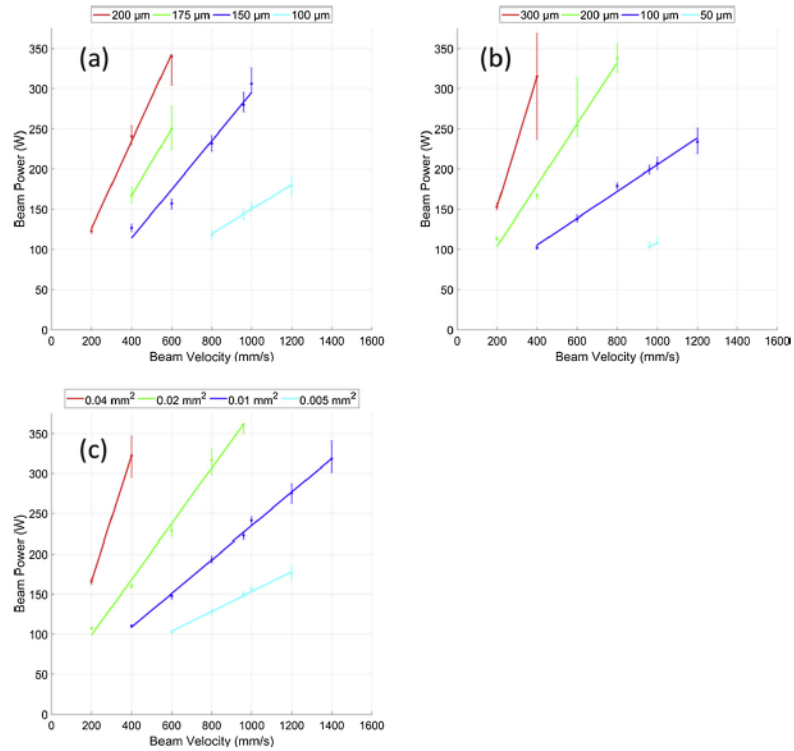


Figure 46) Process map of the cross-sectional melt pool (a) width, (b) depth, (c) area [40].

- Le Zhou studied the microstructure, precipitates and mechanical properties of powder bed fused Inconel 718 before and after heat treatment of solutioning and two-step aging. It was found that precipitates of γ and γ' were not observed in the as-built Inconel 718 but they were observed after two step aging, that solution heat treatment is necessary to dissolve segregated elements and that the hardness of the Inconel alloy slightly decrease after the SHT heat treatment while increase after the two-step aging. The highest hardness was found with SHT at 1065 °C (figure 47) [41].

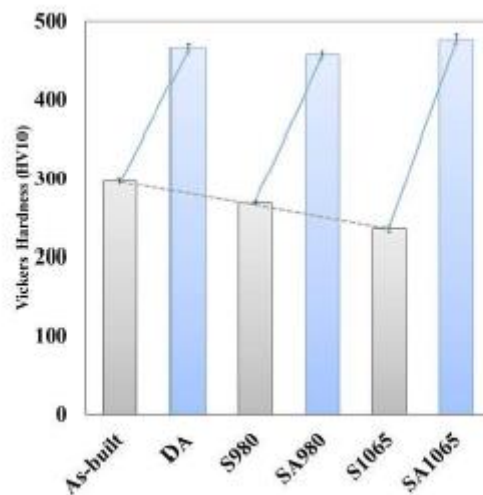


Figure 47) Vickers Hardness change in PBF IN718 alloy samples examined in this study [41]

- Qingbo Jia on October 2013 studied the Densification behavior, microstructural features and properties of In718 parts produced with Selective Laser Melting process (SLM). Multiple Energy Density values (330 J/mm, 300 J/mm, 275 J/mm, 180 J/mm) have been used to produce samples to be analyzed. During this work has been found that is possible to reach a near-full 98,4% density using an Energy Density of 330 J/m (figure 48). The sample shows an uniform microhardness distribution with a mean value of 395,8 HV_{0,2}. In addition with the same Energy Density value the optimum high performance oxidation behavior has been achieved [43].

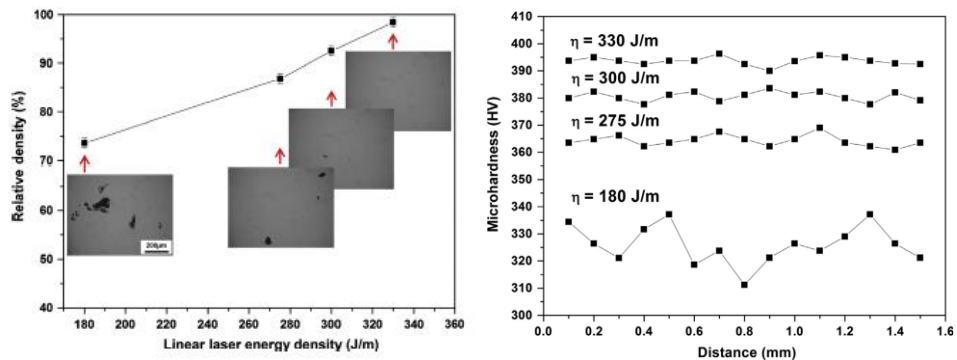


Figure 48) on the left: trend of Relative Density as a function of Linear Energy Density, on the right: microhardness and its distribution of In718 parts under various processing conditions [43].

- Christopher Kantzos on march 2018 studied the effects of the modifications of process parameters on additively Manufactured In718 parts. Four different set of parameters were investigated during this study. The work has highlights that, between the samples printed with different process parameters sets, shown in the figure 49, there has been small changes in microstructure but these changes did not seem to have any effect on mechanical properties (YS and UTS). Parameter sets that have shown an increased porosity percentage, number 2 and number 5, have also shown a shorter fatigue life (figure 50) [44].

Parameter	Power, W	Velocity, mm/s	Hatch spacing, μm	Modification
1	285	960	110	Nominal parameters
2	285	960	150	Increased hatch spacing
3	285	960	80	Decreased hatch spacing
4	300	1200	80	Increased cooling rate
5	200	400	180	Decreased cooling rate

Figure 49) Parameter set information [44]

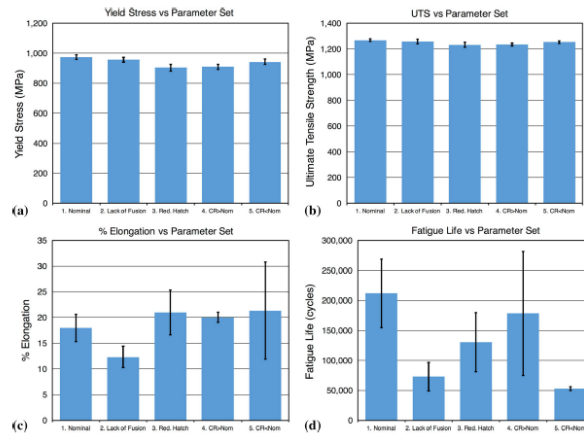


Figure 50) (a) Yield Strength, (b) UTS, (c) %Elongation, (d) Fatigue life as a function of process parameters sets [44]

In this literature review some of the most interesting articles found concerning the production of Inconel 718 fabricated with SLM have been briefly summarized. None of the articles found and analyzed, though, deals specifically on the increasing productivity of the process. Therefore, it will not be possible to make a comparison with the data obtained during this project thesis.

2 Materials and Methods

2.1 Starting material: Inconel 718

For this thesis work the superalloy Inconel 718 was used as starting material in form of powders. It was produced by the company Oerlikon [45] using the Gas Atomized manufacture process. The chemical composition is reported in the table 3 and the characteristics of the powder are reported in the table 4.

	Weight Percentage (Nominal)							
	Ni	Cr	Fe	Nb+Ta	Mo	Al	Ti	other
MetcoAdd 718C	balance	18	18	5	3	0,6	1	< 0,5

Table 3

	Nominal Range [μm]	D90 [μm]	D50 [μm]	D10 [μm]	Hall Flow [s/50 g]	Apparent Density [g/cm ³]	Morphology
Metcoadd 718C	-45 +15	46	30	18	< 18	4 to 5	Spheroidal

Table 4

2.2 Design of Experiment

The Design of Experiment, commonly abbreviated by the acronym DoE, is the set of all parameters used in the test. In powder bed fusion process a lot of parameters can be modified before starting a job. They represent all the work settings required by the machine to create the component from the powders. These are defined process parameters and they can be divided for the sake of simplicity into the 4 categories listed below [34]:

- Laser-related
 - Laser Power
 - Wave length
 - Spot size
 - Pulse duration
 - Pulse frequency
- Scan-related
 - Scanning speed
 - Scanning spacing (or Hatching distance)
 - Scanning pattern
- Powder-related
 - Particle size and distribution
 - Particle shape
 - Powder bed density
 - Layer thickness
 - Material properties

- Temperature-related
 - Powder bed temperature
 - Powder feeder temperature
 - Temperature uniformity

The correct choice of the process parameters is fundamental because the final quality of the product mostly depends on them. It is important to underline how all these parameters interact with each other, and often the change of one parameter or the other can lead to the same result on the properties of the final product. Overall, all parameters must be balanced against each other in order to ensure the maximum possible speed of construction, and thus make the process more and more competitive at an industrial level, and at the same time ensures that the final product has no defects that would penalize the quality. This is in fact the final aim of this thesis project.

Even if all the parameters influence the final products, not all of them have the same impact on the properties. For this reason only the most influential ones were taken into account trying to keep the others as unaltered as possible. The ones that have been proved to be more influential are: layer thickness, laser power, laser spot, scanning speed and hatching distance.

Volumetric Energy density (VED) and the Linear Energy Density (LED) were introduced [35, 36, 37] to obtain a significant value by comparing the various sets of parameters.

$$VED = \frac{P}{v * h * l}$$

$$LED = \frac{P}{v}$$

where:

$$VED = \text{volumetric energy density} \left[\frac{J}{mm^3} \right]$$

$$LED = \text{linear energy density} \left[\frac{J}{mm} \right]$$

$$P = \text{Laser power} \left[\frac{J}{s} \right]$$

$$v = \text{scanning speed} \left[\frac{mm}{s} \right]$$

$$h = \text{hatching distance} [mm]$$

$$l = \text{layer thickness} [mm]$$

VED represents the amount of energy that affects 1 cubic millimeter of the powder bed. It will then be used as an indicative value with the aim of increase the productivity of the process.

2.2.1 The first Design Of Experiment

As a starting point for the setting of the first Design Of Experiment a research in literatures was carried out. This research showed that using a set of parameters that has a Volumetric Energy Density Value between $60\text{J}/\text{mm}^3$ and $110\text{J}/\text{mm}^3$ is possible to reach an acceptable value of density into the sample (greater than 98%) [43,44].

Combining the data found in literature with regard to Inconel 718 and the knowledge of Prima Additive gained through the experience, it was decided to analyze all possible combinations using the speed and power values shown in table 5 while keeping constant the remaining parameters (table 6). The value of laser power, scanning speed and hatching distance is reported as a percentage value for privacy reasons.

Scanning Speed	57%	67%	77%	87%	
Laser Power	27%	31%	35%	39%	43%

Table 5

Constant Parameters	
Laser Spot(mm)	0,07
Hatching Distance	10%
Layer Thickness (mm)	0,02

Table 6

Starting from the chosen value, for each combination of scanning speeds and laser powers reported in table 5 the energy density was calculated in the table 7 with the formula described in the chapter above. During the first DoE a sample with the standard parameter used now by the company Prima Industrie was printed to have a comparison with the results obtained. This sample is the number 3 in the table below.

Sample number	Scanning speed	Laser Power	Hatching distance	Laser spot [mm]	Layer thickness [mm]	Energy density [J/mm^3]
1	87%	39%	10%	0.07	0.02	75,0
2	67%	43%	10%	0.07	0.02	107,5
3	57%	39%	10%	0.07	0.02	114,7
4	77%	39%	10%	0.07	0.02	84,8
5	87%	43%	10%	0.07	0.02	82,7
6	77%	43%	10%	0.07	0.02	93,5
7	57%	43%	10%	0.07	0.02	126,5
8	67%	39%	10%	0.07	0.02	97,5
9	77%	27%	10%	0.07	0.02	58,7
10	67%	31%	10%	0.07	0.02	77,5
11	77%	31%	10%	0.07	0.02	67,4

Sample number	Scanning speed	Laser Power	Hatching distance	Laser spot [mm]	Layer thickness [mm]	Energy density [J/mm ³]
12	77%	35%	10%	0.07	0.02	76,1
13	67%	27%	10%	0.07	0.02	67,5
14	67%	35%	10%	0.07	0.02	87,5
15	57%	27%	10%	0.07	0.02	79,4
16	57%	35%	10%	0.07	0.02	102,9
17	57%	31%	10%	0.07	0.02	91,2
18	87%	27%	10%	0.07	0.02	51,9
19	87%	31%	10%	0.07	0.02	59,6
20	87%	35%	10%	0.07	0.02	67,3

Table 7

The purpose of the first DoE is to identify a windows of Volumetric Energy Density's values generating the best results in terms of porosity. This windows of VED was used later during the second DoE with the aim of increasing productivity. In accordance with the final purpose of the thesis, the productivity values of each sample were also calculated with the formula:

$$Productivity \left[\frac{mm^3}{s} \right] = v * l * h$$

where:

$$v = Scanning\ speed \left[\frac{mm}{s} \right]$$

$$l = layer\ thickness \ [mm]$$

$$h = hatch\ distance \ [mm]$$

To have this value in a more significant unit [cm³/h] the productivity was multiplied by $\frac{3600}{1000}$ (table 8).

Sample Number	Hatching Distance	Layer Thikness [mm]	Scanning Velocity	productivity [cm ³ /h]
1	10%	0,02	87%	9,36
2	10%	0,02	67%	7,20
3	10%	0,02	57%	6,12
4	10%	0,02	77%	8,28
5	10%	0,02	87%	9,36
6	10%	0,02	77%	8,28
7	10%	0,02	57%	6,12
8	10%	0,02	67%	7,20
9	10%	0,02	77%	8,28
10	10%	0,02	67%	7,20

Sample Number	Hatching Distance	Layer Thickness [mm]	Scanning Velocity	productivity [cm ³ /h]
11	10%	0,02	77%	8,28
12	10%	0,02	77%	8,28
13	10%	0,02	67%	7,20
14	10%	0,02	67%	7,20
15	10%	0,02	57%	6,12
16	10%	0,02	57%	6,12
17	10%	0,02	57%	6,12
18	10%	0,02	87%	9,36
19	10%	0,02	87%	9,36
20	10%	0,02	87%	9,36

Table 8

Once the parameters were chosen, the samples were created directly in Materialise Magics. For the sake of simplicity the samples was printed in the shape of a cube with dimensions of 20 mm x 20 mm x 15,4 mm shown in the figure 51. In addition, a label indicating the scanning speed and the Laser power used for the sample was added above each one of them in order to distinguish the samples.

One specimen for each set of parameters was created. Materialise Magics offers the possibility to load your own printing platform in order to organize the job to be printed in the best way possible (figure 52). The work area represented in the figure 52 is the one of "Printsharp 250" and has a dimension of 250mm x 250mm x 350mm. Thanks to this function is possible to organize the available space during the pre-process operation and fill the working area as much as possible.

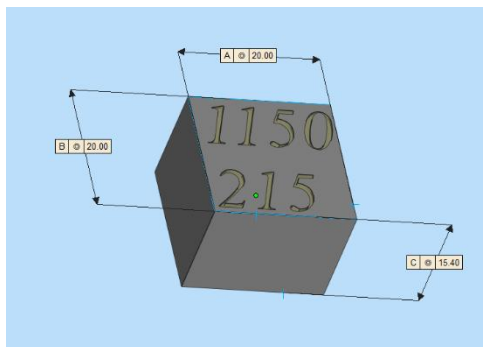


Figure 51

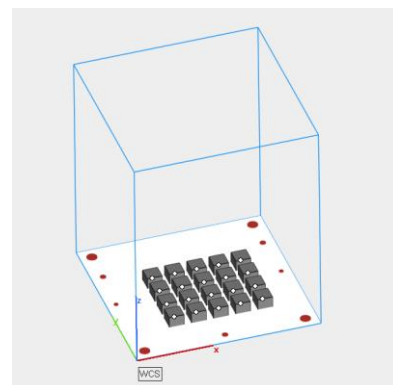


Figure 52

As mentioned in the chapter on the Additive Manufacturing cycle, after creating an STL file it is necessary to divide it into slice. Slicing was performed with the slicer function of Materialise Magics (figure 53). During this step is possible to chose the thickness of each slice that will correspond to the layer thickness during the printing process. For the first DoE the layer thickness was set to 20 micrometers. The output of this tool is a ".CLI" format file.

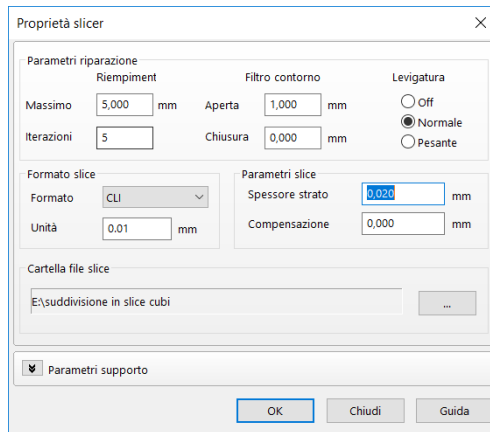


Figure 53) slicing tool Materialise Magics

Once the extension “.cli” is available the files were opened with the post processor software of Prima Additive. The function of this software is to set all the remaining process parameters that the machine will use to print the parts. So through this program the parameters chosen in the DoE was set for each sample and the files were finally saved as “.EPI” format, ready to be inserted in the machine and printed.

The printing of the samples was performed in two separate jobs (figure 54) using the “Printsharp 250” (figure 55). All the specifications of the machine were reported in “APPENDIX A”.

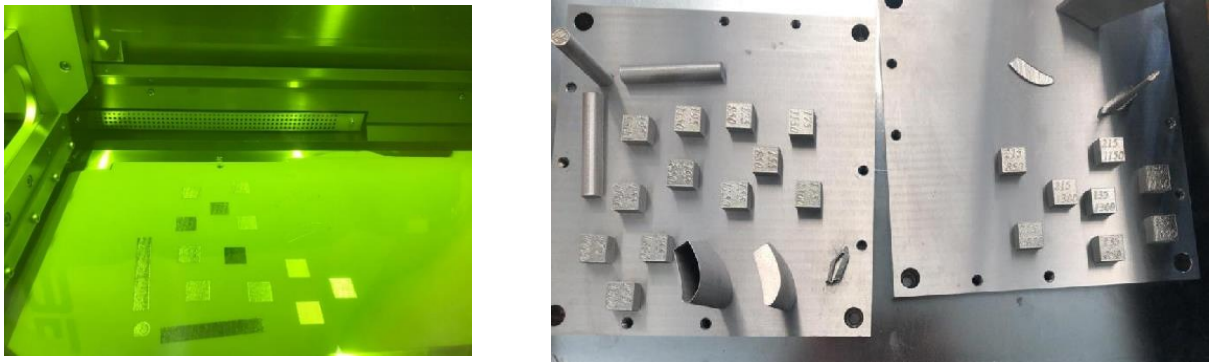


Figure 54) job during the printing and building platforms after the printing



Figure 55) PrintSharp 250

The two building platforms were preheated to 60°C inside the machine before printing began to avoid the creation of thermal stresses at the base of the parts and ensure a proper attachment to the platform. Moreover, after inserting the sieved powders into the machine, an inert environment was created by using nitrogen gas to avoid oxidation and to limit the explosive behavior of the powders with really small granulometry range (15-45 micrometers).

After the printing phase, the specimens in figure 54 was detached by the 2 building platform by the use of wire-cut EDM (Electrical Discharger Machine).

2.2.2 Repeatability Test

Before proceeding with the second phase of this work it was necessary to verify whether the values obtained with the parameters used were repeatable. Not all the combination of parameters of the first DoE was used for this test. A window of volumetric energy density values was chosen where the porosity values reach a sort of “steady state” trend. The samples that have shown this sort of trend were those with VED values between 85 J/mm³ and 115 J/mm³. In this window of values, the samples showed a good and approximately constant percentage of porosity. Another reason for choosing these values was the low standard deviation. This means that the specimens had more or less the same percentage of porosity at various points of the surface where the image analysis was performed. With this aim the VED values used for the samples number 2, 3, 6, 8, 14, 16, 17 of the first DoE were used again for this second DoE. The chosen parameters were reported in the table 9.

Sample number	numeration of DOE1	Laser Power	Scan Velocity	Linear energy density [J/mm]	Volumetric Energy Density [J/mm ³]	Hatch Distance	Layer Thickness [mm]
21	16	35%	57%	0,21	102,9	10%	0,02
22	17	31%	57%	0,18	91,2	10%	0,02
23	8	39%	67%	0,20	97,5	10%	0,02
24	3	39%	57%	0,23	114,7	10%	0,02
25	6	43%	77%	0,19	93,5	10%	0,02
26	2	43%	67%	0,22	107,5	10%	0,02
27	14	35%	67%	0,18	87,5	10%	0,02

Table 9

With the same procedure made for the first DoE the job was prepared using Materialise Magics and printed with the Printsharp 250 (figure 56) in Prima Industrie. The specimens were created of the same size and shape as the previous one.

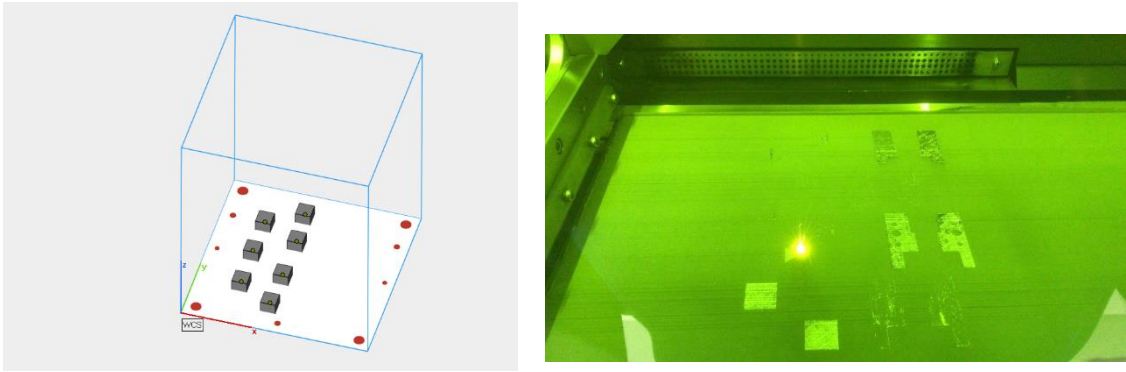


Figure 56) Repeatability job prepared on the left and on the right the printing with PrintSharp 250

2.2.3 The Second Design of Experiment

The objective of this second DoE was to obtain more productive parameters while maintaining the level of porosity below a certain threshold. Based on the results of the first Design of Experiment and the confirmation obtained by the repeatability test, it was decided to use VED values, between 85 J/mm³ and 115 J/mm³. The process parameters that influence the productivity are basically three as can be seen by looking at the formula reported below. The first and the most influential is certainly the thickness of each layer, but the objective of this work was to improve productivity without increase the slicing effect and therefore without modifying the layer thickness. The other two parameters that can influence the productivity are the laser scanning speed and the hatching distance. The hatching distance used for the first DoE was 10%. With the aim of increasing the productivity it was decided to print eight samples using a value of hatching distance of 11% and other eight samples using a value of 12%. On the other hand, as far as the scanning speed of the laser is concerned, it was decided to use 57%, 67%, 77% and 87%. Each of these speed values was then used for 4 samples of which two with a hatching distance of 11% and two with a hatching distance of 12%, trying to modify the laser power so that the VED value of each sample remained within the selected window.

$$Productivity \left[\frac{cm^3}{h} \right] = v * l * h * 3,6$$

where:

$$v = Scanning \ speed \left[\frac{mm}{s} \right]$$

$$l = layer \ thickness \ [mm]$$

$$h = hatch \ distance \ [mm]$$

The parameters chose for each sample are reported in table 10

Sample Number	Laser Power	Scanning Velocity	Linear energy density [J/mm]	Volumetric Energy Density [J/mm ³]	Hatch Distance	Layer Thickness [mm]	Productivity [cm ³ /h]	Increase in Productivity [%]
31	35%	57%	0,21	93,58	11%	0,02	6,7	10,0
32	39%	57%	0,23	104,28	11%	0,02	6,7	10,0
33	40%	67%	0,20	90,91	11%	0,02	7,9	29,4
34	48%	67%	0,24	109,09	11%	0,02	7,9	29,4
35	48%	77%	0,21	94,86	11%	0,02	9,1	48,8
36	50%	77%	0,22	98,81	11%	0,02	9,1	48,8
37	52%	87%	0,20	90,91	11%	0,02	10,3	68,2
38	60%	87%	0,23	104,90	11%	0,02	10,3	68,2
39	40%	57%	0,24	98,04	12%	0,02	7,3	20,0
40	47%	57%	0,28	115,20	12%	0,02	7,3	20,0
41	44%	67%	0,22	91,67	12%	0,02	8,6	41,2
42	52%	67%	0,26	108,33	12%	0,02	8,6	41,2
43	52%	77%	0,23	94,20	12%	0,02	9,9	62,4
44	54%	77%	0,23	97,83	12%	0,02	9,9	62,4
45	58%	87%	0,22	92,95	12%	0,02	11,2	83,5
46	60%	87%	0,23	96,15	12%	0,02	11,2	83,5

Table 10

The last column of the tab 10 shows the increase in the productivity value related to the standard one used in Prima Industrie that is 6,12 cm³/h.

2.2.4 Tensile Properties

Once the porosity values were obtained, it was also considered to carry out tensile test to verify the actual mechanical properties obtained with the new and more productive process parameters set. Therefore, 2 sets of parameters were chosen to verify the yield and the ultimate tensile strength: the parameters used for the sample number 33, which showed an increase in productivity of 29,41% compared to the standard parameters, and the ones used for specimen 44, which leads to an increase in productivity of 62,35%. The set of parameters of specimen 33 was chosen because it was the specimen with the lowest percentage of porosity. The parameters used for the sample 44, on the other hand, are not those that showed the lowest percentage of porosity, $0,3 \pm 0,07\%$ against $0,18 \pm 0,09\%$ for sample 33. But taking into account both the high increase in productivity and the relatively low percentage of porosity these parameters were found to be an optimal choice. In order to have a comparison, it was also decided to print tensile bars with the standard parameters used by the company.

In the table 11 the parameters used for printing the tensile bar were reported.

sample Number	Laser Power	Scanning Velocity	LED [J/mm]	VED [J/mm ³]	Hatch Distance	Layer Thickness [mm]	Productivity [cm ³ /h]	Increase in productivity [%]
33	40%	67%	0,20	90,9	11%	0,02	7,9	29,4
44	54%	77%	0,23	97,8	12%	0,02	9,9	62,4
standard	39%	57%	0,23	114,7	10%	0,02	6,12	0,00

Table 11

The dimension of these bars were decided on the basis of the standard required for the tensile tests to which they will be subjected (height: 140 mm , diameter: 15 mm). For each set of parameters three bars were created. It was Important to print all the bar in the same direction. That's because the mechanical properties of the bars change along with the direction where they are printed: horizontal or vertical. Usually the inclination in the "xy plane" does not cause discrepancies between the results obtained for the tensile tests. But to avoid problem all the tensile bars of this work were printed with the same angle in the "xy plane". The orientation of a piece of any shapes, as explained in the previous chapters, is very important for successful printing. For example, in this case, considering that the re-coater blade lays the powder in the negative direction of the x-axis, was important to avoid positioning the bars with the long side perpendicular to the direction of movement of the "re-coating blade". The bars in this case were tilted of 3° with respect to the x-axis to prevent them also from being exactly parallel to the direction of movement of the re-coater blade.

In addition, a small area below each bar was supported (in blue in the figure 57) to dissipate stresses and avoid bending. On the right side of the figure 57 the block structure of the supports can be seen from below.

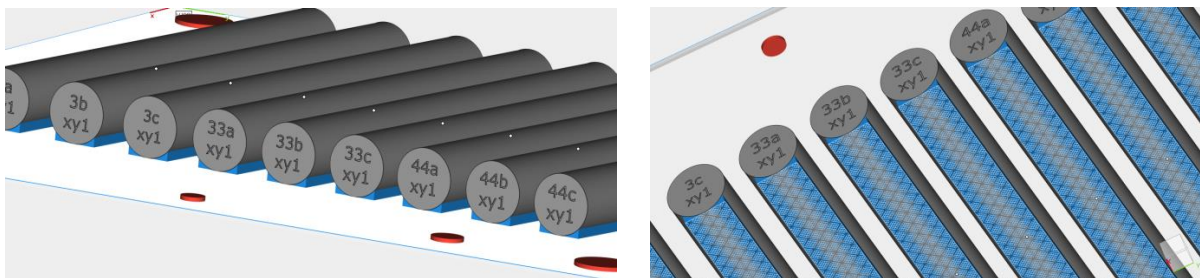


Figure 57) tensile bar prepared using Materialise Magics

For each tensile bar a label was added in order to distinguish them. For each set of parameter as mentioned above 3 tensile bars, respectively called "a", "b" and "c", were chosen to print.

The tensile bars were printed in Prima Industrie plant in Collegno with the PrintSharp 250. Figure 58 shows a photo taken during the printing of the tensile bars and a photo of the building platform once the printing was done. After the bars were detached from the platform by EDM, using a Dremmel the support structures were manually removed as shown in figure 59.

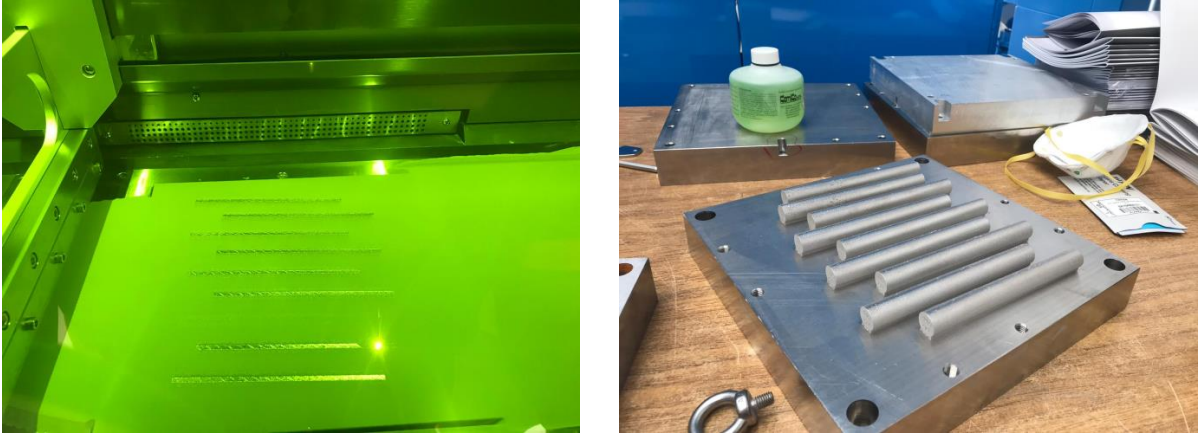


Figure 58) on the left :Tensile bars during the printing, on the right: the building platform after the job was completed



Figure 59) supports removal

2.2.5 Characterization

2.2.5.1 Metallography

2.2.5.1.1 Cutting

With the aim of analyze the density of each sample, the latter were cut by means of a cut-off machine (figure 60) at the laboratories of the DISAT department of the Politecnico di Torino. The blade used was the so called “diamond blade” (figure 61 (1)) running at about 290rpm.



Figure 60) cutting machine with positioning system (1)

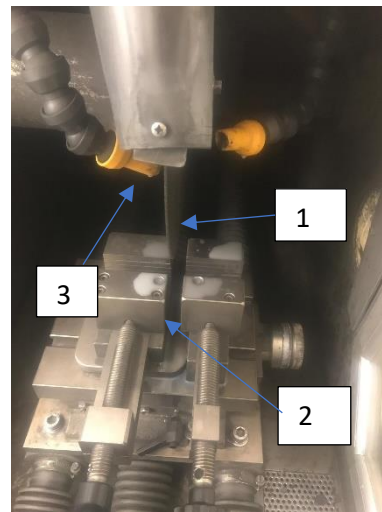


Figure 61) Diamond blade (1), vices (2) and tubes (3)



Figure 62) specimen fixed in the vice

A very important point before starting the cut, is the fixing of the sample to the 2 vices (figure 61(2)) and position it by means of the appropriate positioning system (figure 60 (1)) exactly under the blade to ensure maximum cutting efficiency. In this case the samples were too small to be fixed with both

clamps so only the first one was used to clamp the samples and the second one was used only as a reference point in order to cut them all in the same section (figure 62). In order to avoid overheating, creation of sparks and excessive wear of the blade, two tubes shoot a mixture of water and lubricant on the blade (figure 61(3)). The cutting machine was also equipped with a special hood in order to aspirate the fumes created during the operation of cutting. Once the cutting was complete, the specimens were removed from the clamp. To avoid confusion between the samples, each of them has been marked with its number (figure 63).



Figure 63) sample marked with his number

2.2.5.1.2 Polishing

The sample immediately after the cutting are full of scratches (figure 64). For this reason to analyze the samples it was necessary to polish the surfaces.



Figure 64) specimen after cutting

For this phase was used the polishing machine (figure 65) in the DISAT department at Politecnico di Torino. Six different abrasive papers with increasing level of abrasion were used in succession. Respectively P400 (grain size: 35 μm), P600 (grain size: 25,8 μm), P800 (grain size: 21,8 μm), P1200 (grain size: 15,3 μm), P2400 (grain sizes: 8,4 μm), P4000 (grain size: 5 μm) (figure 67).

The first abrasive paper (600) was placed on the rotating plate of the machine and fixed by means of a special ring (1). Then the polishing machine was switched on, setting a speed of the rotating plate of about 250 rpm using the interface of the machine (2). In order to reduce the friction force that would be created between the sample and the rotating paper, a constant flow of water was directed to the rotating plate through the small tube (3) above the plate. At this point the sample was manually placed in contact with the abrasive paper, trying to maintain a constant pressure during the polishing (figure

66). This procedure was repeated for all the specimens and for each abrasive paper. The purpose of each polishing with different abrasive papers is to completely eliminate the scratches created by the previous papers. For each abrasive paper, the samples have been kept in contact at a different angle so as to make it easier to identify the scratches created by the previous paper. Moreover, between one paper and the next the sample have always been carefully dried with a compressor to avoid any oxidation on the polished surface.

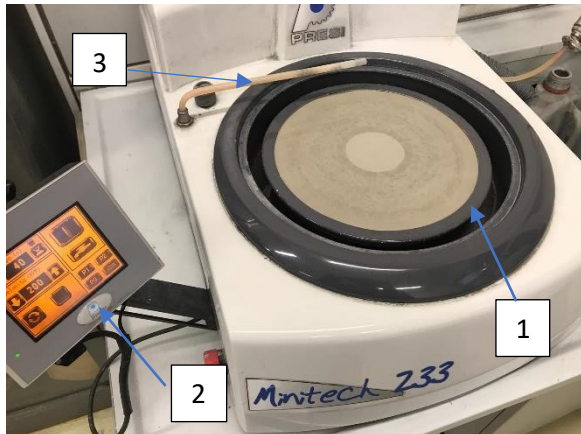


Figure 65) Polishing machine: (1) special ring to fix the paper, (2) small tube, (3) interface of the polishing machine

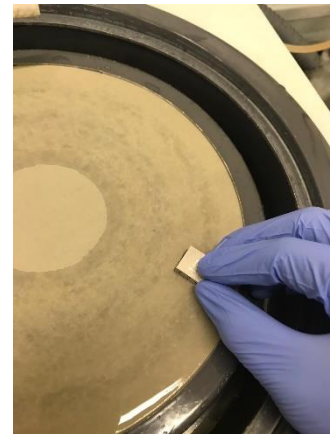


Figure 66) sample held manually in contact with the rotating paper



Figure 67) abrasive papers: P400, P600, P800, P1200, P2400, P4000

After polishing all the samples with all the abrasive papers, to further reduce the depth of the scratches, the same were still polished by the use of two pans (figure 68) fixed to the rotating plate in the same way as the abrasive papers. On the first pan was applied a diamond paste with a grain size of $3\ \mu\text{m}$ (figure 69) and the polishing was done adding lubricant instead of the water to avoid damaging the surface of the pan and decrease the friction's force at the same time. On the second one was placed a diamond past with a grain size of $1\ \mu\text{m}$ (figure 69). After polishing the samples using both pans the surface of the same was carefully washed under running water gently passing a cotton-fioc with a drop of liquid soap (figure 70) to ensure that no particles of the diamond paste remained on the surface. Finally, all the samples were carefully dried using a flow of compressed air to avoid any

phenomenon oxidation or corrosion on the polished surface. The final results of the polished surface is shown in figure 71 .



Figure 68) pans



Figure 69) Diamond stick : 1µm and 3µm



Figure 70) surface cleaned using a drop of liquid soap and a cotton-fioc.



Figure 71) sample after cutting on the left and after polishing on the right

2.2.5.2 Image Analysis

After polishing it was possible to look at the sample's surface under an optical microscope. The optical microscope used for this study is the "LEICA" (figure 72). LEICA is an Optical Microscope with a manual x-y stage and with an objectives from 50x and 1000x. Calibrated imaging can be performed by a black/white camera. The microscope is also interfaced with a software with advanced image processing capability.

The samples were placed on a dedicated plane with the surface to be analyzed facing downwards (figure 73). It was decided to analyze the surface by setting the optical microscope at a zoom of 100x. Thanks to the knobs, it is possible to move the sample in order to see the whole surface of each sample.

Then ten pictures were taken at different points on the surface of each sample as random as possible. The focus of the microscope was adjusted for each picture so that the pores present on the surface were as defined as possible.



Figure 72) Optical Microscope Leica



Figure 73)

As the picture points out, the black dots on white background are the pores present in the section of the material. Thanks to the software it has been possible to measure the percentage of the pores on the surfaces and their size. Adjusting the threshold in such a way as to exclude the wakes of the pores that have been created by polishing (figure 74) and the remaining scratches it was possible to measure the percentage of the shaded areas that represent the pores of the samples. All the picture were collected and analyzed, and for each sample the largest pore present on the surface was identified. The length of this pore was measured and reported on the graph that is presented in the following chapter.



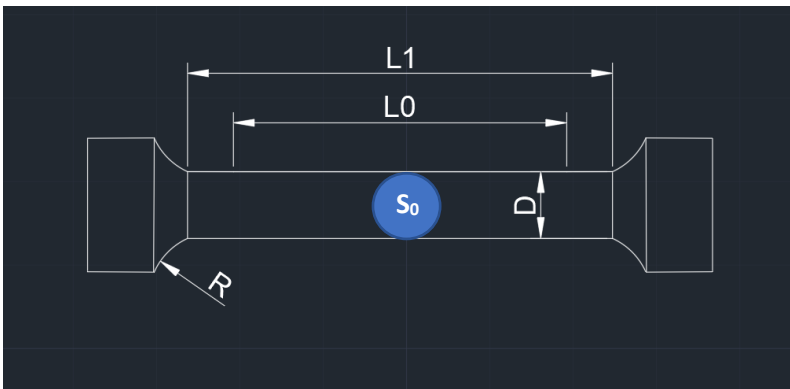
Figure 74) pore's wake created by polishing

All the pictures collected were reported in the APPENDIX B.

2.2.5.3 Mechanical testing

2.2.5.3.1 Tensile Test

All the nine tensile bars were sent to the laboratories of Politecnico di Torino in Alessandria to be subjected to tensile test. Before the tensile test, the bars were machined with the aim to have the dimension reported in figure 75. Subsequently the tensile test was performed with the "Zwisch-Roell BT1-FR100" figure 76.



Symbol	
L_1 (mm)	40
L_0 (mm)	51
D (mm)	8
S_0 (mm ²)	50,26
R (mm)	8

Figure 75) dimensions of machined bars



Figure 76) Zwisch-Roell BT1-FR100

Thanks to the tensile test the Ultimate Tensile Strength (UTS) and the Yield Strength (YS) were computed and reported in the chapters below.

2.2.5.3.2 Microhardness

Among all the cubic samples produced, those printed with the two most promising sets of parameters were selected to be subjected to microhardness test. For comparison, the same test was also carried out on the sample printed with the standard set of parameters used in Prima Industrie. (Figure 77).

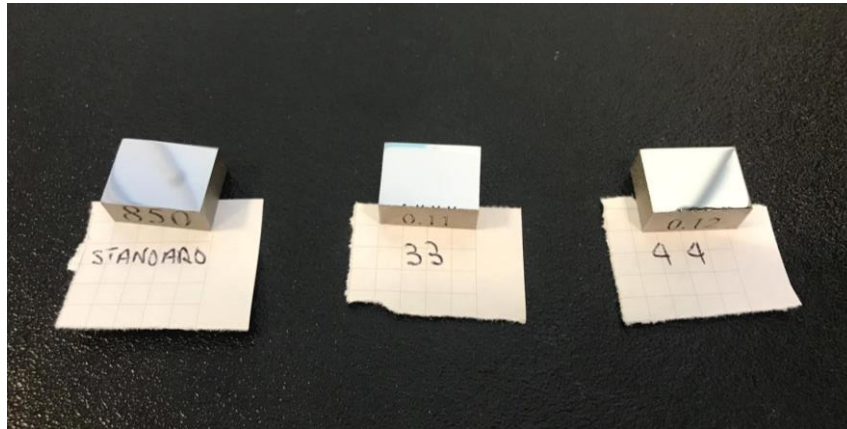


Figure 77

The selected samples were brought to the laboratories of the Politecnico di Torino in Alessandria to be tested. The microhardness was computed with the machine "LEICA VMHT" in figure 78 using the Vickers method in five randomly chosen point on the polished surface of each sample in order to have a more reliable value. This method uses a pyramidal tip that is pressed against the surface with certain load for a time interval usually between 10 and 15 seconds. Once the tip has been removed, it leaves a mark on the surface as shown in the figure 79.



Figure 78) Leica VMHT

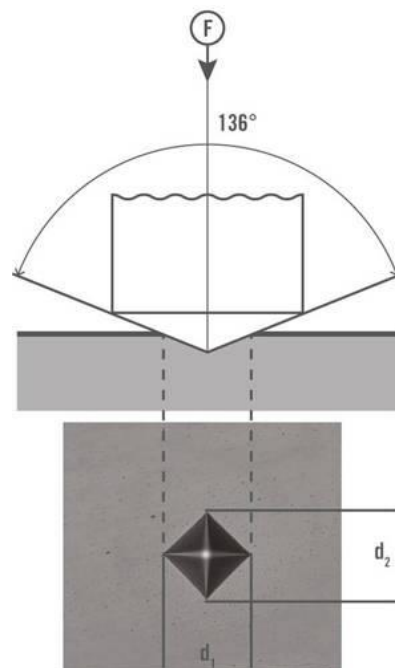


Figure 79) Vickers Hardness test [51]

Measuring the two diagonal of the imprint and knowing the load used, the microhardness can be calculated as:

$$HV = constant * \frac{\text{test force } F}{\text{surface of the indentation}} = 0,102 * \frac{2 * F * \sin \frac{136^\circ}{2}}{d^2} = 0,1891 * \frac{F}{d^2}$$

$$d = \text{average diagonal lenght} = \frac{d_1 + d_2}{2}$$

Before starting to record the data, the different possible loads that can be used for the test were evaluated analyzing the shape of the imprint left by the tip. At the end of the evaluation, it was considered appropriate to use a load of 300gf maintained for 15 seconds. This amount is the one that left the most regular trace on the surface of the sample. Moreover the size of the diagonals measured were all between 30 μm and 50 μm .

3 Results & Discussion

3.1 First DoE

The data collected concerning the calculation of the porosity values were reported in table 12. As can be seen, ten values of porosity for each sample are reported in the table. Each value represents the percentage of porosity in one of the ten randomly taken photos along the polished surface of the specimen.

Sample Number	Image Analysis porosity [%]									
	1	2	3	4	5	6	7	8	9	10
1	0,045	0,058	0,392	0,395	0,334	0,408	0,154	0,207	0,367	0,120
2	0,923	0,788	0,841	0,825	0,857	0,896	0,953	1,343	0,900	1,085
3	0,309	0,239	0,357	0,217	0,250	0,331	0,249	0,218	0,189	0,222
4	0,169	0,167	0,257	0,189	0,190	0,185	0,212	0,237	0,244	0,199
5	0,441	0,431	0,460	0,374	0,260	0,387	0,390	1,001	0,321	0,423
6	0,088	0,094	0,121	0,130	0,184	0,116	0,152	0,170	0,129	0,148
7	0,128	0,160	0,173	0,283	0,133	0,305	0,116	0,322	0,178	0,248
8	0,213	0,082	0,118	0,154	0,301	0,074	0,237	0,105	0,132	0,164
9	0,130	0,255	0,209	0,152	0,713	0,154	0,615	0,194	0,145	0,195
10	0,127	0,061	0,191	0,097	0,201	0,184	0,193	0,130	0,193	0,075
11	0,125	0,561	0,338	0,672	0,384	0,655	0,200	0,169	0,277	0,176
12	0,209	0,052	0,089	0,105	0,183	0,069	0,243	0,172	0,165	0,078
13	0,108	0,139	0,434	0,046	0,117	0,126	0,085	0,063	0,043	0,033
14	0,061	0,044	0,081	0,073	0,085	0,081	0,062	0,089	0,091	0,115
15	0,181	0,140	0,110	0,072	0,109	0,114	0,067	0,063	0,122	0,152
16	0,041	0,031	0,045	0,043	0,046	0,041	0,081	0,103	0,043	0,065
17	0,122	0,167	0,263	0,171	0,207	0,138	0,114	0,091	0,082	0,118
18	0,666	0,186	0,492	2,576	0,815	3,721	0,793	0,386	1,371	0,106
19	0,788	0,282	1,303	1,123	0,372	0,519	0,447	0,648	0,833	0,651
20	0,099	0,082	0,085	0,121	0,065	0,075	0,079	0,083	0,137	0,097

Table 12

The average porosity, the average density and the standard deviation were subsequently calculated with the followings formulas:

$$\mu [\%] = \frac{\sum_{i=1}^N x_i}{N}$$

$$d[\%] = 100 - \mu$$

$$\sigma = \sqrt{\sum_{i=1}^N \frac{(x_i - \mu)^2}{N}}$$

Where:

μ = average value of porosity [%]

d = Average Density [%]

σ = deviation standard

x_i = porosity percentage in the i^{th} photo

N = total number of pictures taken for each sample = 10

The values obtained are reported in the table 13 together with the maximum dimension of the biggest pore measured in each sample. The two specimens that gave the best and the worst results are respectively highlighted in green and red.

Sample Number	Energy density [J/mm ³]	Density min [%]	Density max [%]	Average Porosity [%]	Standard Deviation σ	Average density [%]	Maximum Porosity Dimension [μ m]
1	75,0	99,59	99,96	0,25	0,15	99,75	29,47
2	107,5	98,66	99,21	0,94	0,16	99,06	20,69
3	114,7	99,64	99,81	0,26	0,06	99,74	15,25
4	84,8	99,74	99,83	0,20	0,03	99,80	22,65
5	82,7	99,00	99,74	0,45	0,20	99,55	28,31
6	93,5	99,82	99,91	0,13	0,03	99,87	16,66
7	126,5	99,68	99,88	0,20	0,08	99,80	21,42
8	97,5	99,70	99,93	0,16	0,07	99,84	30,02
9	58,7	99,29	99,87	0,28	0,21	99,72	69,75
10	77,5	99,80	99,94	0,15	0,05	99,85	40,69
11	67,4	99,33	99,88	0,36	0,21	99,64	78,42
12	76,1	99,76	99,95	0,14	0,07	99,86	37,43
13	67,5	99,57	99,97	0,12	0,12	99,88	105,32
14	87,5	99,89	99,96	0,08	0,02	99,92	50,18
15	79,4	99,82	99,94	0,11	0,04	99,89	29,91
16	102,9	99,90	99,97	0,05	0,02	99,95	22,00
17	91,2	99,74	99,92	0,15	0,06	99,85	19,91
18	51,9	96,28	99,89	1,11	0,58	98,89	122,14
19	59,6	98,70	99,72	0,70	0,33	99,30	111,41
20	67,3	99,86	99,94	0,09	0,02	99,91	21,02

Table 13

To better visualize and understand the meaning of the results obtained in the first Design Of Experiment these data were represented in graphs. The graph in figure 80 shows the porosity trend as a function of the Volumetric Energy Density Value of the respective samples. To visualize this trend for the samples number 18, 11, 16 and 3, respectively characterized by a VED of 51.9, 67.4, 102.9 and 114.7 J/mm³, one of the ten captured images was also reported. Tracing the trend line we can see that the average porosity show a parabolic trend.

Specimens printed using an energy density below 60 J/mm³ showed in fact a high percentage of porosity. The worst case was the sample number 18 with a porosity value of 1,11 ± 0,58 % and a density of 98,89 %. On the other hand, printed specimens with a Volumetric Energy Density between 85 and 110 J/mm³ showed an almost constant trend in the porosity percentage with values below 0,3%. The only exception in this range was the sample number 2 (VED = 107,5 J/mm³) which showed an unexpected porosity value of 0,9 ± 0,16 %. The sample number 16 (VED=102,9 J/mm³) was the one that highlighted the best result in terms of porosity with a value of 0,05 ± 0,02 %. Finally the samples with a value of VED above 105 J/mm³ show again a slight increase in porosity percentage.

Considering this parabolic trend, the range of Volumetric Energy Density with the most promising characteristics in terms of porosity was between 85 J/mm³ and 115 J/mm³. This windows of VED values were subsequently used both for repeatability test and for the second DoE.

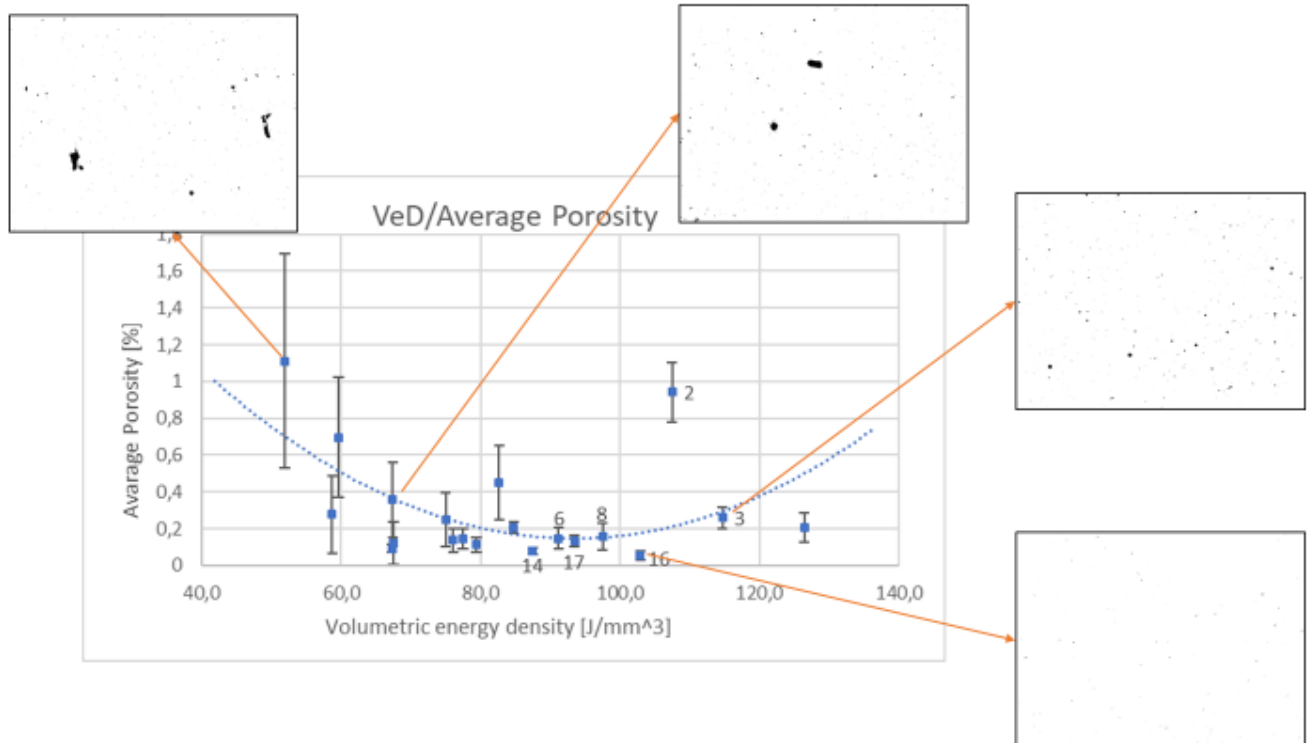


Figure 80

The graph in figure 81 shows the porosity percentage as a function of Linear Energy Density. By modifying, in this first DoE, only the laser power and scanning speed values, LED and VED values remain equal except for one constant.

$$VED = \frac{1}{\text{hatching distance} * \text{layer thickness}} * LED$$

For this reason the trend of the porosity percentage as a function of LED matches exactly with the trend of porosity in the graph presented in figure 80. The same observations ,therefore, also apply to this graph.

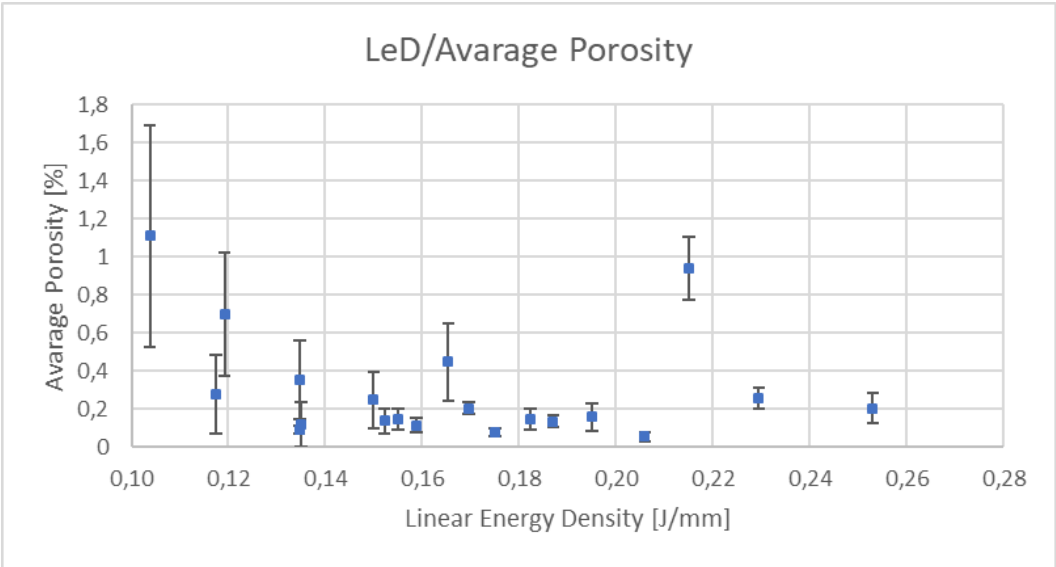


Figure 81

Finally the graph in figure 82 shows the max porosity dimension measured for each samples as a function of the Volumetric Energy Density. The images were added with the aim of highlighting not only the dimension of the pores but also the shape. Three images were chosen to represent respectively the shapes of the pores in the three different zones of the graph: the first among the low VED samples (below 60 J/mm³), the second among the samples with intermediate VED value (between 60 and 105 J/mm³) and the third for the high VED samples (above 105 J/mm³). In the first area, a high number of pores with large size and very irregular shapes were found. This form was probably due to a lack of volumetric energy density that affected the powder bed. The low amount of energy used to print the samples wasn't able to melt all the powder particles creating these big irregular pores into the samples. In the second area it was seen that the number and the size of pores decreased, and the shapes of them began to regularize and to resemble more and more to a circle. This second area is, in fact, the one that showed the best results in terms of average porosity percentage as can be seen looking at the previous graph. In the last area, the shape of the pores became circular and smaller but the number of them increased significantly. The perfect circular shape of the pores means that some alloys remained trapped in form of gas: some elements probably started to evaporate without having enough time to go out. This process led to the creation of a large amount of small circular pores into the samples.

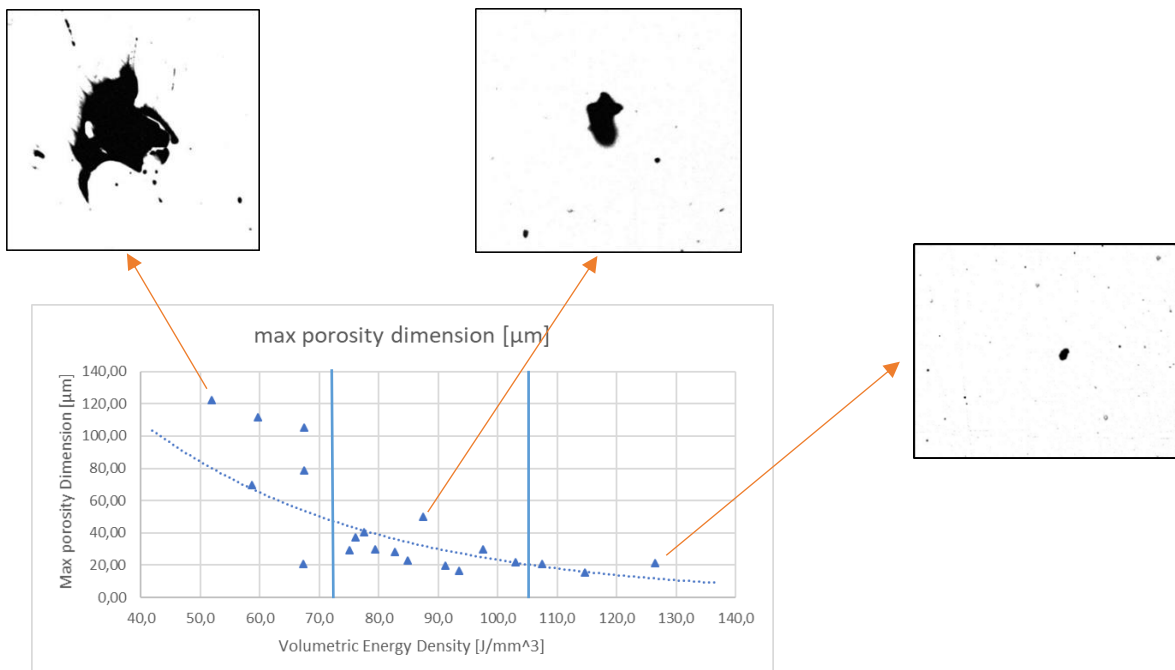


Figure 82

3.2 Repeatability Test

In the table 14 all the porosity value measured in the photos for each of the seven sample were reported.

Sample Number	image									
	1	2	3	4	5	6	7	8	9	10
27	0,112	0,095	0,194	0,159	0,163	0,338	0,161	0,117	0,156	0,128
22	0,170	0,167	0,209	0,136	0,150	0,178	0,198	0,176	0,165	0,135
25	0,204	0,167	0,221	0,259	0,175	0,123	0,092	0,109	0,198	0,136
23	0,229	0,198	0,199	0,184	0,209	0,149	0,165	0,115	0,174	0,097
21	0,363	0,258	0,288	0,308	0,320	0,285	0,311	0,323	0,294	0,321
26	0,197	0,170	0,197	0,161	0,193	0,173	0,178	0,169	0,171	0,178
24	0,191	0,193	0,140	0,157	0,144	0,131	0,120	0,142	0,148	0,167

Table 14

Starting from this data the average porosity, the standard deviation and the density of each sample were extracted (tab 15).

Sample Number	Average porosity [%]	Density max [%]	Density min [%]	Average Density [%]	Standard Deviation σ	Max porosity Dimension [μm]
21	0,307	99,74	99,64	99,69	0,03	10,548
22	0,168	99,87	99,79	99,83	0,02	13,852
23	0,172	99,90	99,77	99,83	0,04	13,351
24	0,153	99,88	99,81	99,85	0,02	30,306
25	0,168	99,91	99,74	99,83	0,05	18,239
26	0,179	99,84	99,80	99,82	0,01	12,830
27	0,162	99,91	99,66	99,84	0,07	13,647

Table 15

To interpret the collected data, the following graphs may help. The first two graph, figure 83 and figure 84, show the porosity trend as a function of the Volumetric Energy Density and Linear Energy Density respectively. In addition, in both of them, the porosity values found in the first DoE were added in order to compare the results. The figure clearly confirms the high repeatability of the process, as the samples showed almost the same level of porosity in two different jobs.

The only exception is represented by the sample number 26 printed with a VED of 107,5 J/mm³ that has a porosity value much lower than its counterpart of the first DoE (sample number 2). In fact, sample

number 26 is characterized by a porosity of $0,179\% \pm 0,01\%$, while sample 2 by a porosity of $0,941\% \pm 0,16\%$. The anomalous porosity found in the specimen 2 it is probably the consequence of an experimental error and may be related to the position of the specimen in the job or to the presence of other pieces in the building platform that causes some defects into the sample. In almost all cases, as we can see, the porosity found into the samples of the first DoE was less than the one in the samples of the second print. This is probably due to the fact that between the first job and the second one the powder was used several time. On this subject there are some case studies in literature that showed how the reuse of the powders increases their oxygen content. The higher percentage of oxygen can leads to the formation of more pores in the printed parts [50].

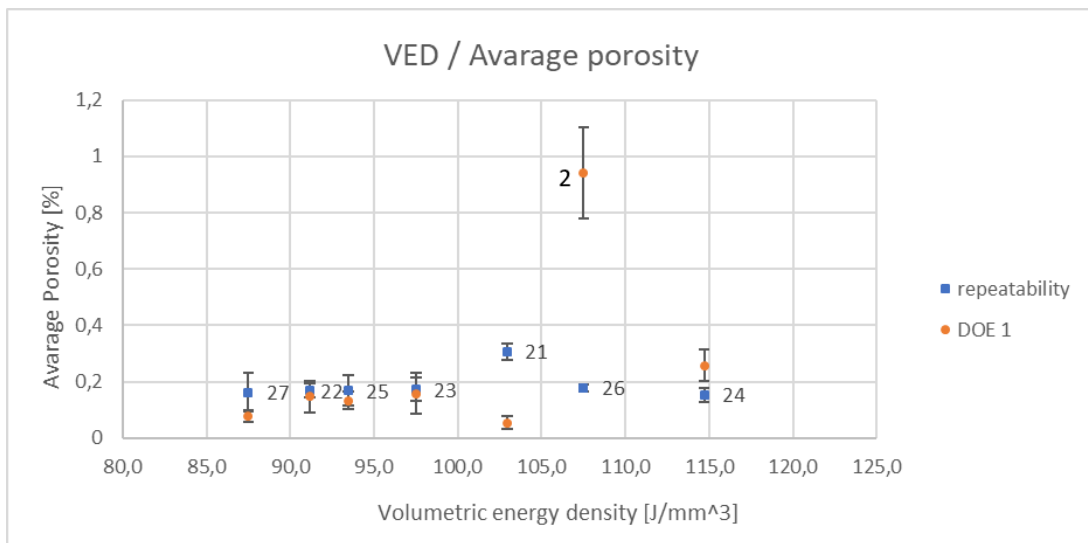


Figure 83

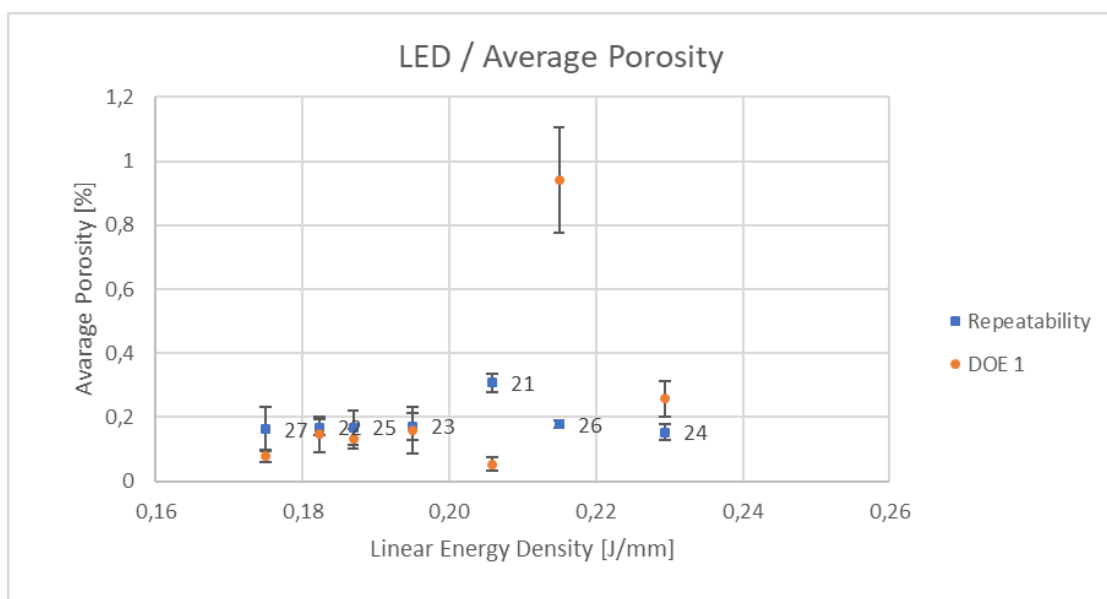


Figure 84

The graph in figure 85 represents the trend of the maximum porosity dimension found in the samples as a function of the Volumetric Energy Density. What can be seen is that the size of the largest pores of each specimen seems to be consistent with the size found in the first DoE maintaining a maximum size between 10 μm and 35 μm . In addition, the shape of the largest pores was also consistent with those of the first DoE. Almost all of them showed a circular shape and they didn't present irregular and serrated shapes. Table 16 shows one representative picture for each sample.

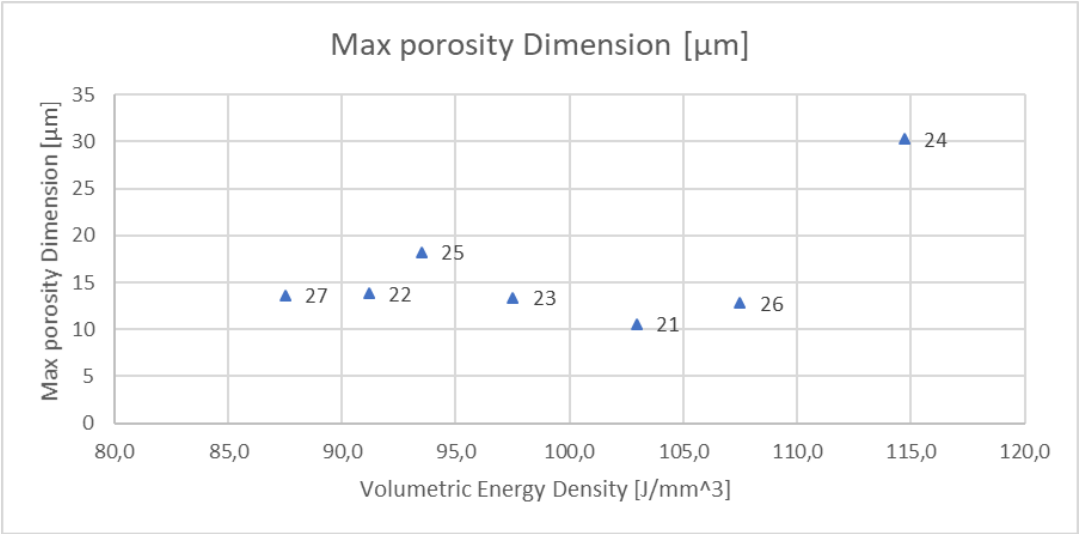


Figure 85

21	22	23	24
25	26	27	

Table 16

3.3 Second DoE

The data measured concerning the porosity analysis of the samples are reported in table 17.

Sample Number	image									
	1	2	3	4	5	6	7	8	9	10
31	0,403	0,123	0,124	0,115	0,664	0,121	0,102	0,291	0,296	0,175
32	0,119	0,151	0,176	0,287	0,327	0,217	0,191	0,177	0,128	0,399
33	0,204	0,199	0,200	0,196	0,320	0,084	0,303	0,108	0,130	0,144
34	0,601	0,730	0,625	0,430	0,510	0,478	0,528	0,528	0,491	0,351
35	0,242	0,355	0,323	0,273	0,178	0,326	0,454	0,251	0,282	0,419
36	0,358	0,345	0,533	0,357	0,235	0,700	0,460	0,328	0,300	0,288
37	0,370	0,263	0,234	0,536	0,172	0,181	0,314	0,503	0,352	0,320
38	0,403	0,380	0,531	0,590	0,420	0,460	0,430	0,450	0,432	0,443
39	0,391	0,405	0,319	0,259	0,325	0,576	0,415	0,413	0,368	0,474
40	0,220	0,225	0,191	0,266	0,278	0,374	0,194	0,270	0,156	0,168
41	0,361	0,281	0,247	0,263	0,356	0,279	0,284	0,172	0,228	0,437
42	0,200	0,253	0,244	0,412	0,338	0,197	0,237	0,126	0,235	0,195
43	0,537	0,492	0,537	0,555	0,592	0,368	0,403	0,375	0,328	0,429
44	0,263	0,474	0,250	0,358	0,284	0,346	0,197	0,285	0,328	0,286
45	1,042	0,793	0,746	1,247	0,475	0,822	0,514	0,711	0,485	0,586
46	0,525	0,492	0,589	0,593	0,523	0,774	0,554	0,431	0,633	0,556

Table 17

Manipulating the collected data as in the two previous cases, it was possible to calculate: the average and maximum porosity, the minimum and maximum density, the average density and the standard deviation of each sample (table 18).

Sample Number	Volumetric Energy Density [J/mm ³]	Average Porosity [%]	Deviation Standard σ	Max Density [%]	Min Density [%]	Average Density [%]	Max Porosity Dimension [μm]
31	93,6	0,2414	0,180204	99,898	99,336	99,7586	23,13
32	104,3	0,2172	0,09187	99,881	99,601	99,7828	46,691
33	90,9	0,1888	0,077276	99,916	99,680	99,8112	43,363
34	109,1	0,5272	0,105757	99,649	99,270	99,4728	12,797
35	94,9	0,3103	0,083499	99,822	99,546	99,6897	23,423
36	98,8	0,3904	0,138226	99,765	99,300	99,6096	18,145
37	90,9	0,3245	0,122643	99,828	99,464	99,6755	21,745
38	104,9	0,4539	0,062264	99,62	99,410	99,5461	45,904
39	98,0	0,3945	0,088028	99,741	99,424	99,6055	53,275
40	115,2	0,2342	0,064997	99,844	99,626	99,7658	82,877
41	91,7	0,2908	0,075707	99,828	99,563	99,7092	46,991
42	108,3	0,2437	0,080097	99,874	99,588	99,7563	35,738

43	94,2	0,4616	0,092273	99,672	99,408	99,5384	86,043
44	97,8	0,3071	0,075418	99,803	99,526	99,6929	53,541
45	92,9	0,7421	0,251365	99,525	98,753	99,2579	127,67
46	96,2	0,567	0,092181	99,569	99,226	99,433	38,432

Table 18

The two specimens that gave the best and the worst results respectively are highlighted in green and red. To make the analysis of the results obtained more understandable, they are translated into graphs. The graph in figure 86 reports the trend of the average porosity as a function of the volumetric energy density. The graph in figure 87 presents the trend of porosity as a function of linear energy density. From neither of the two graphs, however, it was possible to identify a clear trend in the porosity value as a function of energy density in the window of chosen VED. The specimen that shows the best characteristics in terms of porosity is the specimen number 33 printed using a VED value of 90,9 J/mm³. The worst case was found to be the specimen number 45 printed with a VED value of 92,9 J/mm³. The measured standard deviation for each test specimen was found to be quite low despite a significant increase in productivity (with the exception of test specimen number 45 that shows an average porosity value of 0,742 ± 0,25%).

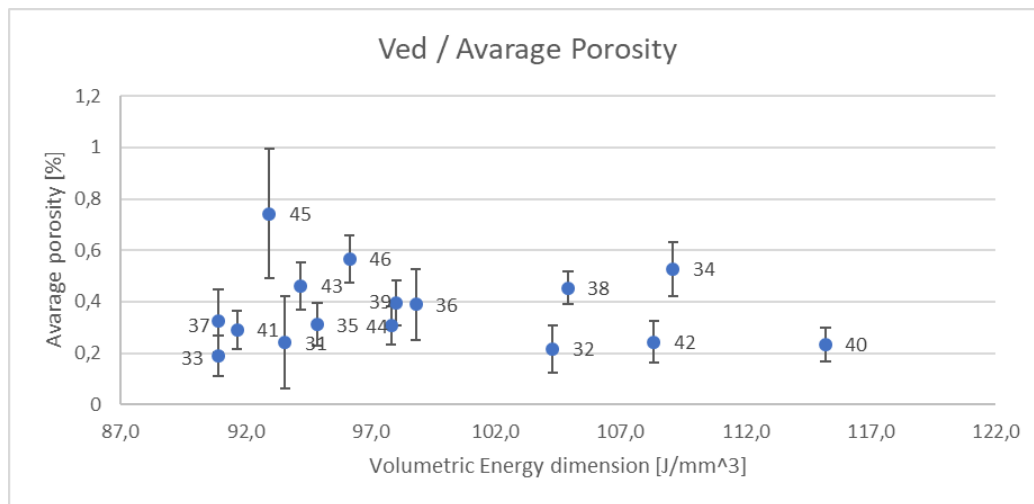


Figure 86

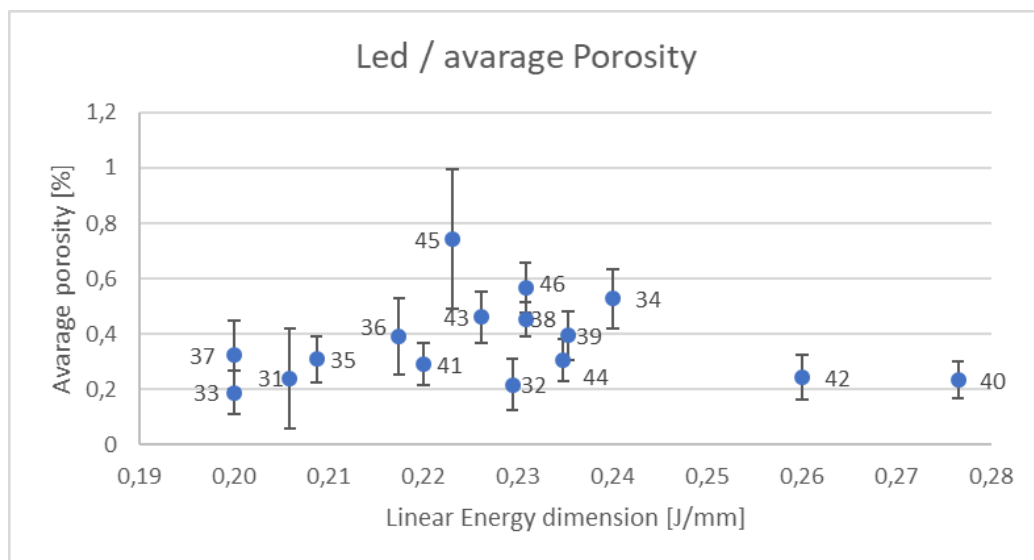


Figure 87

The graph in figure 88 shows the trend of the maximum pore dimension found in the surface of each sample as a function of volumetric energy density. In most of the sample it was noted that the pore with the largest dimension had an irregular shape with jagged edges. This could be a consequence of the increased productivity of the parameters used to print the samples. Around the graph there are three images of the measured pores. In the specimen number 45 we measured the largest pore with a length of 127,67 μm .

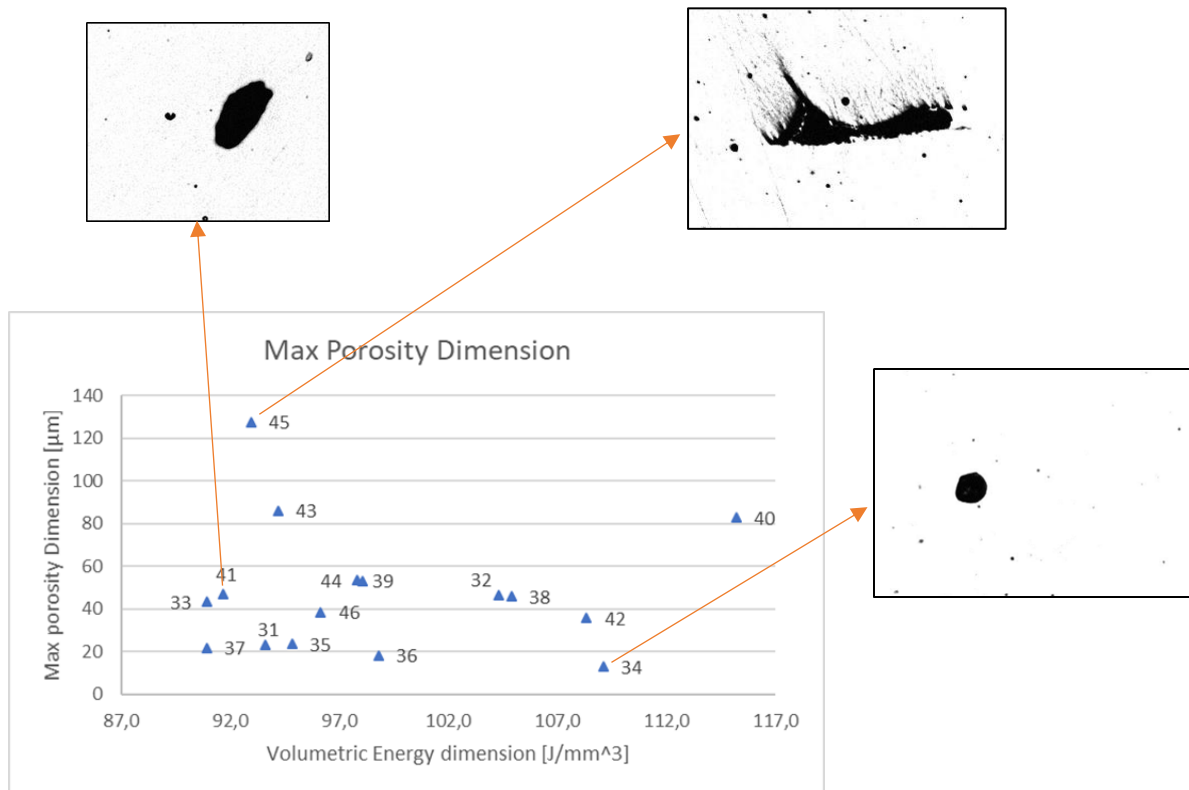


Figure 88

To understand the trend of the porosity found in the samples, the obtained values were plotted as a function of productivity in figure 89. Thanks to this graph, it immediately emerged that the porosity found in the samples had a linear trend depending on the productivity. To display this trend, three images were added. The first for the sample number 31 to represent the ones with the lower values of productivity, the second for the sample number 36 to represent those with an intermediate productivity value and the third one for the sample number 45 to represents the one with the highest productivity value. As two samples were printed for each productivity value, it was seen that an higher VED doesn't necessarily means a lower porosity percentage despite the irregular shape of the pores shown in the graph 84 may suggest a lack of energy density.

Comparing the results with the standard parameters, it was seen that it is possible to print with a productivity greater than 29% and obtain the same porosity value, less than 0,2%, in the sample as the sample number 33 showed. Another specimen that has given excellent results considering both productivity and porosity it the sample number 44. This sample showed in fact a value of porosity

relatively low ($0,31 \pm 0,07 \%$) considering the increase of productivity of 62,35% with respect to the standard.

These are the reasons why the sets of optimized parameters used to print the sample number 33 and the sample number 44 were selected to find the achievable mechanical properties. We are confident that they can constitute a sustainable starting point for the printing process of Inconel718 fabricated by Additive Manufacturing in Prima Industrie Spa.

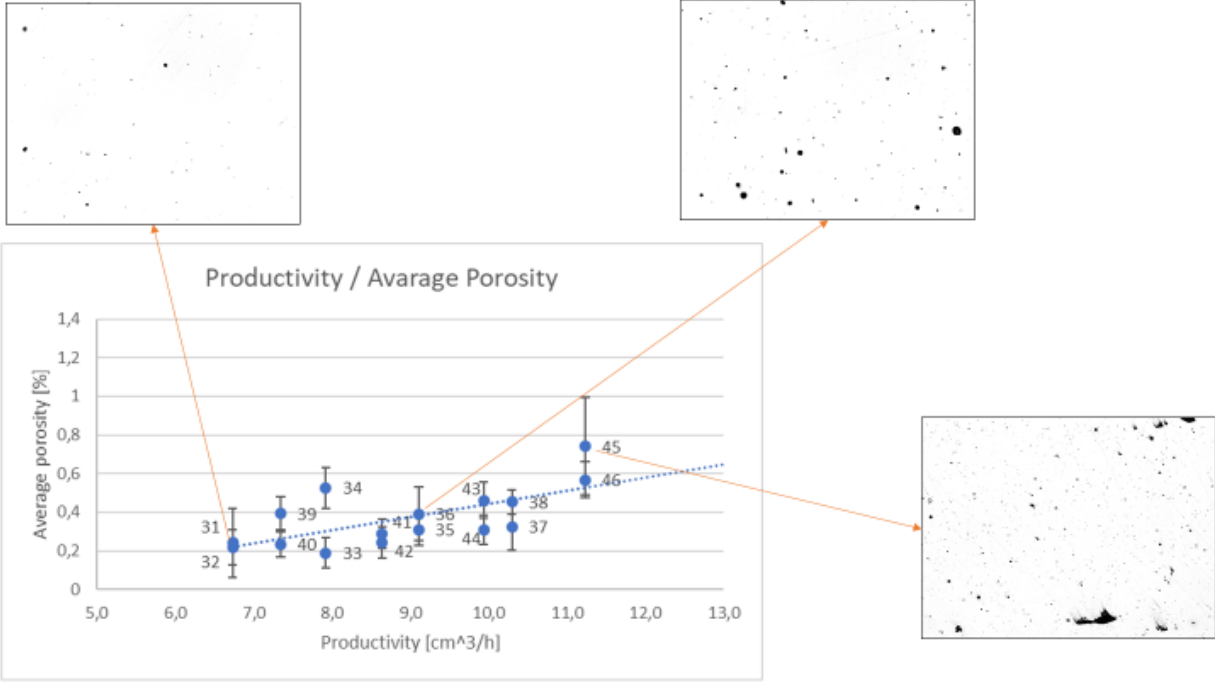


Figure 89

3.4 Tensile Test

Unfortunately it was not possible to have the results of the tensile test because the lathes to machine the samples in the laboratories of Politecnico in Alessandria is broken. As soon as possible the data will be updated.

3.5 Microhardness

All the data collected during the microhardness test were reported in the table 19. The medium value and the standard deviation of the data were reported in table 20.

		test 1	test 2	test 3	test 4	test 5
3	d1 [μm]	37,6	35,8	36,4	35,8	38,9
	d2 [μm]	35,5	36,6	36,4	38	39,7
	HV	400	425,2	420	408,8	360,7
33	d1 [μm]	39	38,9	38,7	37	37,1
	d2 [μm]	38,6	39,7	38,6	38,1	37,4
	HV	369,3	369,7	372,7	394	401
44	d1 [μm]	39,9	41,1	42,3	40,2	41,1
	d2 [μm]	40,1	40,9	40,7	39,5	42
	HV	348,2	330,7	323,5	350,9	322,3

Table 19

	HV	st dev	Decrease [%]
3	402,9	25,6	0
33	381,4	15,1	5,4
44	335,1	13,6	16,8

Table 20

The data found were plotted to analyze the result in figure 90.

The sample printed with the standard set of parameters showed a microhardness of $402,9 \pm 25,6$ HV. The sample printed with the optimized set of parameter number 33 showed a slightly lower value than the standard one despite the percentage of porosity of those two sample is very similar. The last sample instead, with a microhardness of $335,1 \pm 13,6$ HV, showed a decrease of 16,8% as a consequence of higher percentage of porosity.

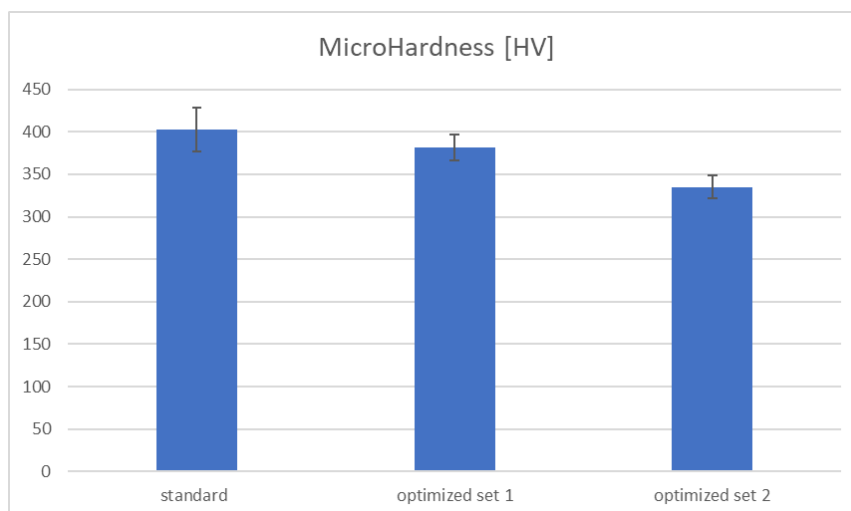


Figure 90

4 Case Of study

In order to show the advantages of the most productive set of parameters a complex commercial piece (figure 91) was analyzed in 3 different production conditions: the first using the standard set parameters in use at Prima Additive, the second using the optimized set of parameters number 33 and the third one using the optimized set of parameters number 44. This commercial part is not a piece intended for production; it has the function of highlighting all the possible structures that can be created with the additive manufacturing machines, such as the small holes on the top (1) or the thin wall at the base (2) or the lattice internal structure (3) or the little tubes with an internal diameter of 1,5 mm that grows in the shape of a spiral entering and leaving the main body of the piece (4). This part was chosen because, being self-supported, it is a very good example for evaluating the production time. Table 21 reports the volume and the height of the commercial part.

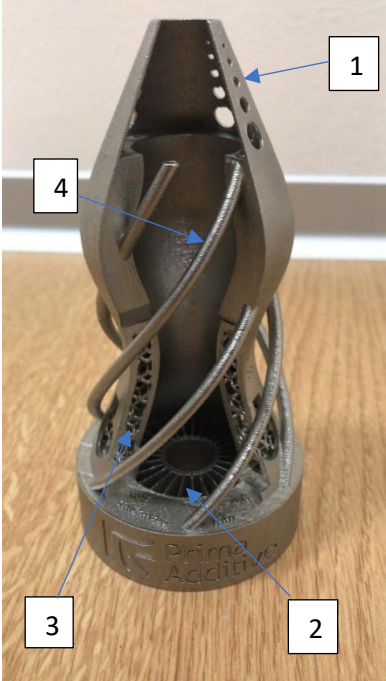


Figure 91) Commercial piece of Prima Additive

Volume [cm ³]	Heigh [cm]	Total number of layer at 20 μm
78	12,1	6054

Table 21

The value of productivity reported in this thesis project are only theoretical since they do not consider the time required by the re-coater to lay a new layer of powder. This movement, in the Printsharp 250 used for this work, takes 12 seconds for each layer. Table 22 reports the data concerning the real production time required by the 3 identical commercial pieces under 3 respective process conditions.

	Productivity [cm³/h]	Total recoating time [h]	Production time [h]	Total time [h]
Standard parameters	6,12	20,18	12,7	32,9
Optimized parameters 1	7,9	20,18	9,9	30,1
Optimized parameters 2	9,9	20,18	7,9	28,1

Table 22

The total recoating time and the production time were computed with the formulas:

$$\text{Total Recoating Time [s]} = \text{number of layers} * \text{recoating time [s]}$$

$$\text{Production time [s]} = \frac{\text{volume of part [cm}^3\text{]}}{\text{productivity [}\frac{\text{cm}^3\text{]}{\text{s}}\text{]}}$$

The total time required to produce one commercial piece in one job with the standard parameters is 33 hours. Using the optimized set of parameters 1 is possible to print the same part in 30 hours, reducing the working hours of the machine of 8,7%. The second set of optimized parameters, on the other hand, leads to a reduction of the working hours of 14,8%, producing the part in 28 hours.

The use of optimized parameters not only leads to time advantages, but also to cost savings. The two things are interrelated because reducing machine working hours means reducing the costs of the entire process. In addition, it is possible to increase even more the savings for each job by printing more than one commercial piece in the same job. Is indeed possible to place up to ten commercial pieces on the same building platform. In table 23 are reported the costs of the jobs with 1 and 10 pieces for the 3 sets of parameters.

	Number of part per job	Working hours [h]	Cost of the job [€]	Cost per part [€]	Savings per job [€]	Savings [%]
Standard parameters	1	33	801	801	-	-
	10	148	3717,1	371,7	-	-
Optimized parameters 1	1	30	741,7	741,7	59,4	7,4%
	10	119	3123,3	312,32	593,6	16,0%
Optimized parameters 2	1	28	700,4	700,4	100,6	12,6%
	10	99	2710,8	271,1	1006,4	27,1%

Table 23

The cost of the job was computed with the formula:

$$\mathbf{Cost\ of\ the\ job\ [€]=}$$

$$\mathbf{material\ cost[€] + total\ gas\ cost[€] + machine\ operation\ cost[€] + electricity\ cost\ [€]}$$

$$\mathbf{material\ cost\ [€] = m * lp * cpk}$$

$$\mathbf{total\ gas\ cost\ [€] = wh * g * GVP + * g * GVC}$$

$$\mathbf{electricity\ cost\ [€] = wh * econ * ecost}$$

$$\mathbf{machine\ operation\ cost\ [€] = wh * hourly\ cost\ of\ the\ machine}$$

Where:

\mathbf{m} = mass of the part [g]

\mathbf{lp} = loss powder factor = 1,5

\mathbf{cpk} = cost of the powder per kilogram $\left[\frac{€}{g}\right]$

\mathbf{wh} = working hours of the process [h] = total time required

\mathbf{g} = gas cost per m^3 $\left[\frac{€}{m^3}\right]$

\mathbf{GVP} = gas volume required by process $\left[\frac{m^3}{h}\right]$

\mathbf{GVC} = gas volume to fullfill the working chamber [m^3]

\mathbf{econ} = energy consumed [kW]

\mathbf{ecost} = electricity cost [€/kWh]

As the table 20 shows, using the optimized parameter 1, it is possible to save about the 7,4 % printing only 1 commercial piece per job, while, printing 10 parts in one job, it is possible to save about 16,0 % (594 €) per job. Using the optimized set of parameters 2, otherwise, it is possible to save up to 27,1% (1006 €) printing ten part in the same job.

5 Conclusion & Future works

The results of this thesis project show that using the Printsharp 250 it is possible to increase productivity on one hand and maintain an acceptable percentage of porosity in the components produced by SLM on the other hand.

The two best sets of parameters chosen, according to the second DoE, were the number 33, with a volumetric energy density of 90,9 J/mm³, and the number 44, with a volumetric energy density of 97,8 J/mm³. The first set, which showed a percentage porosity of 0,19%, had a productivity of 7,9 cm³/h, which corresponded to an increase over the standard of 29,41%. The second set, with a percentage porosity of 0,3%, had a productivity of 9,9 cm³/h, which corresponded to an increase of 62,4% compared to the standard parameters. Both sets of parameters could be an excellent choice from the point of view of productivity so far. But it is also necessary to consider the increase in porosity involved and their effect on the mechanical properties. Set number 33 generated an increase in porosity of 0,04% compared to the standard. However, this difference in porosity seemed to have a relatively low effect on the hardness showing a decrease of 5,4% with respect to the standard. Consequently, parameter set 33 could be an optimum candidate to replace the standard parameters used so far. In the case of set number 44 the increase in porosity (+0,15%) affected the hardness of the component more significantly, decreasing the value of 16,8% with respect to the standard.

In conclusion, we can affirm that it is possible to obtain a component with good mechanical properties using parameter set number 33, which allows an increase in productivity of 29,4%. The further increase in productivity, through the use of parameter set number 44, leads to an increase in porosity and a worsening in the mechanical properties of the products. But this does not preclude the use of parameter set 44 which can be used to speed up the production of applications which do not require high mechanical properties. As pointed out in the case study in fact, the increase in productivity of the parameters set number 44 can lead to great advantages both in terms of time and in terms of cost. Using this set of parameters is in fact possible to save up to 1000€ per job (for the case taken into account in chapter 4).

Further analysis could be developed by considering other parameter combinations within the same VED value window used in this thesis project. In particular, it would be interesting to verify whether they are repeatable and whether it is possible to further increase productivity while keeping porosity below the 0,2% level.

Moreover, this thesis project did not consider the influence of the positioning of the samples within the work platform and the presence of other components on it. Expanding the analysis to include these variables and verify their influence on the results obtained could improve production performance.

A possible cause of error in the data reported in this thesis could be the degradation of powder. Studies [50] showed that the percentage of oxygen present in the powder increases linearly with the number of processes to which this powder is subjected to. It was also verified that this increase in the percentage of oxygen in the powder also affected the final mechanical properties of the component. In the case of this thesis project, for business and cost reasons, it was not possible to use new powder for each print. In fact, the powder has been subjected to many SLM processes before and during the printing of the samples and the bars. This may have affected the results obtained in terms of porosity and mechanical properties. It would be appropriate to re-test the best samples by printing them with virgin powder.

During this project we only worked on process parameters but there are a lot of things that can be done to increase the productivity of the SLM process. Industries are currently working on the reduction of the downtime, for example the recoating time, during the process to decrease the time required by the process. Another possible improvement can be the use of two or more lasers working simultaneously on the same powder bed. Prima Industrie has commercialized, for this purpose, a new machine, called "Print Genius". Thanks to the simultaneous use of two lasers and cutting the recoating time (almost halved) , this machine can theoretically double the productivity of the whole process.

6 Acronyms

CAD	Computer Aided Design
AM	Additive Manufacturing
RP	Rapid Prototyping
SLA	Stereolithography
FDM	Fusion Deposition molding
SLS	Selective Laser Sintering
BJ	Binder Jetting
SLM	Selective Laser Melting
CNC	Computer Numerical Control
STL	Standard triangulation language
GD & T	Geometric Dimensional and Tolerances
PBF	Powder Bed Fusion
LMD	Laser Metal Deposition
LBM	Laser Beam Melting
EBM	Electron Beam Melting
DED	Directed Energy Deposition
LENS	Laser Engineered Net Shaping
DMD	Direct Metal Deposition
LPBF	Laser Powder Bed Fusion
EDM	Electrical Discharger Machine
LED	Linear Energy Density
VED	Volumetric Energy Density
SHT	Short-term Heat Treatment
YS	Yield Strength
UTS	Ultimate Tensile Strength

7 Bibliography

- [1] Julien Gardan, Additive manufacturing technologies: state of the art and trends, International Journal of Production Research, 2015
- [2] Ian Gibson, David Rosen, Brent Stucker, "Additive Manufacturing Technologies: 3DPrinting, Rapid Prototyping, and Direct Digital manufacturing", pp.1-4 Springer 2015
- [3] <https://www.sculpteo.com/blog/2016/12/14/the-history-of-3d-printing-3d-printing-technologies-from-the-80s-to-today/>
- [4] <https://www.sculpteo.com/blog/2017/03/01/whos-behind-the-three-main-3d-printing-technologies/>
- [5] <https://nephrology.wustl.edu/3d-printed-kidney-models-change-way-surgeons-prepare-surgery/>
- [6] <https://www.innovationpost.it/2018/09/17/tutto-quello-che-ce-da-sapere-sulladditive-manufacturing-guida/>
- [7] <http://www.replicatore.it/il-mercato-della-manifattura-additiva-vale-9-miliardi-di-dollari/>
- [8] Ian Gibson, David Rosen, Brent Stucker, "Additive Manufacturing Technologies: 3DPrinting, Rapid Prototyping, and Direct Digital manufacturing", Springer 2015
- [9] Zhongji, Sun Xipeng, TanShu, BengTorWai, YeeYeong, "Selective laser melting of stainless steel 316L with low porosity and high build rates", 2016
- [10] Ian Gibson, David Rosen, Brent Stucker, "Additive Manufacturing Technologies: 3DPrinting, Rapid Prototyping, and Direct Digital manufacturing", pp.7-15 Springer 2015
- [11] <https://www.materialise.com/en/software/magics>
- [12] http://www.fabbers.com/tech/STL_Format
- [13] <https://it.3dsystems.com/quickparts/learning-center/what-is-stl-file>
- [14] <https://www.materialise.com/en/resources/software/webinar-recording/metal-am-webinar-usa>
- [15] Paramita Das, Ramya Chandran, Rutuja Samant and Sam Anand, Optimum Part Build Orientation in Additive Manufacturing for Minimizing Part Errors and Support Structures, 2015
- [16] Bastien , Nicolas Gardan , Gauthier Wahu, Methodology for Part Building Orientation in Additive Manufacturing, 2019
- [17] Luca Iuliano, Department of Management and Production Engineering, Design guidelines for Direct Metal Laser Sintering (DMLS), Politecnico di Torino, 2018
- [18] Ian Gibson, David Rosen, Brent Stucker, "Additive Manufacturing Technologies: 3DPrinting, Rapid Prototyping, and Direct Digital manufacturing", pp 329-349, Springer 2015
- [19] John O. Milewski, "Additive Manufacturing of Metals", Springer, volume 258
- [20] <https://www.3dprintingcreative.it/additive-manufacturing-metalli-picco-2019/>
- [21] J.-P. Kruth, P. Mercelis, J. Van Vaerenbergh, L. Froyen, M. Rombouts, Binding mechanisms in selective laser sintering and selective laser melting, 2005

- [22] <https://www.lboro.ac.uk/research/amrg/about/the7categoriesofadditivemanufacturing/powderbedfusion/>
- [23] Ian Gibson, David Rosen, Brent Stucker, "Additive Manufacturing Technologies", second edition, Springer, 2015, pp. 107-109
- [24] John O. Milewski, "Additive Manufacturing of Metals", Springer, volume 258, pp. 134-135, 2017
- [25] Dongdong Gu, "Laser Additive Manufacturing of High-Performance Materials", Springer, pp.16-23, 2015
- [26] John O. Milewski, "Additive Manufacturing of Metals", Springer, volume 258, pp. 135-140, 2017
- [27] John O. Milewski, "Additive Manufacturing of Metals", Springer, volume 258, pp. 140-146, 2017
- [28] Körner, "Additive manufacturing of metallic components by selective electron beam melting — a review", International Materials Reviews, 2016, DOI: 10.1080/09506608.2016.1176289
- [29] Li Yang, Keng Hsu, Brian Baughman Donald Godfrey, Francisco Medina, Mamballykalathil Menon, Soeren Wiener "Additive Manufacturing of Metals: The Technology, Materials, Design and Production", Springer, pp. 65-70, 2017
- [30] John O. Milewski, "Additive Manufacturing of Metals", Springer, volume 258, pp.90, 2017
- [31]] John O. Milewski, "Additive Manufacturing of Metals", Springer, volume 258, pp. 157-161, 2017
- [32] Iuliano L., Department of Management and Production Engineering, Politecnico di Torino, Tecniche di Fabbricazione Additiva, Letto di polvere EBM, 2018
- [33] http://www.specialmetals.com/assets/smc/documents/inconel_alloy_718.pdf
- [34] S. Sun, M. Brandt, M. Easton, "Powder Bed fusion process : an overview", 2017
- [35] Optimizing quality of additively manufactured Inconel 718 using powder bed laser melting process, Magda Sadowski, Leila Ladani, William Brindley, John Romano, July 2016
- [36] Thijs L., Verhaeghe F., Craeghs T., Humbeeck J.V., Kruth J.P. (2010). "A study of the microstructural evolution during selective laser melting of Ti–6Al–4V." Acta Materialia 58: 3303- 3312
- [37] Dirk Herzog, Vanessa Seyda, Eric Wycisk, Claus Emmelmann, "Additive manufacturing of metals", 2016
- [38] Xiaoqing Wang, Tahmina Keya, Kevin Chou, " Build Height Effect on the Inconel 718 Parts Fabricated by Selective Laser Melting", 2016
- [39] Y. Gao, D. Zhang, M. Cao, R. Chen, Z. Feng, R. Poprawe, J.H. Schleifenbaum, S. Ziegler, Effect of δ phase on high temperature mechanical performances of Inconel 718 fabricated with SLM process, Materials Science & Engineering A (2019), doi: <https://doi.org/10.1016/j.msea.2019.138327>
- [40] Luke Scime, Jack Beuth, Melt pool geometry and morphology variability for the Inconel 718 alloy in a laser powder bed fusion additive manufacturing process, 2019
- [41] Zhou L, Mehta A, McWilliams B, Cho K, Sohn Y, Microstructure, precipitates and mechanical properties of powder bed fused Inconel 718 before and after heat treatment, Journal of Materials Science and Technology (2018), <https://doi.org/10.1016/j.jmst.2018.12.006>
- [42] Gianni Nicoletto, Directional and notch effects on the fatigue behavior of as-built DMLS Ti6Al4V, 2018, <https://doi.org/10.1016/j.ijfatigue.2017.10.004>

- [43] Selective laser melting additive manufacturing of Inconel 718 superalloy parts: Densification, microstructure and properties, Qingbo Jia, Dongdong Gu, February 2014
- [44] An Investigation of Process Parameter Modifications on Additively Manufactured Inconel 718 Parts, Christopher Kantzos, Joseph Pauza, Ross Cunningham, Sneha P. Narra, Jack Beuth, Anthony Rollett, 2018
- [45] <https://www.oerlikon.com/en/>
- [46] Ian Gibson, David Rosen, Brent Stucker, "Additive Manufacturing Technologies", second edition, Springer, 2015, pp. 245-260
- [47] A. Salmi, Department of Management and production (DIGEP), Politecnico di Torino, Additive Manufacturing, 2018
- [48] Silvio Parise, "Basic Application Training for Printsharp 250", Prima Additive, 2018
- [49] David J. Newell, Ryan P. O'Hara, Gregory R. Cobb, Anthony N. Palazotto, Michael M. Kirka, Larry W. Burggraf, Joshuah A. Hess, "Mitigation of scan strategy effects and material anisotropy through supersolvus annealing in LPBF IN718" 2019
- [50] LPW case of study 5: "Powder degradation"
- [51] <https://www.emcotest.com/it/il-mondo-della-prova-di-durezza/nozioni-sulla-durezza/teoria-della-prova-di-durezza/vickers/svolgimento-della-prova-di-durezza-vickers/>

8 APPENDIX A

“Print Sharp 250 is the medium volume machine for Powder Bed Fusion applications, developed for industrial production of complex components. Suitable also for Additive Manufacturing service oriented companies and for prototyping purposes, exhibits a high flexibility in terms of part management and operation performance.” [<https://www.primaadditive.com>]

In the Table below the technical specification of the machine are reported.

Dimension (LXWXH)	1300 (L) – 110 (W) – 1900 (H)
Weight	1400kg
Power Supply	380 V / 50 Hz / 8 kW
Type of Laser	Yb (Ytterbium) Fiber laser
Laser Power	200 W / 500 W (Optional)
Laser Focus Diameter	70 – 100 μ m
Beam Wavelength	1060 – 1080 nm
Building Volume	250 x 250 x 300
Beam Deflection Speed	8 m/s
Positioning Speed	10 m/s
Build Rate	12 – 30 cm ³ /h
Layer Thickness	0.02 mm – 0.1mm
Layer Width	0.1 mm (single line width)
Recoater Specs	Travel: 380 mm / Speed: max 500 mm/s
Building Platform Z-axis	Travel: 300mm / Speed: max 6 mm/s / Res:0.01 mm
Heating Platform	Up to 200°C
Monitoring Of O ₂ Level	Below 100 ppm (0,01%)
Permissible Room Temperatures	15 – 30°C
Gas (Consumption – running / filling)	7 l/min (running)
System Fill Consumption	50 l
Cam Software	Materialise Magics
Control & Other software	Eplus control software (EPC)
Industrial Interfaces	Ethernet

Size & Power

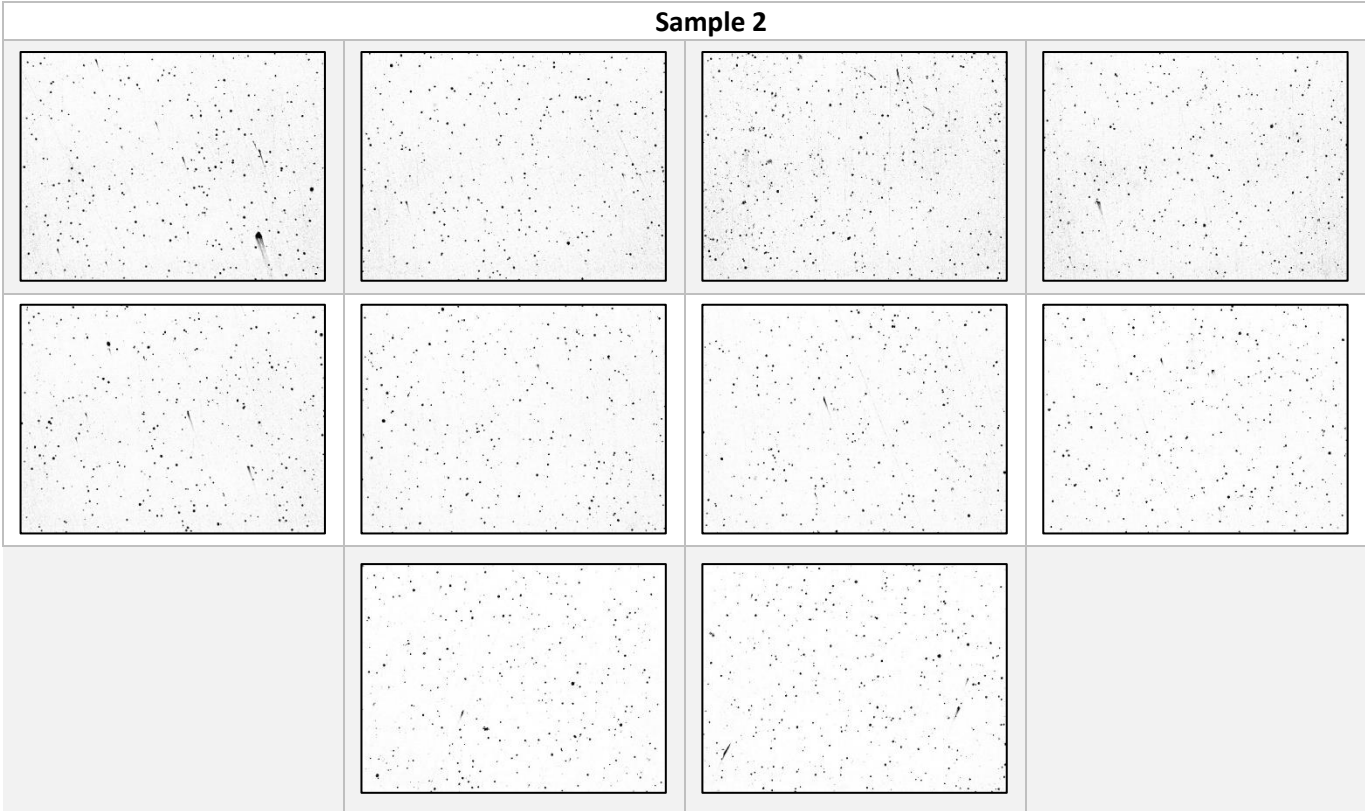
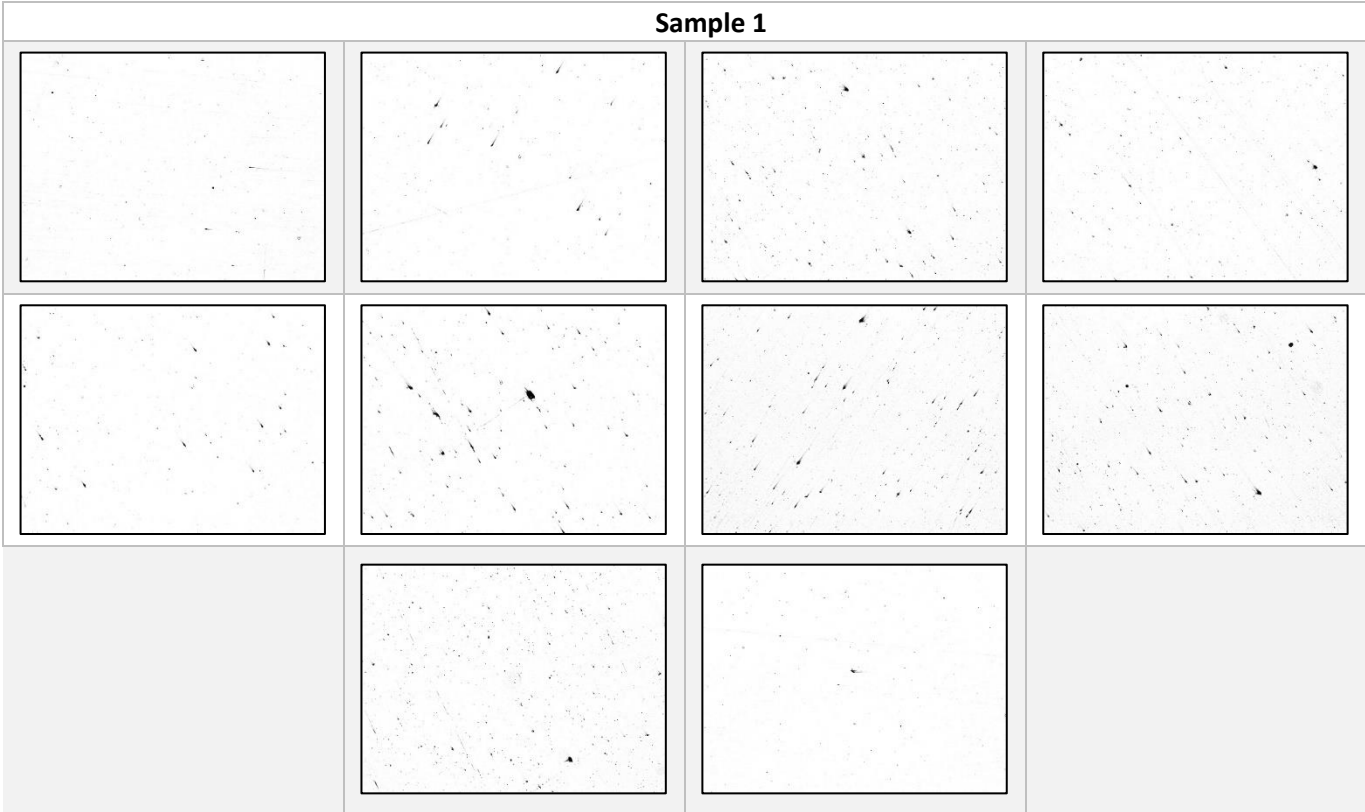
Laser

Machine and Additive process details

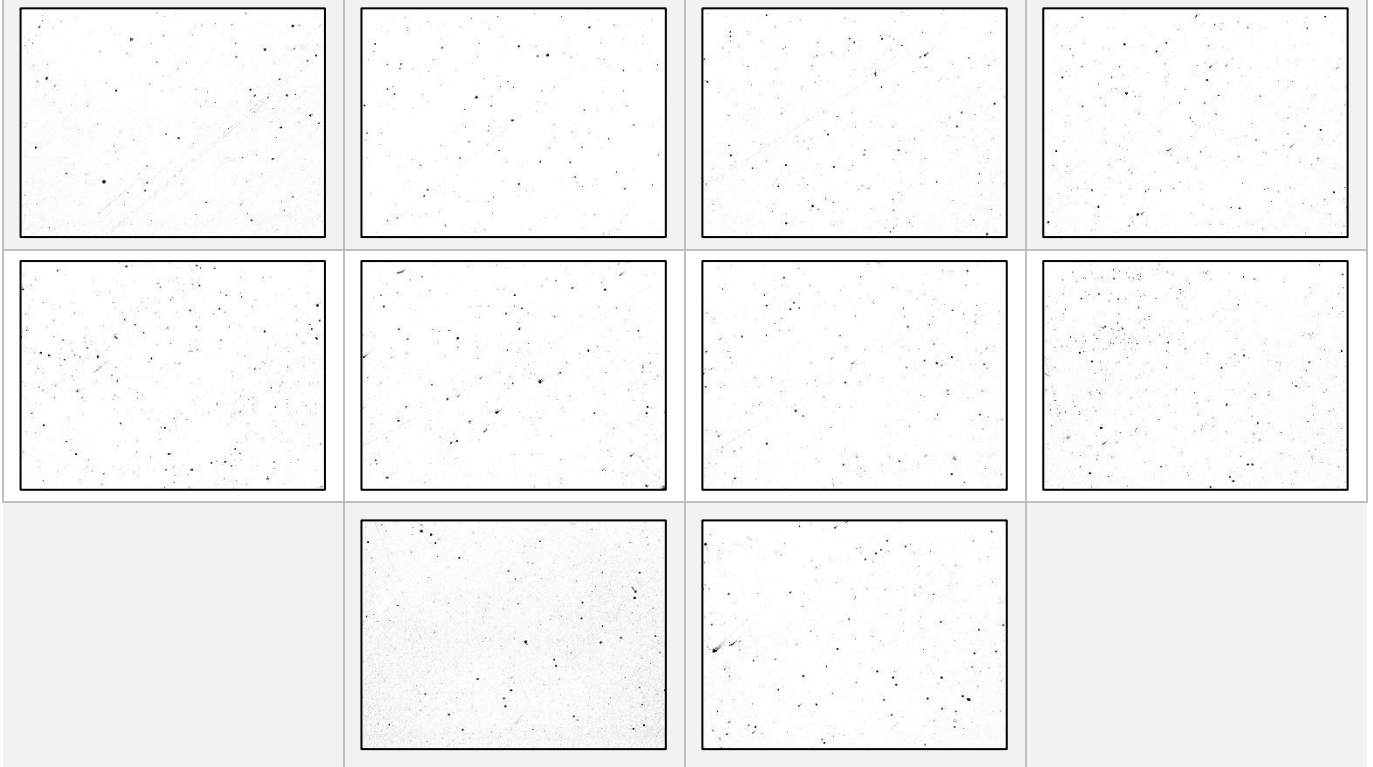
Peripheral & auxiliaries – Software

9 APPENDIX B

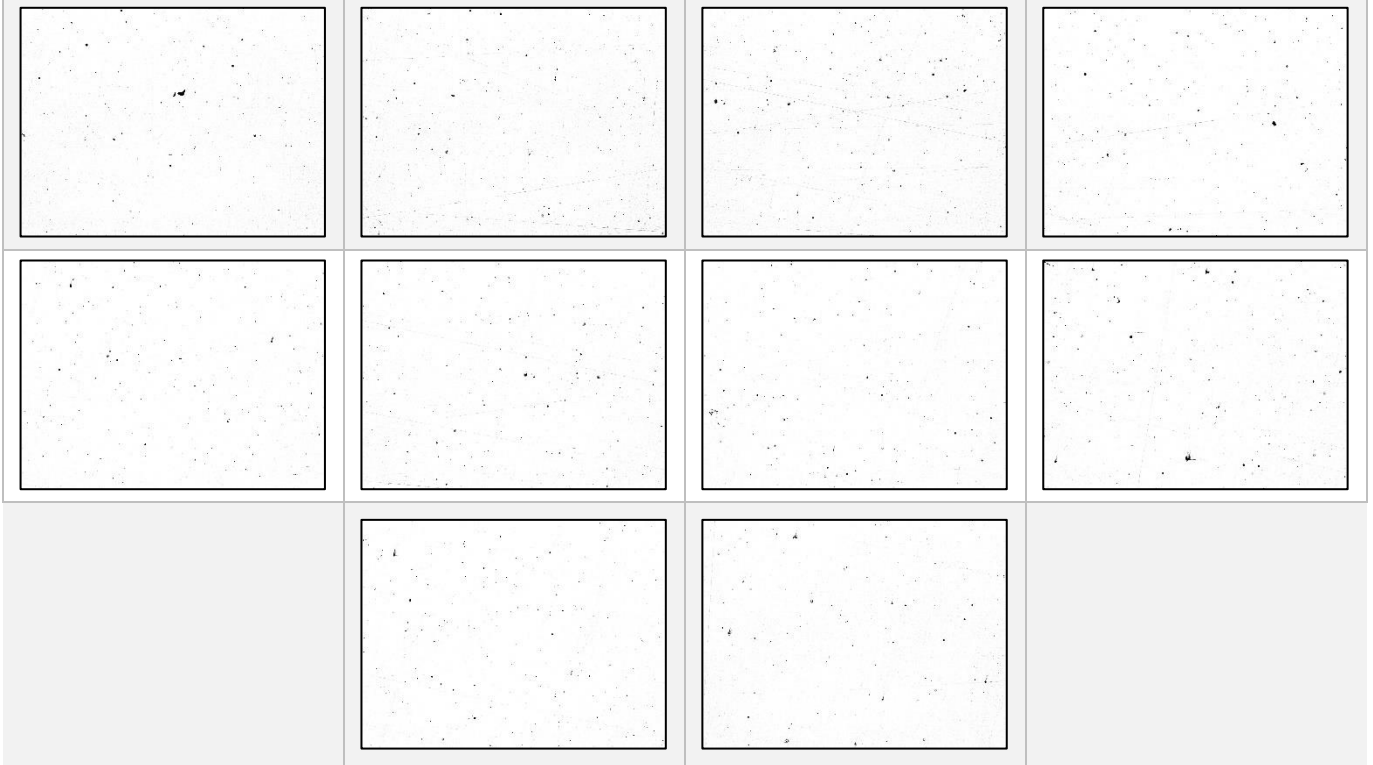
In this appendix were reported all the pictures taken for all the samples for the image analysis



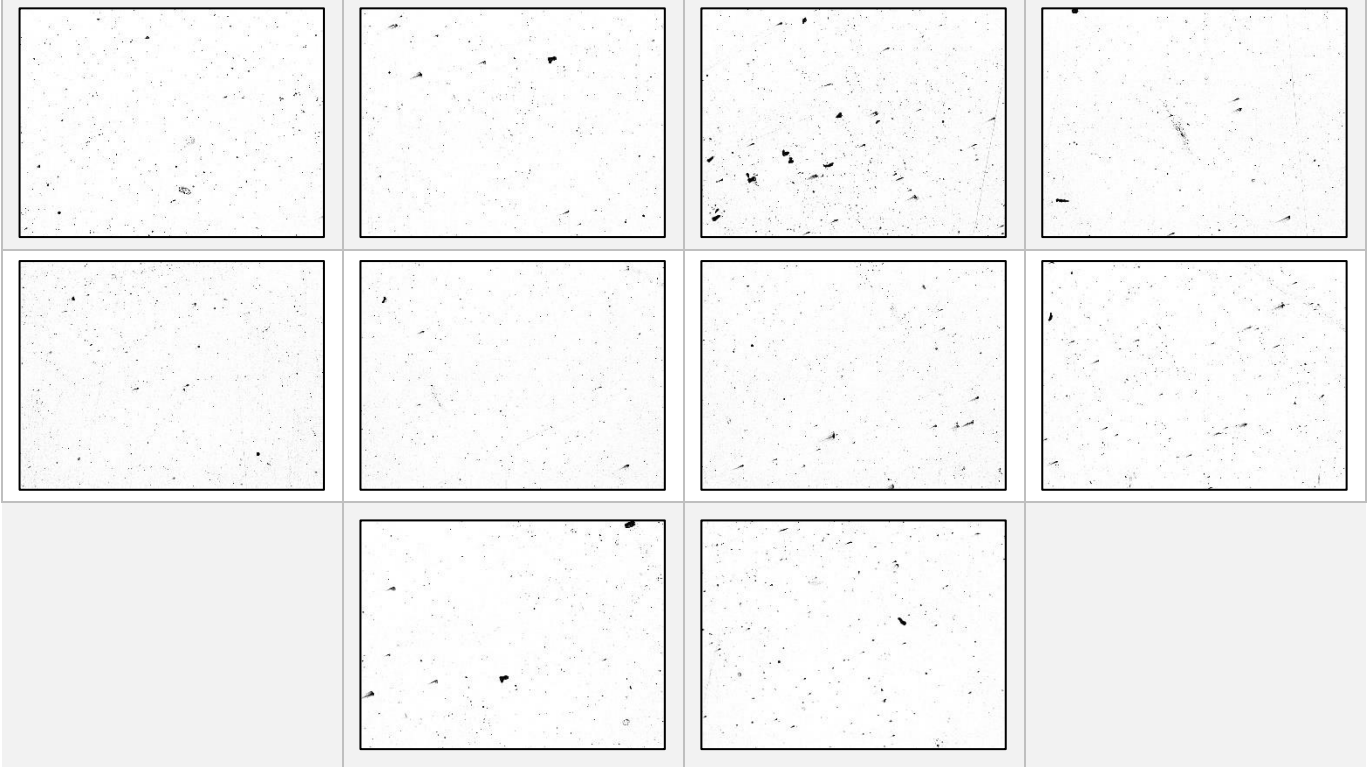
Sample 3



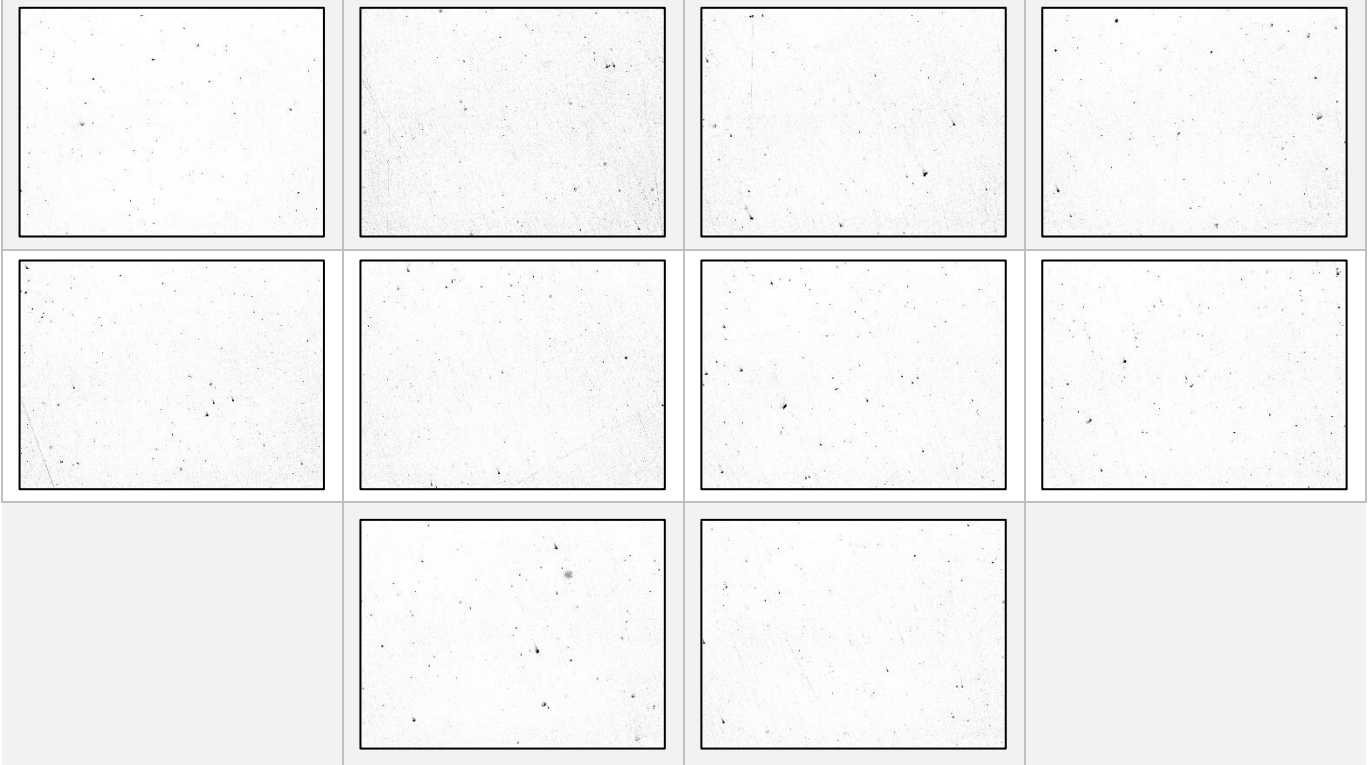
Sample 4



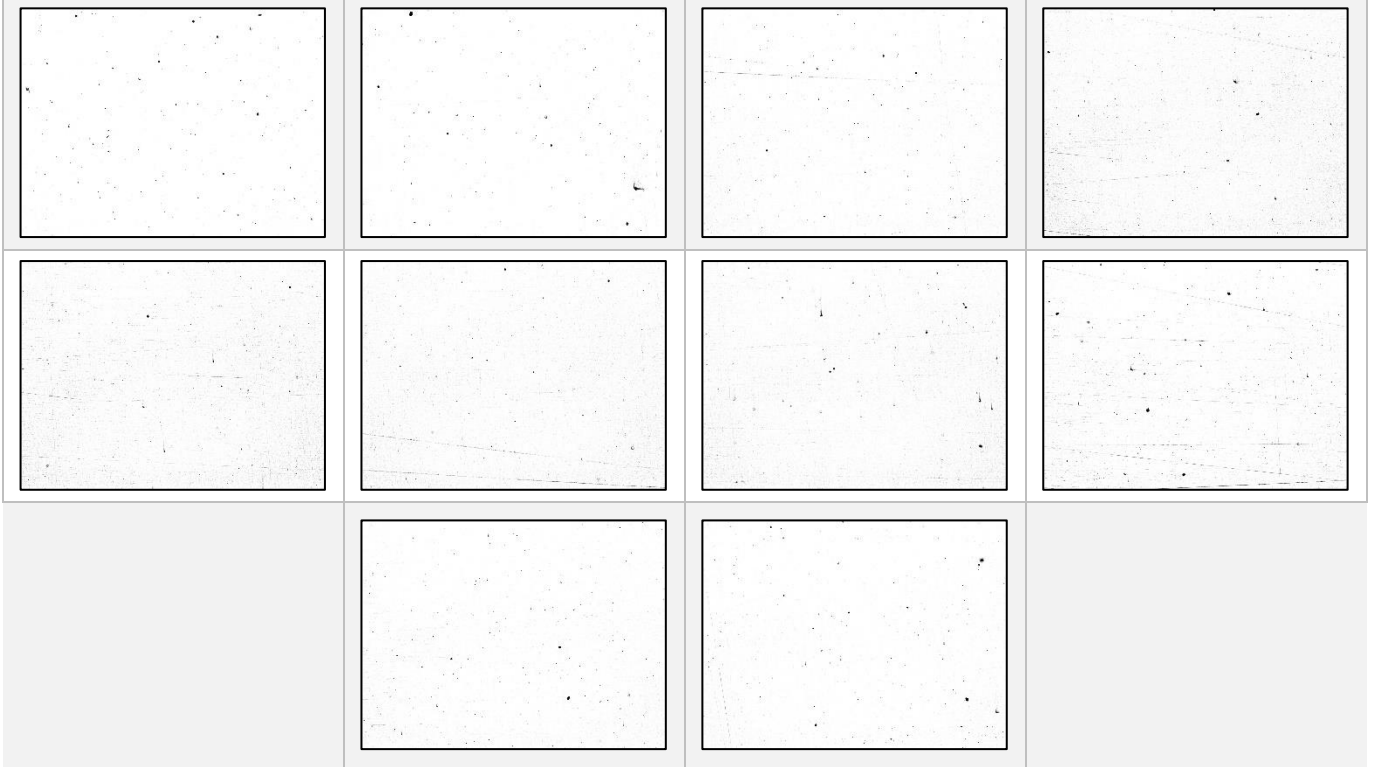
Sample 5



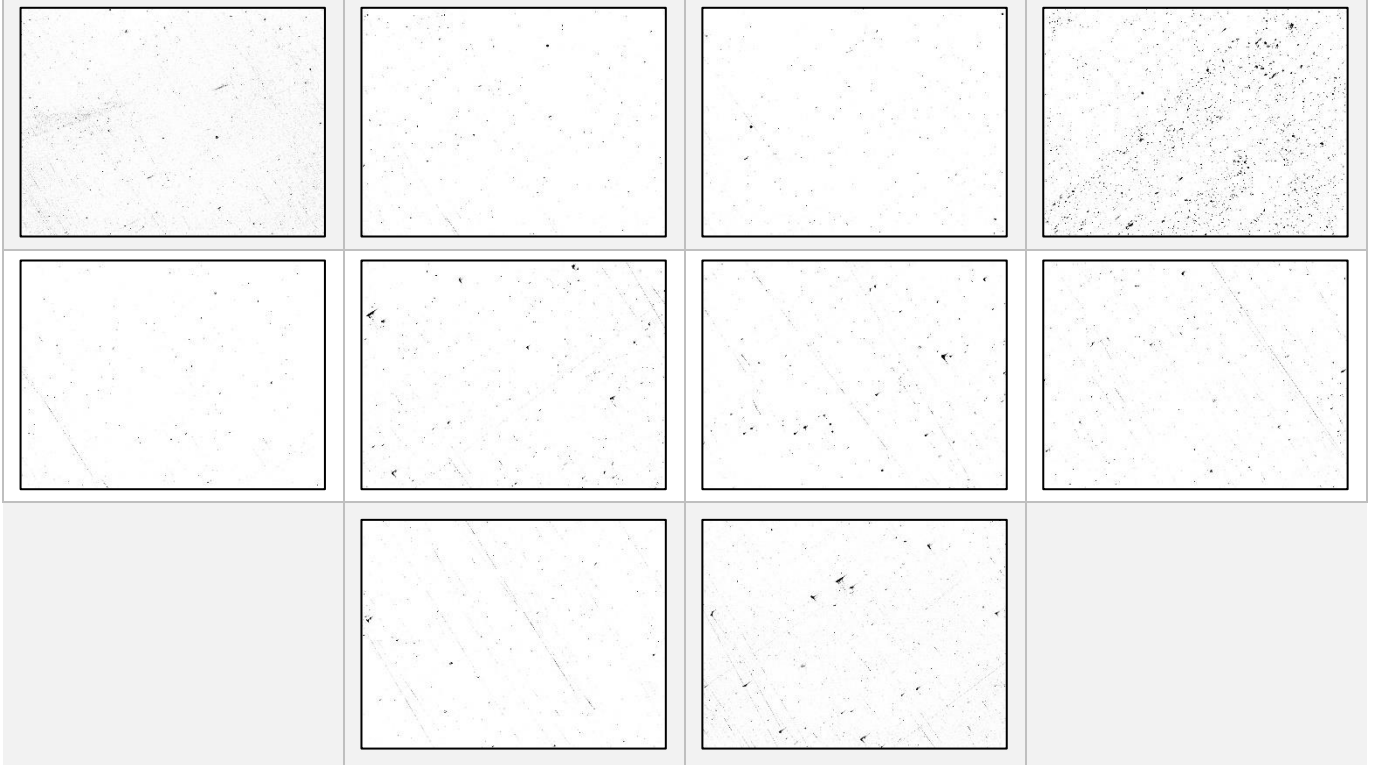
Sample 6



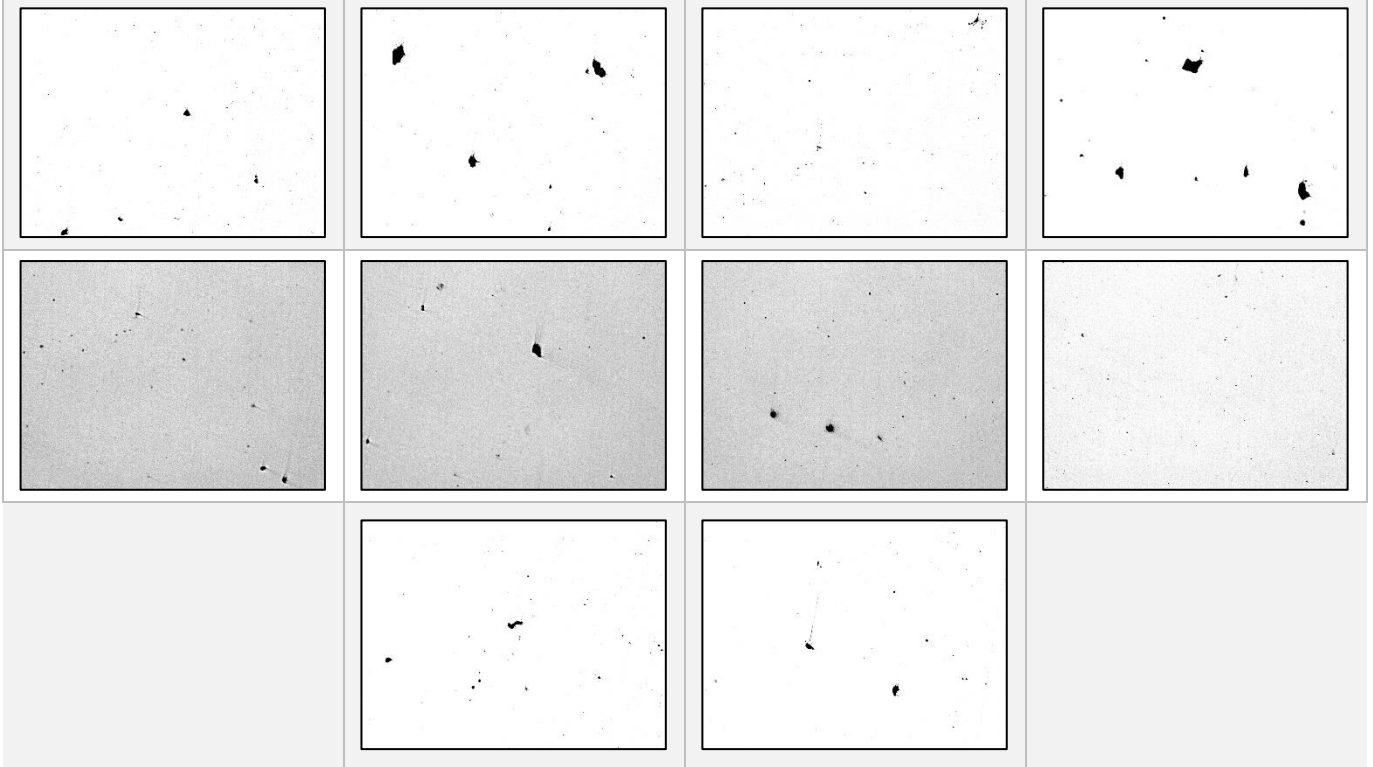
Sample 7



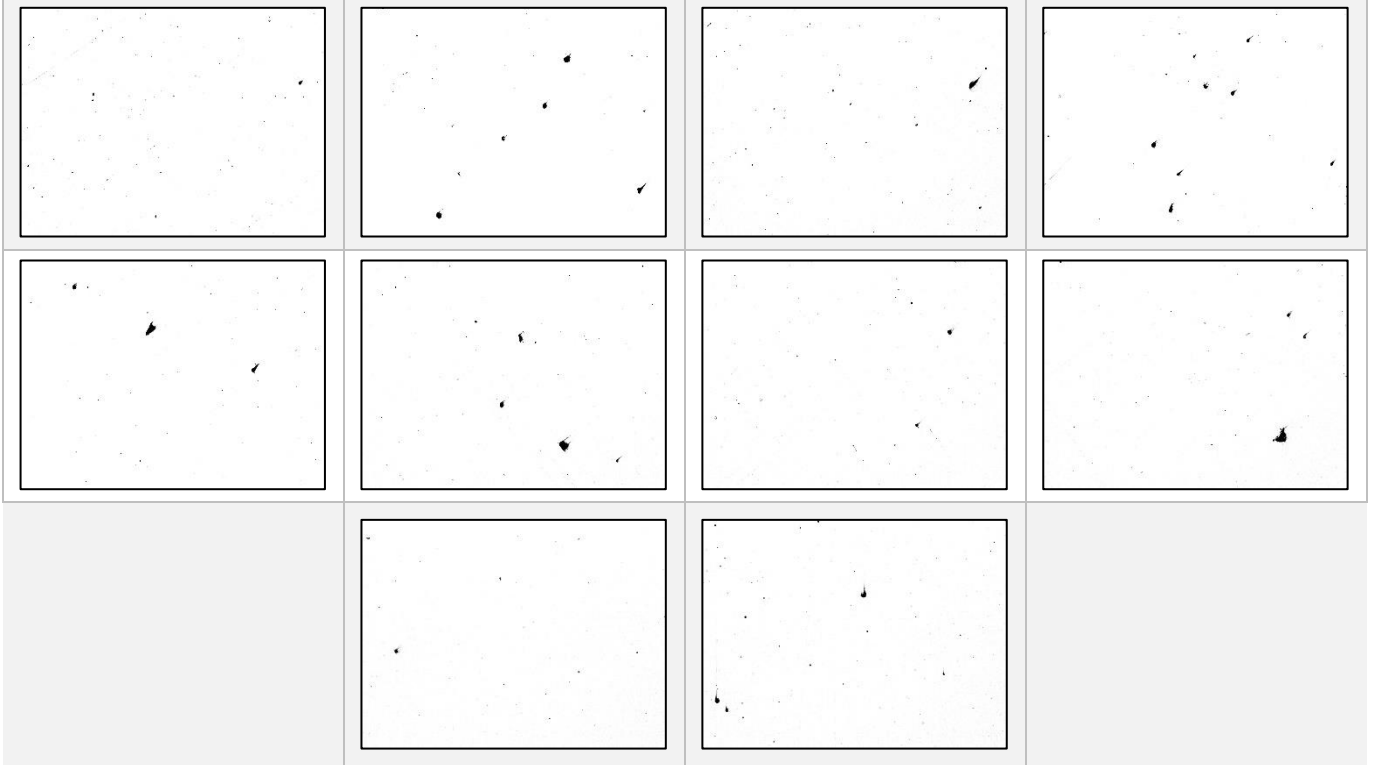
Sample 8



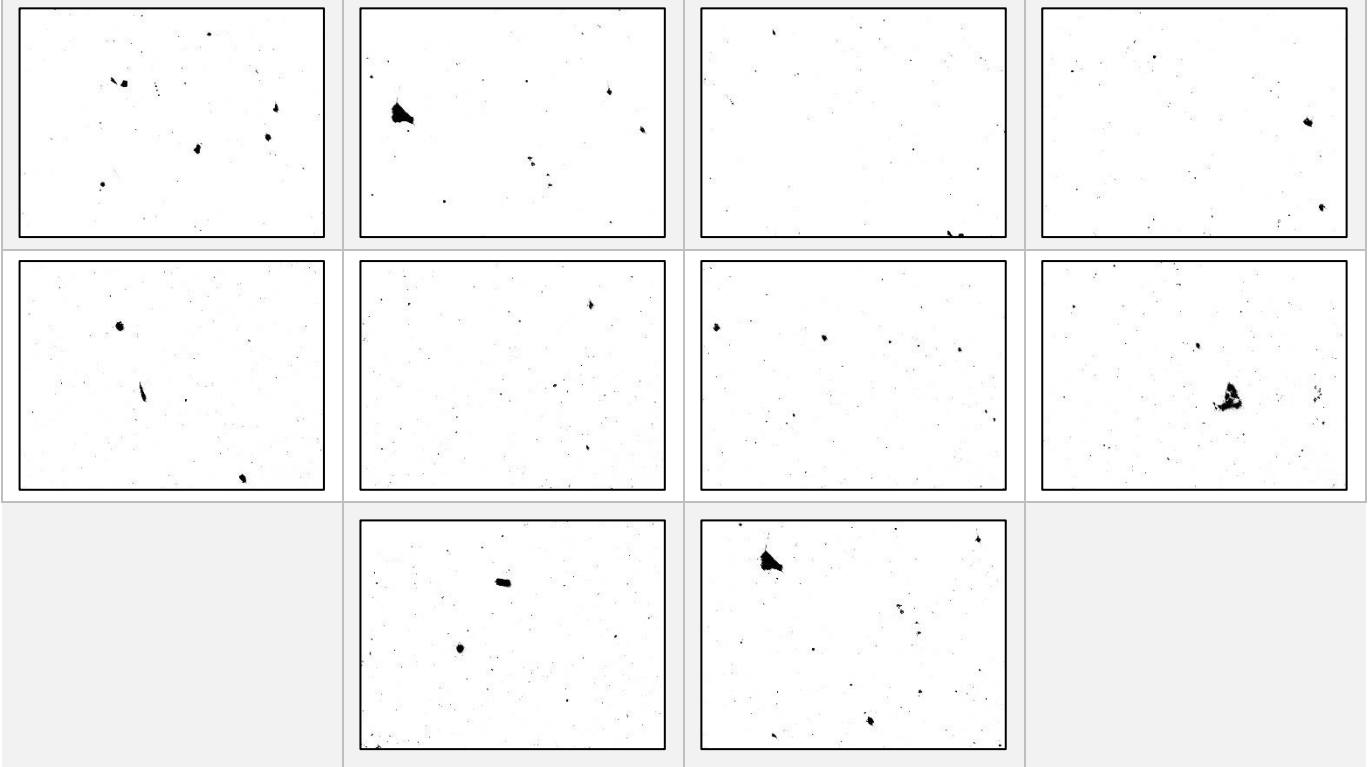
Sample 9



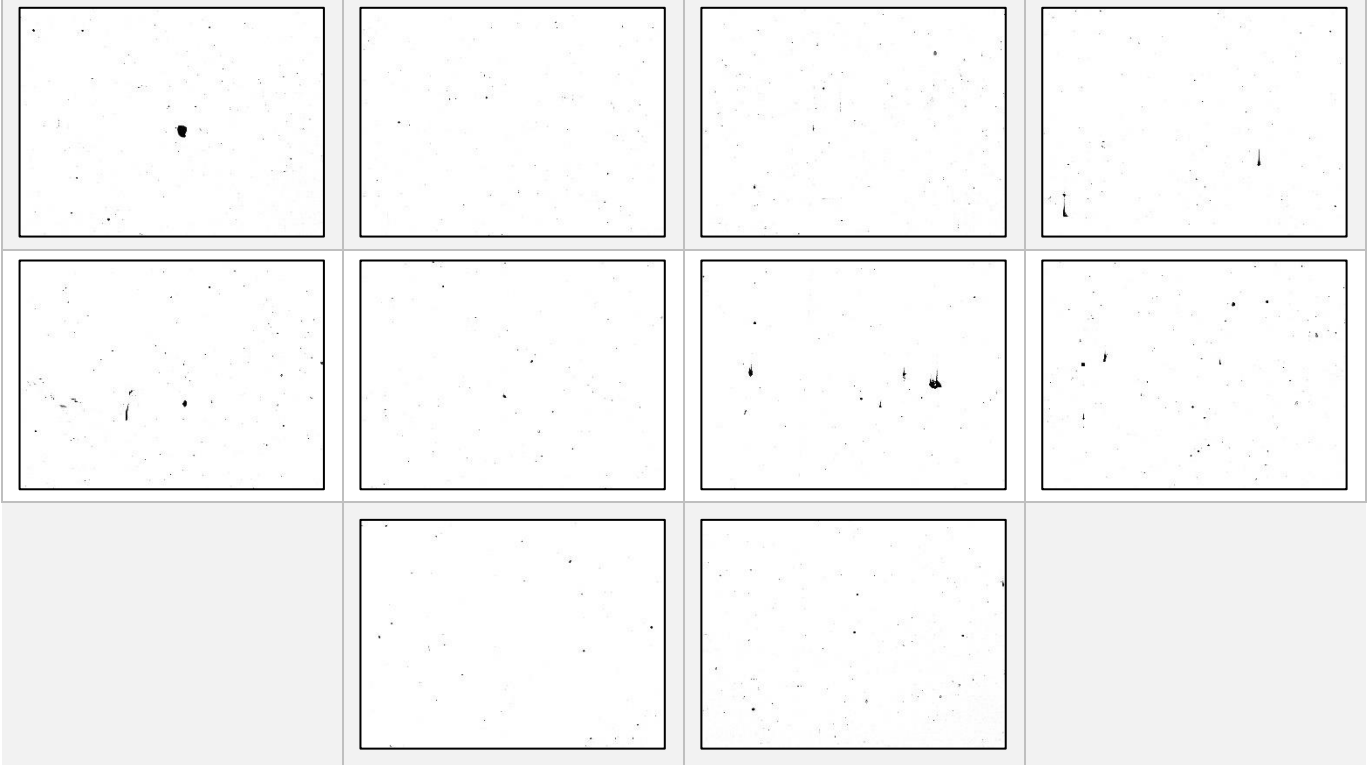
Sample 10



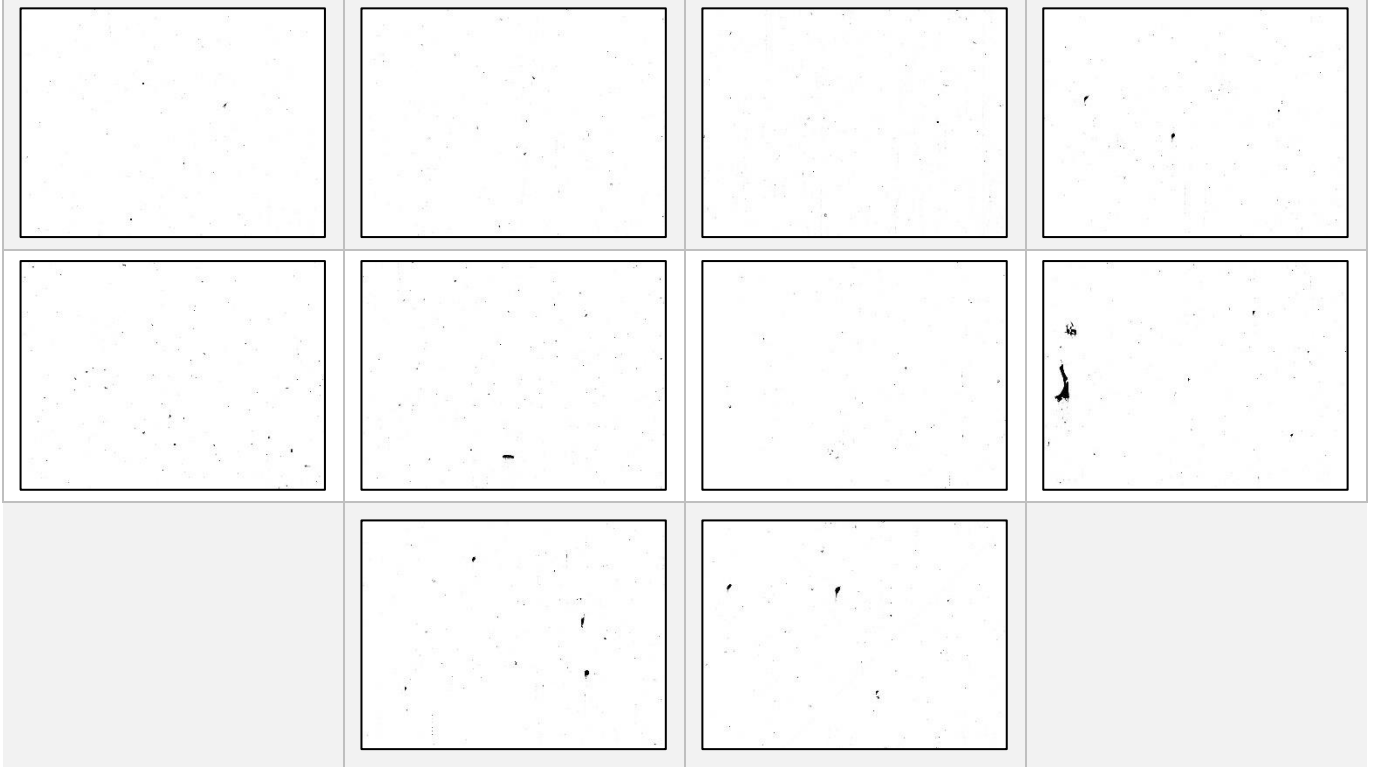
Sample 11



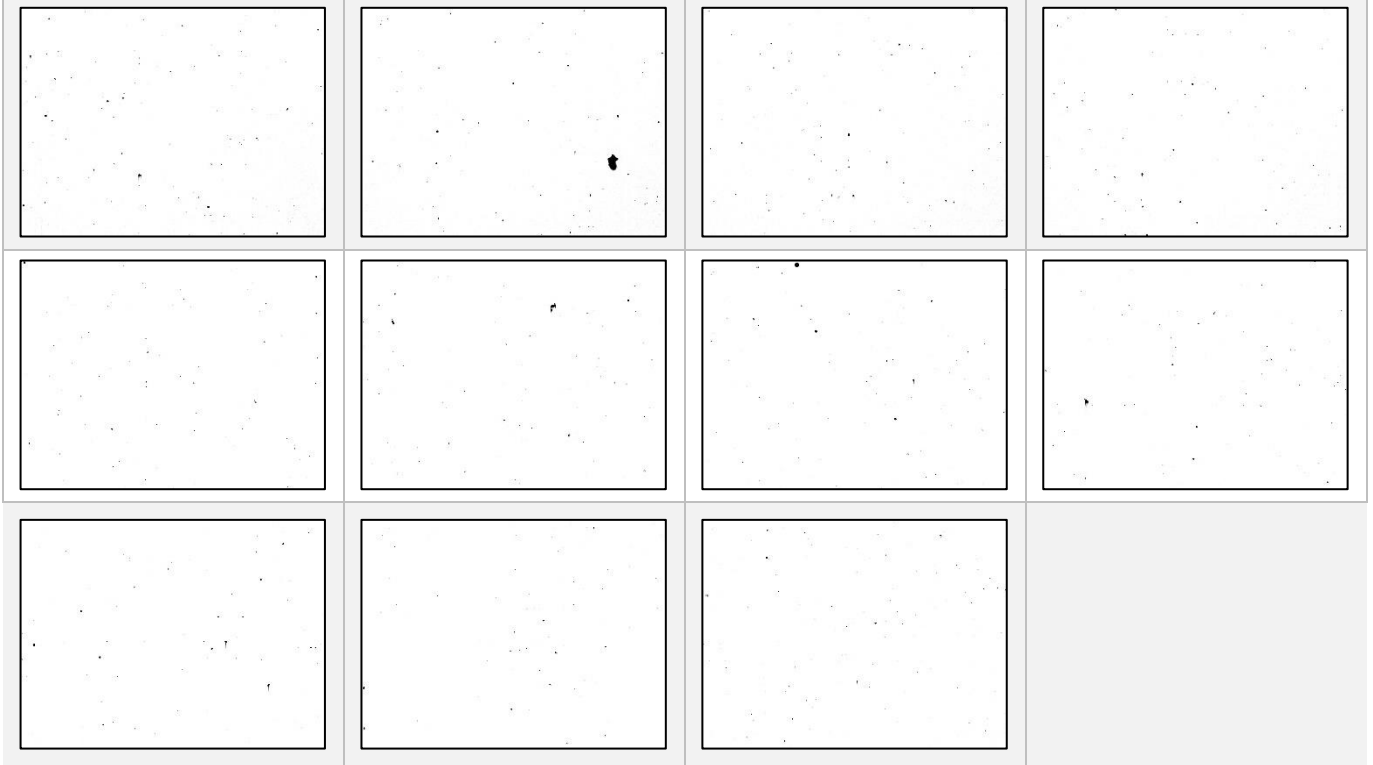
Sample 12



Sample 13



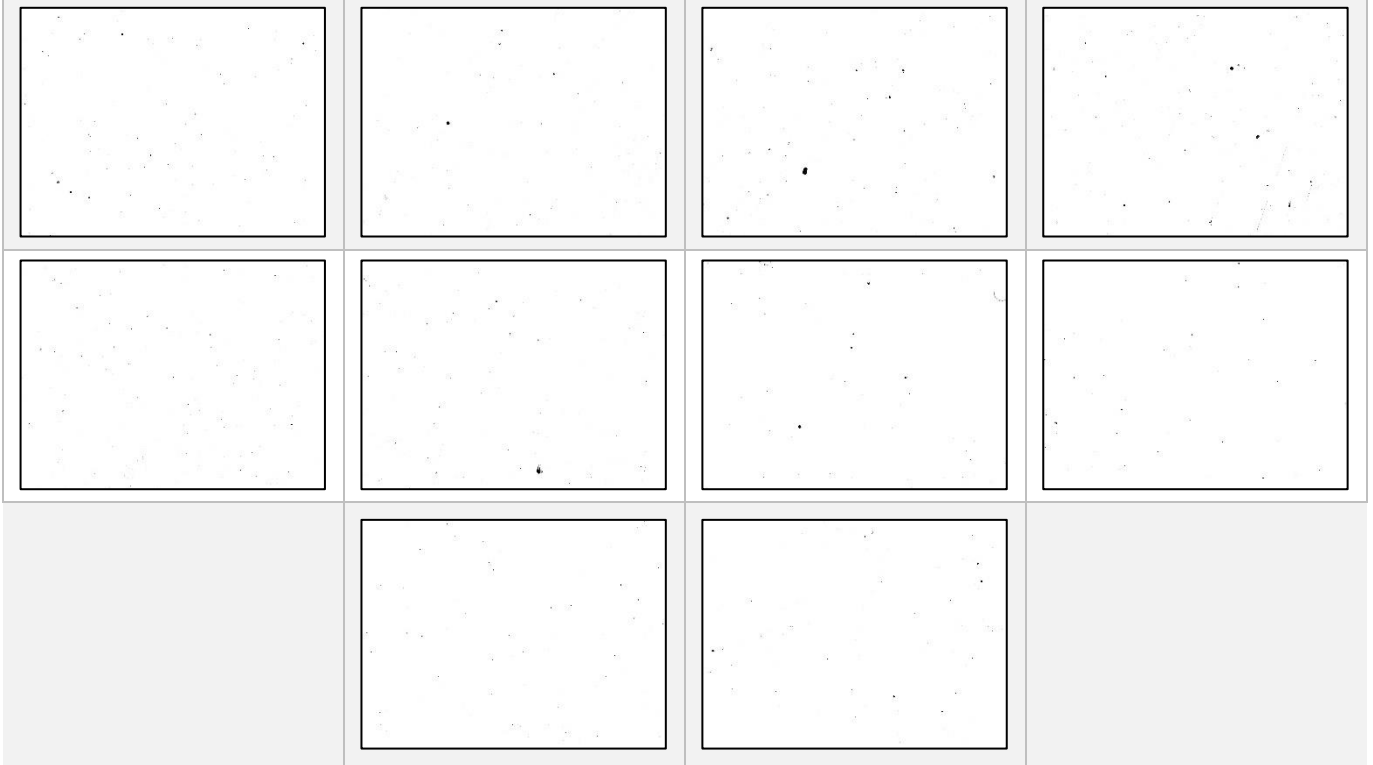
Sample 14



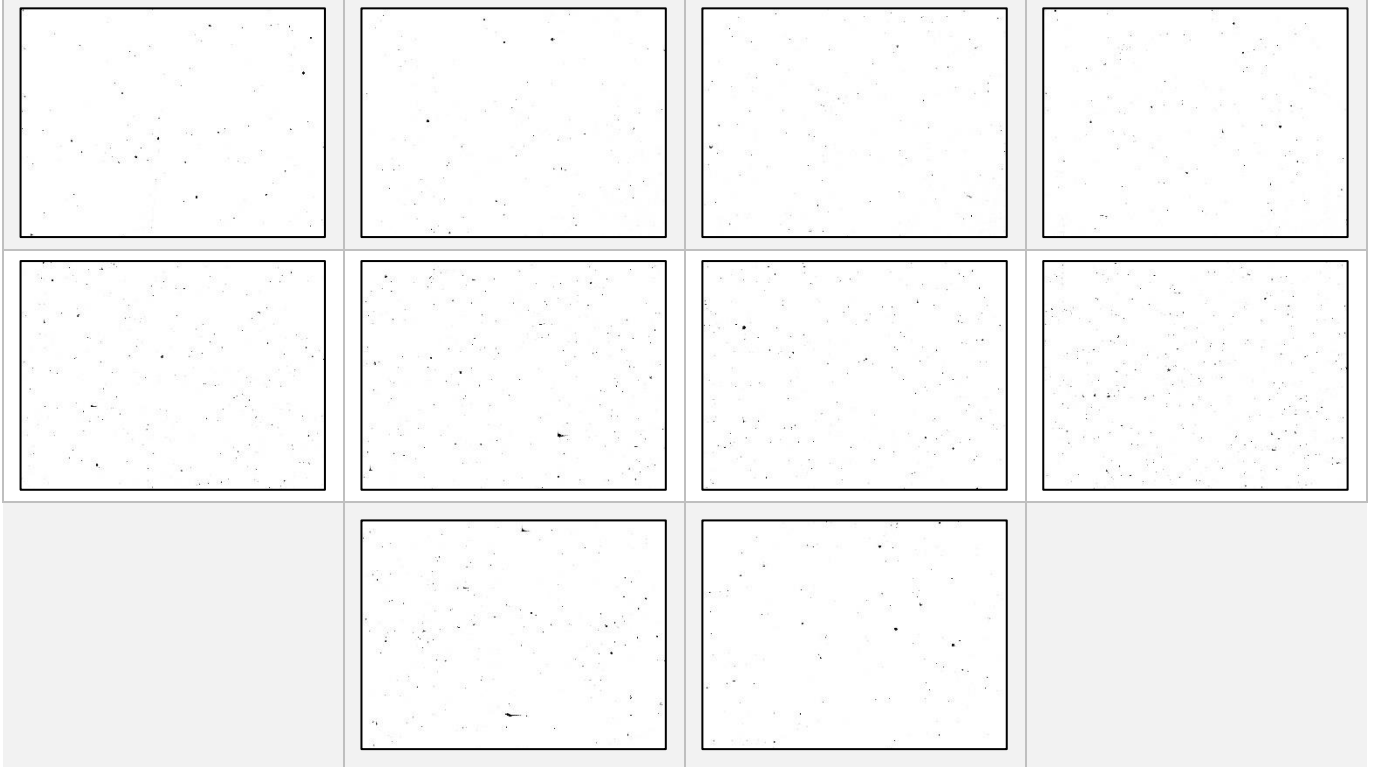
Sample 15



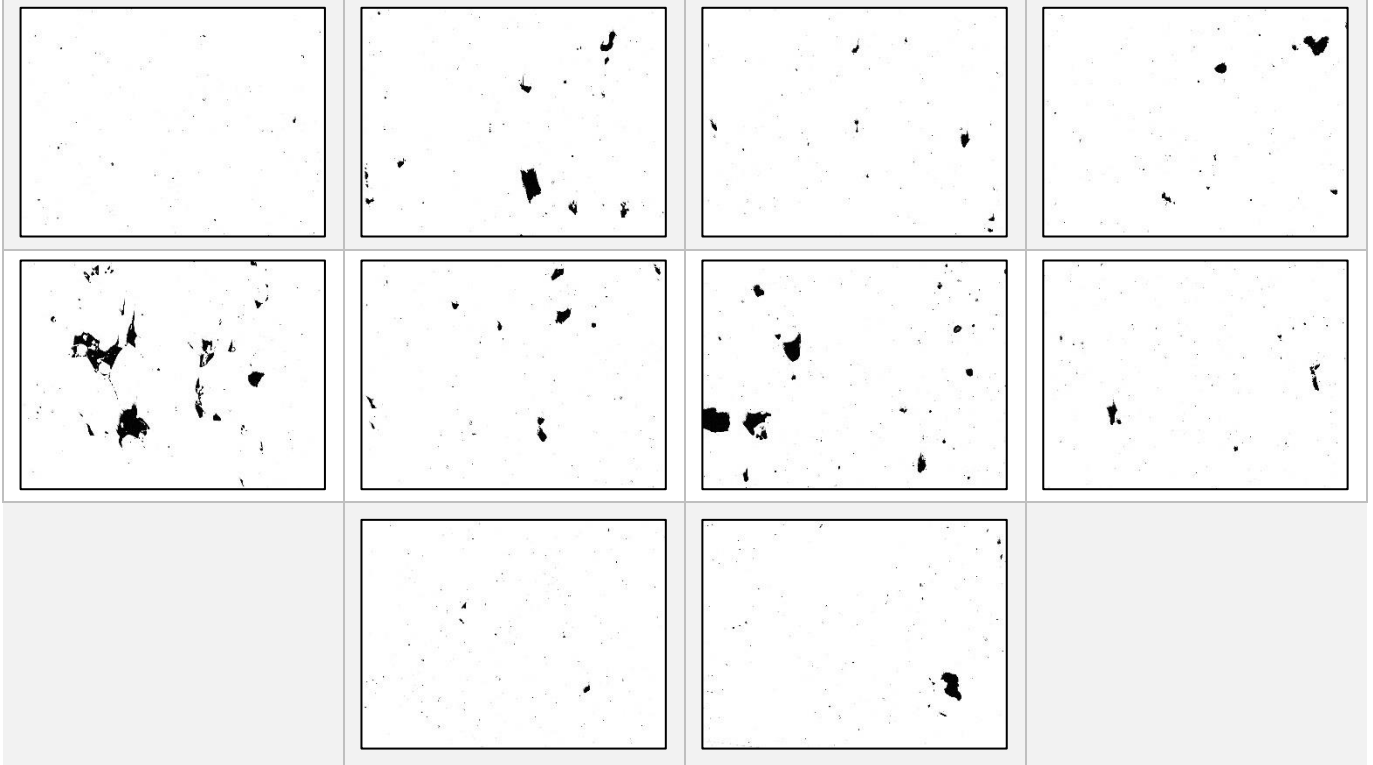
Sample 16



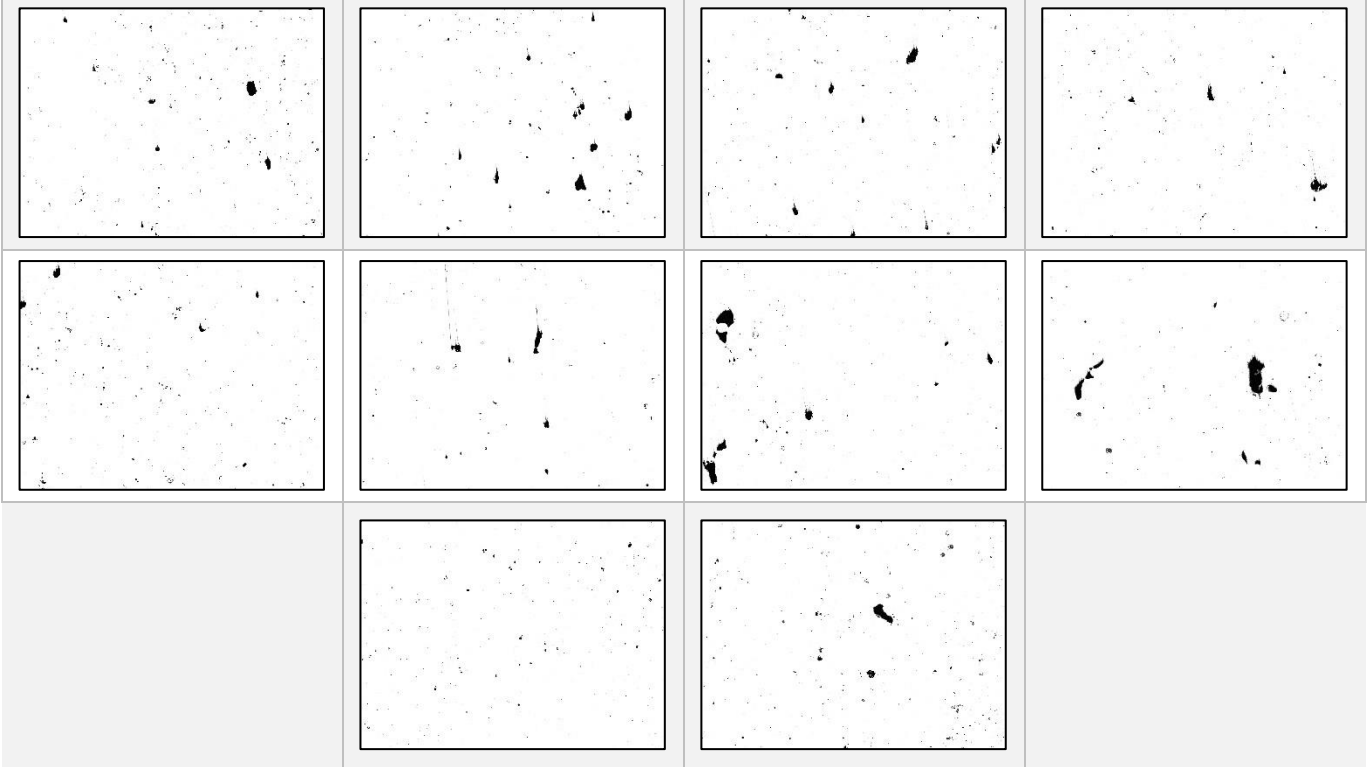
Sample 17



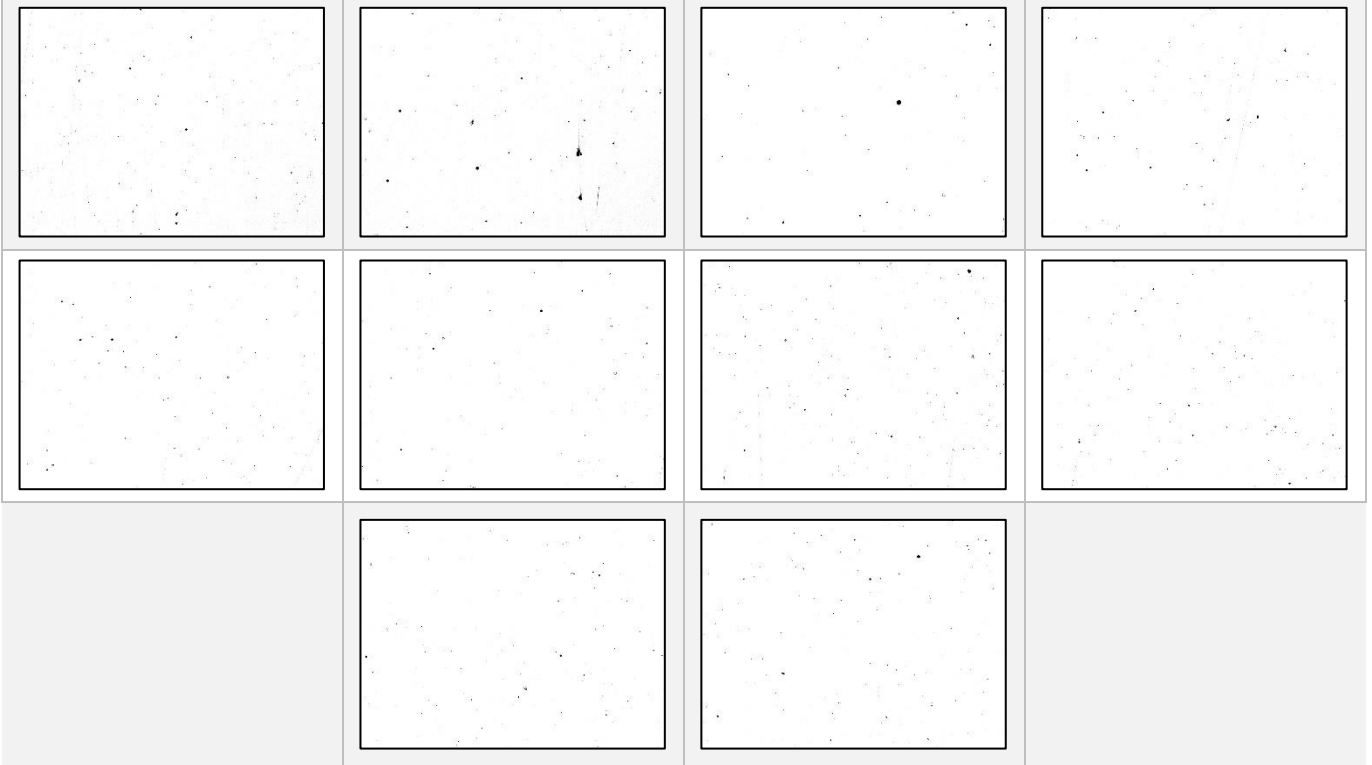
Sample 18



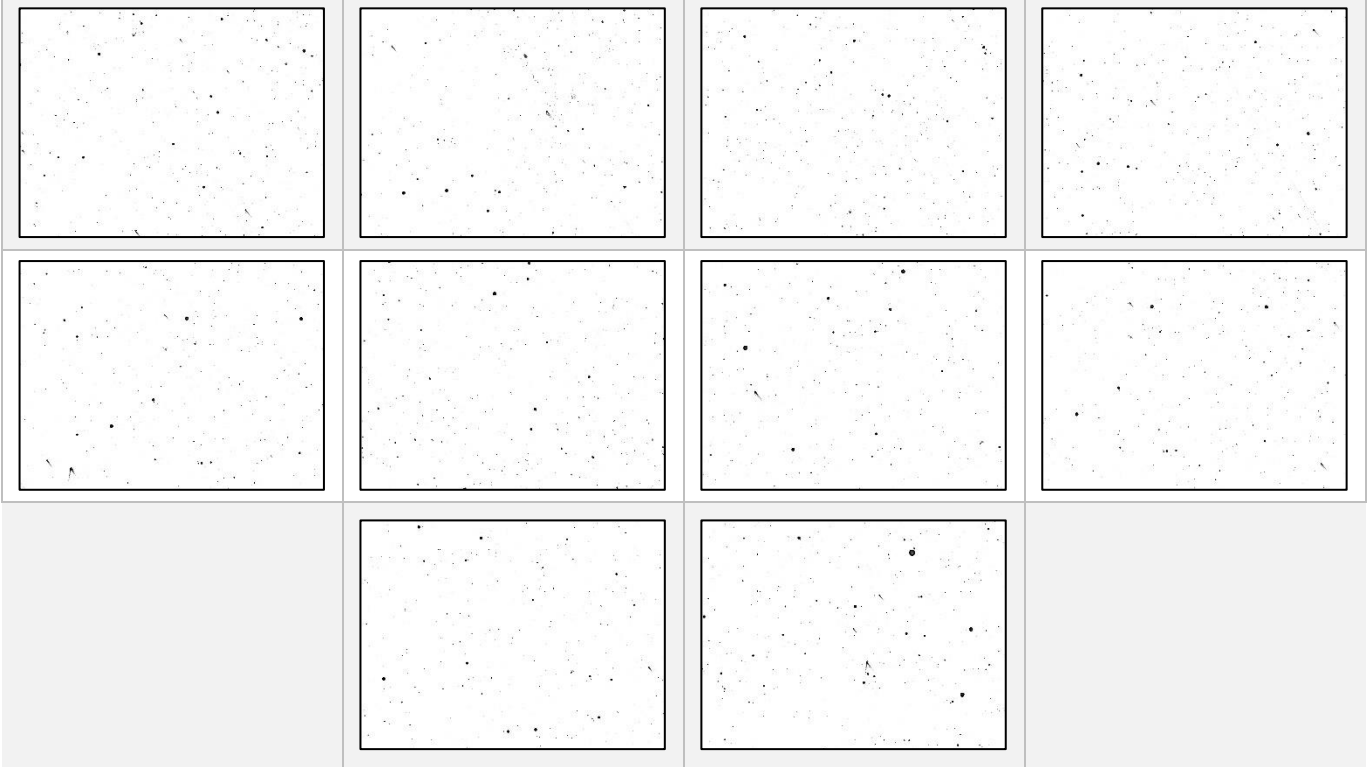
Sample 19



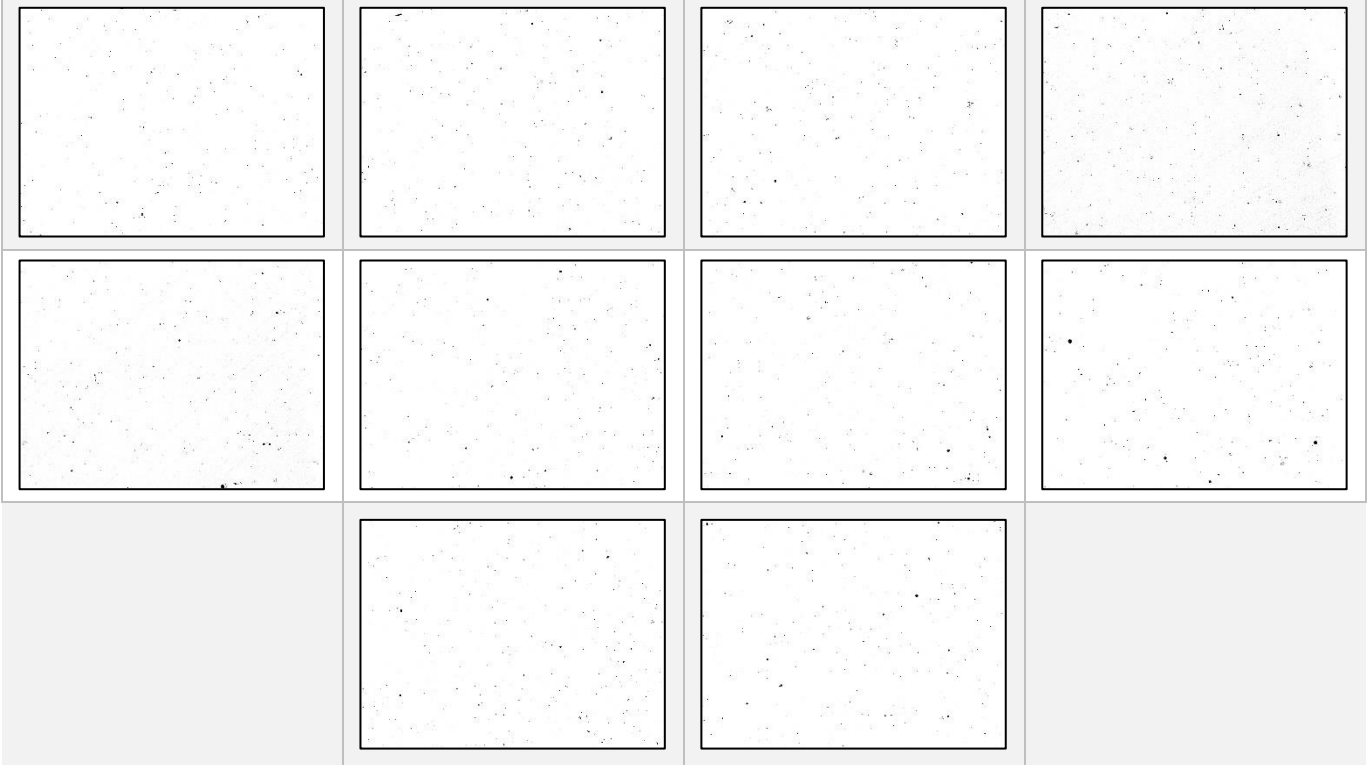
Sample 20



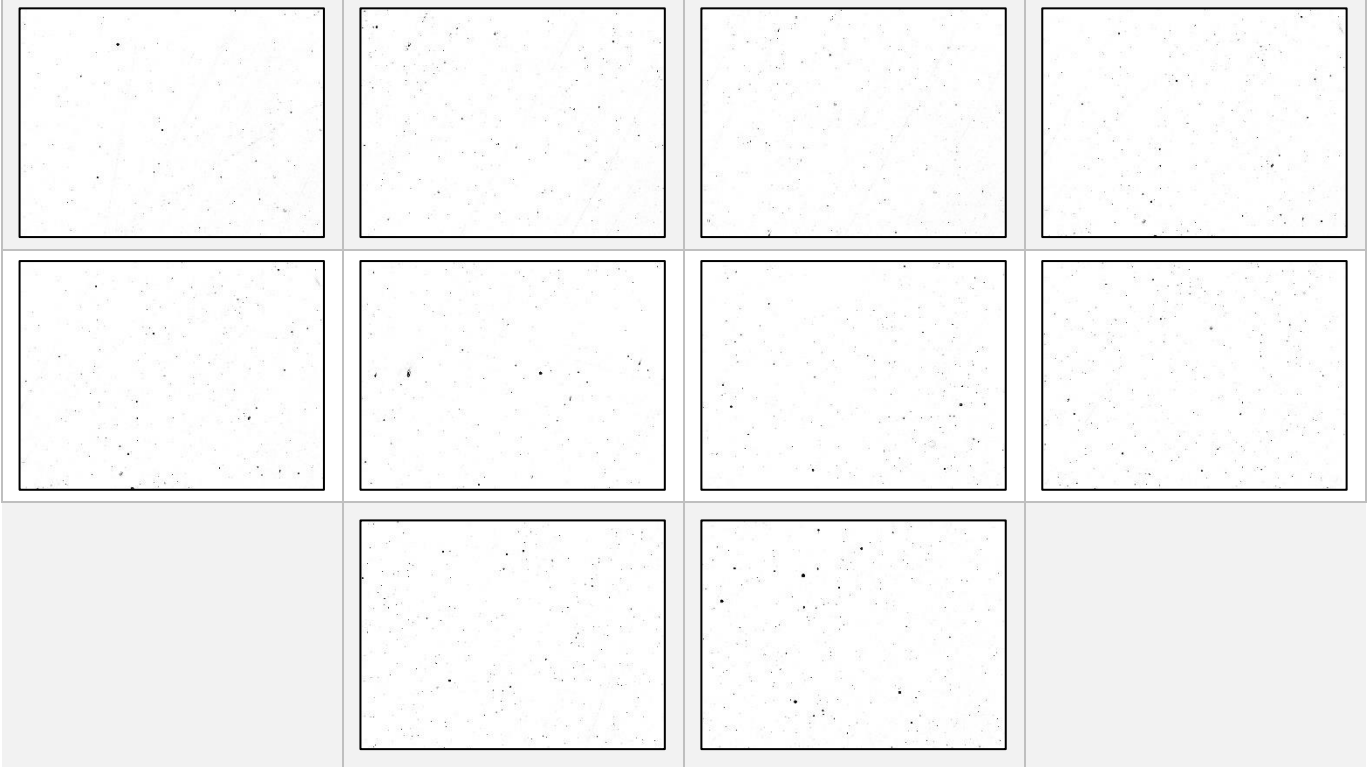
Sample 21



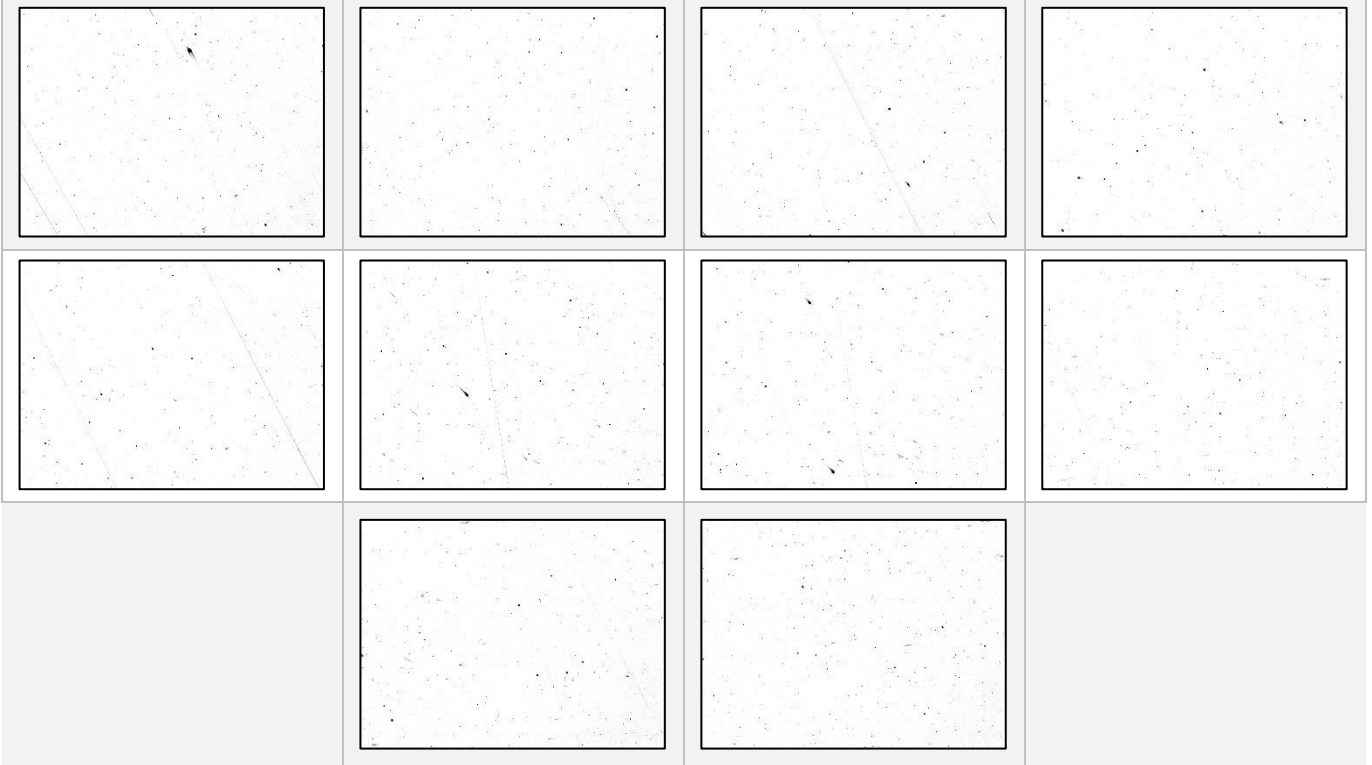
Sample 22



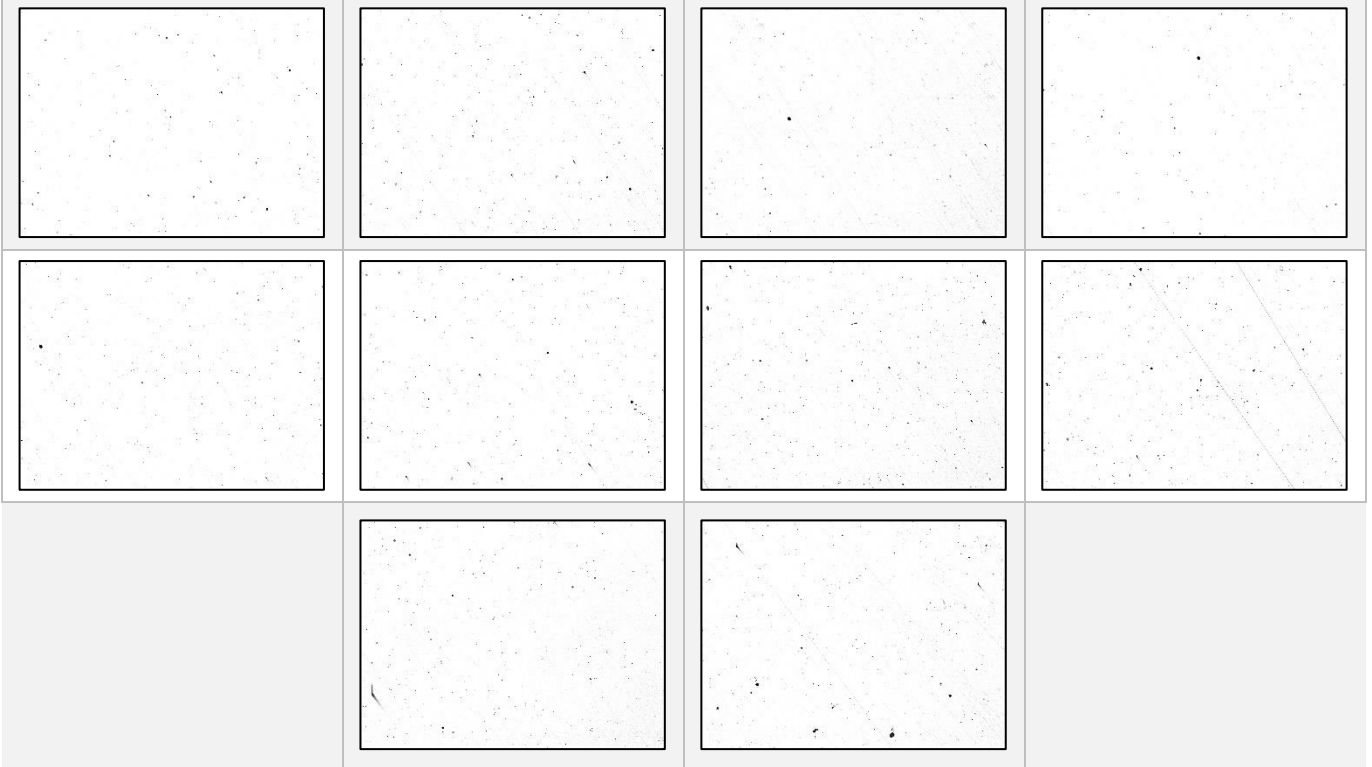
Sample 23



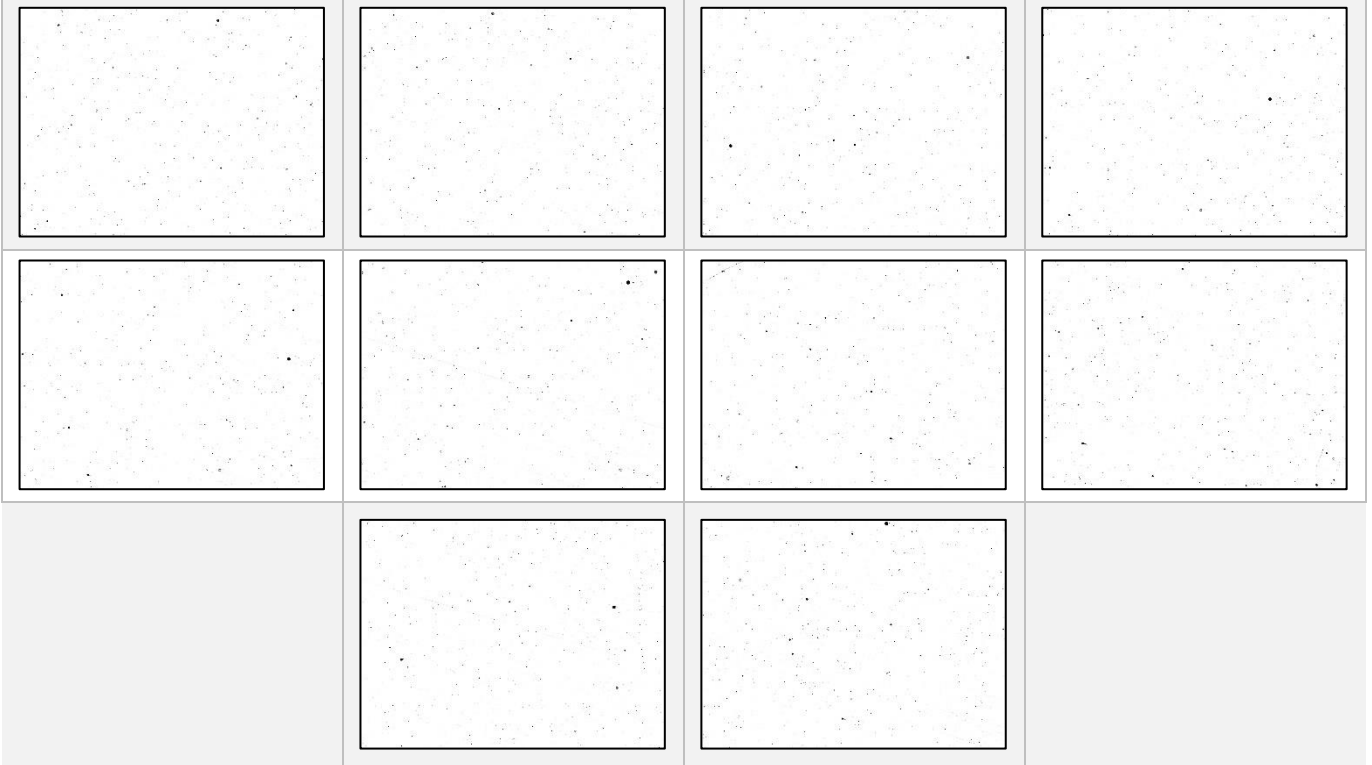
Sample 24



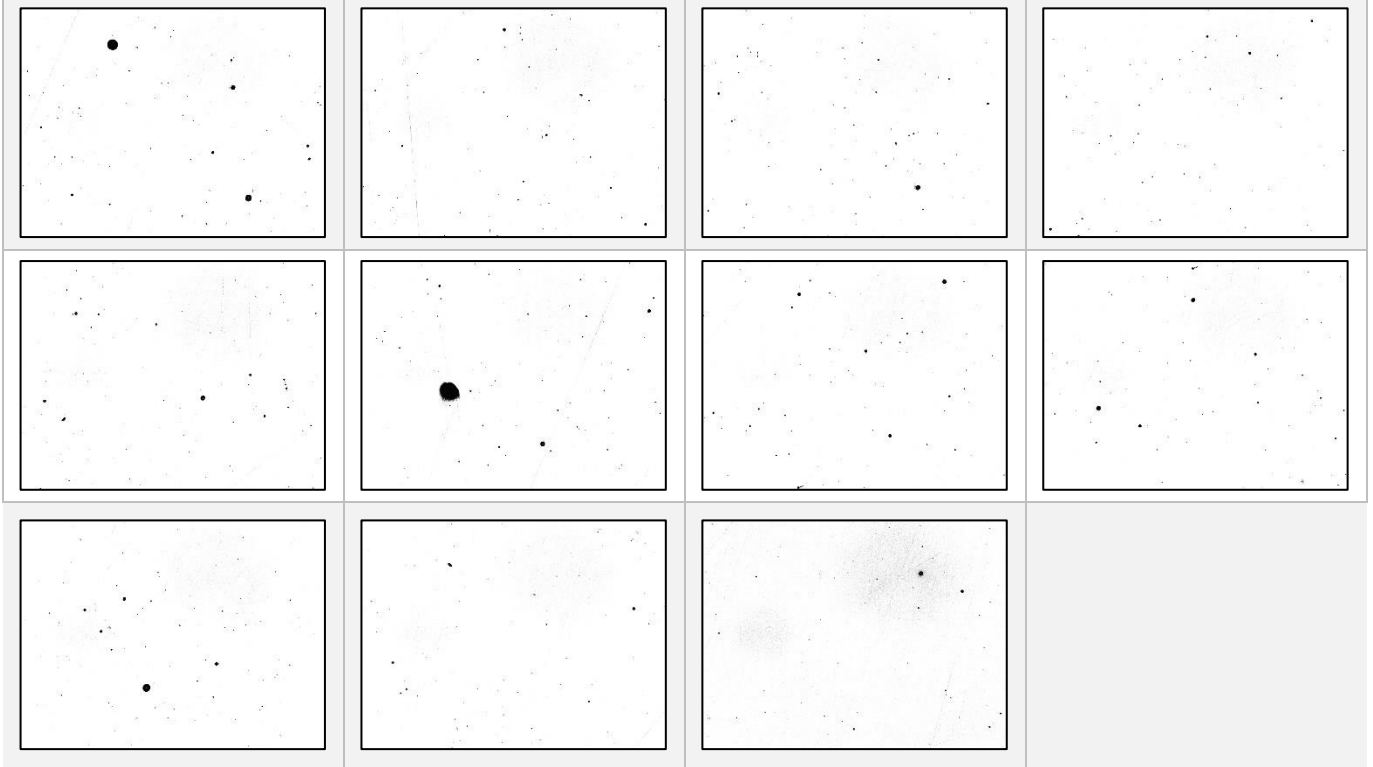
Sample 25



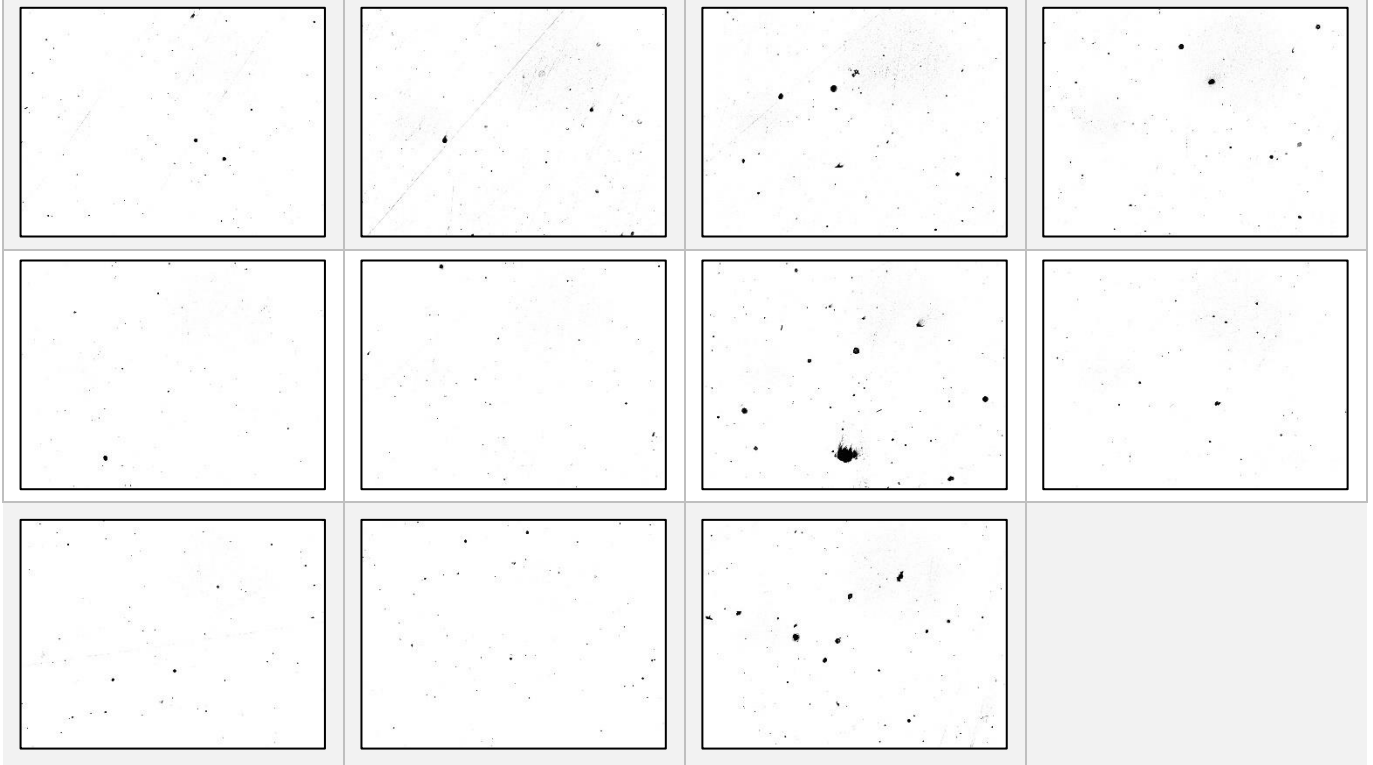
Sample 26



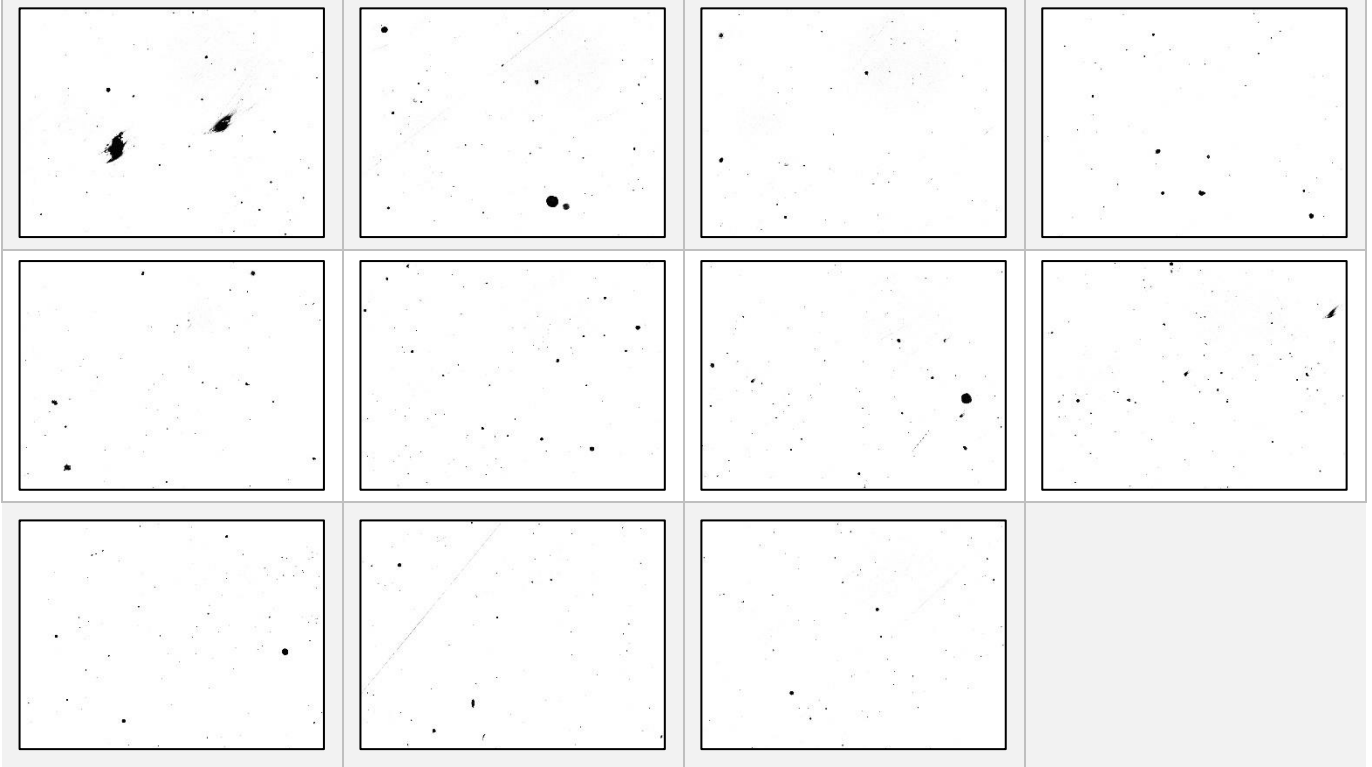
Sample 27



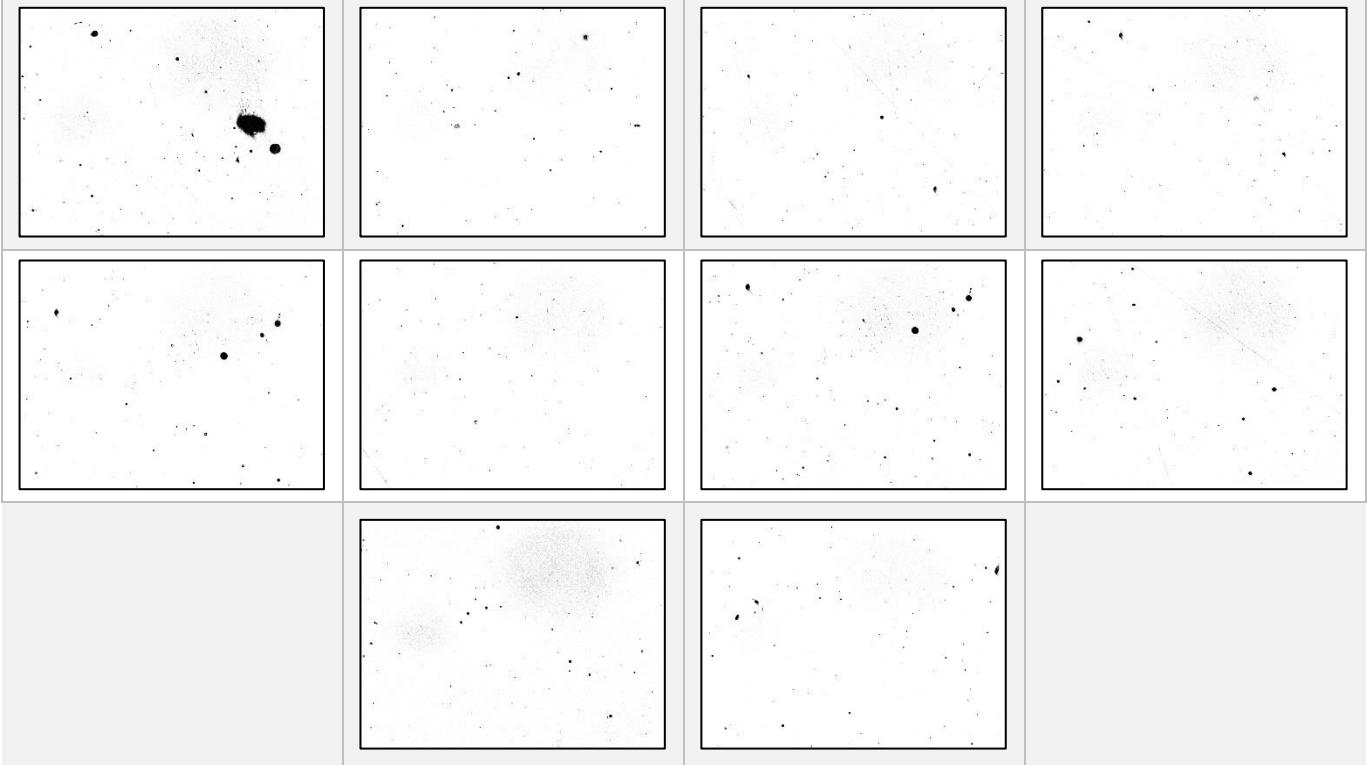
Sample 31



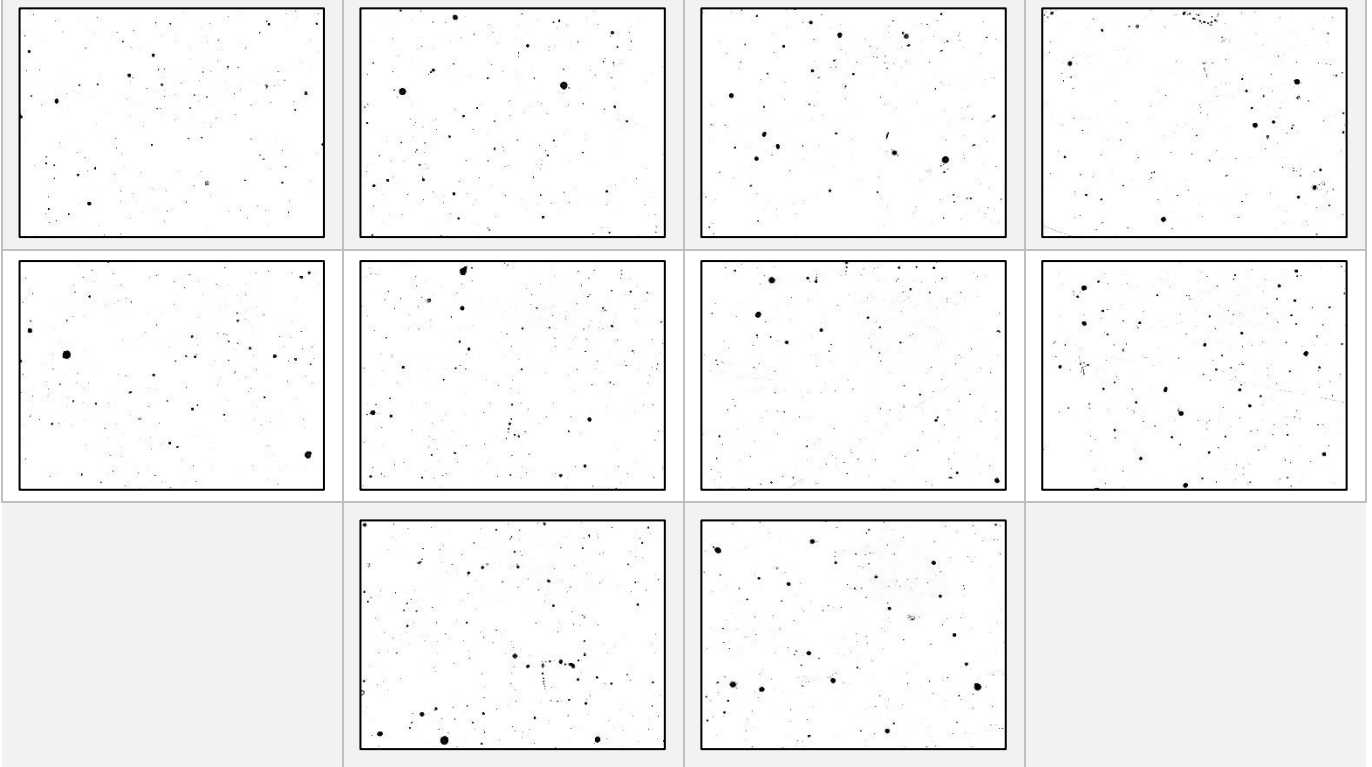
Sample 32



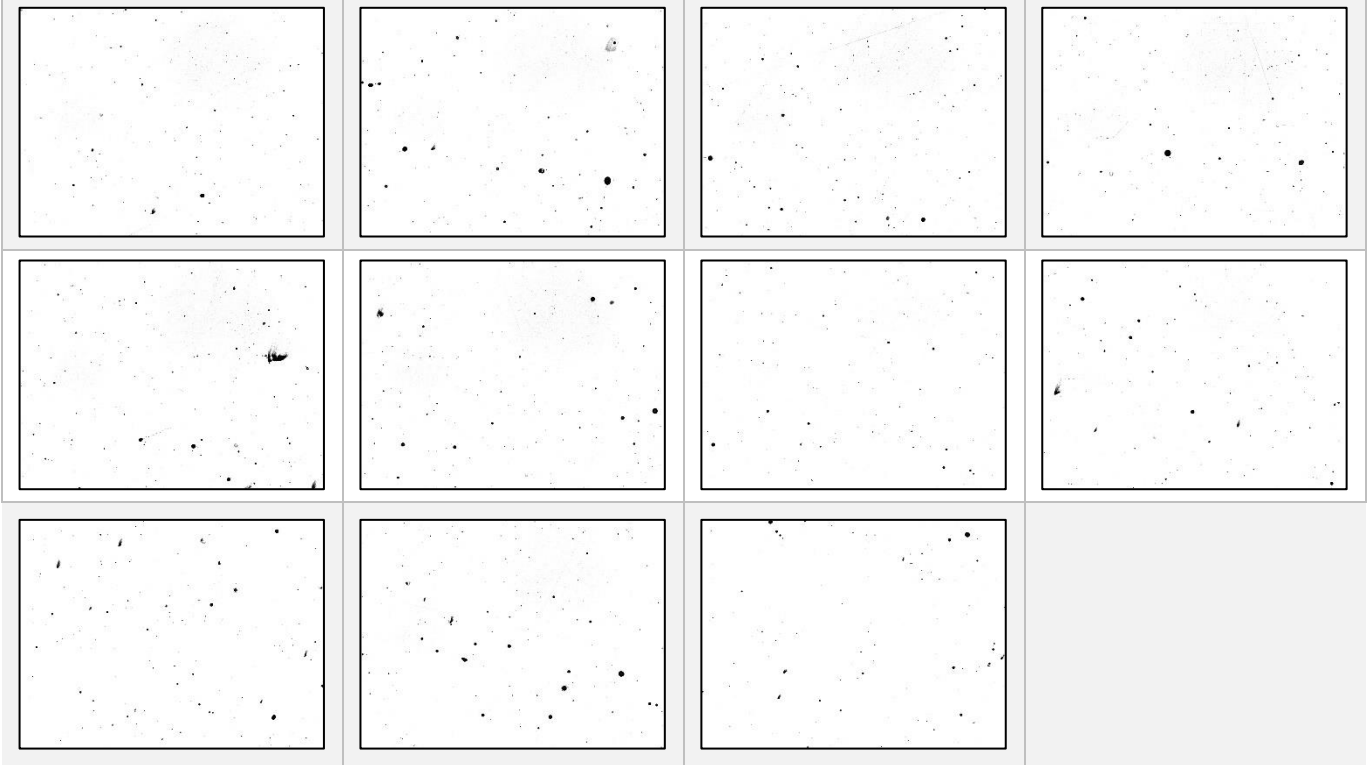
Sample 33



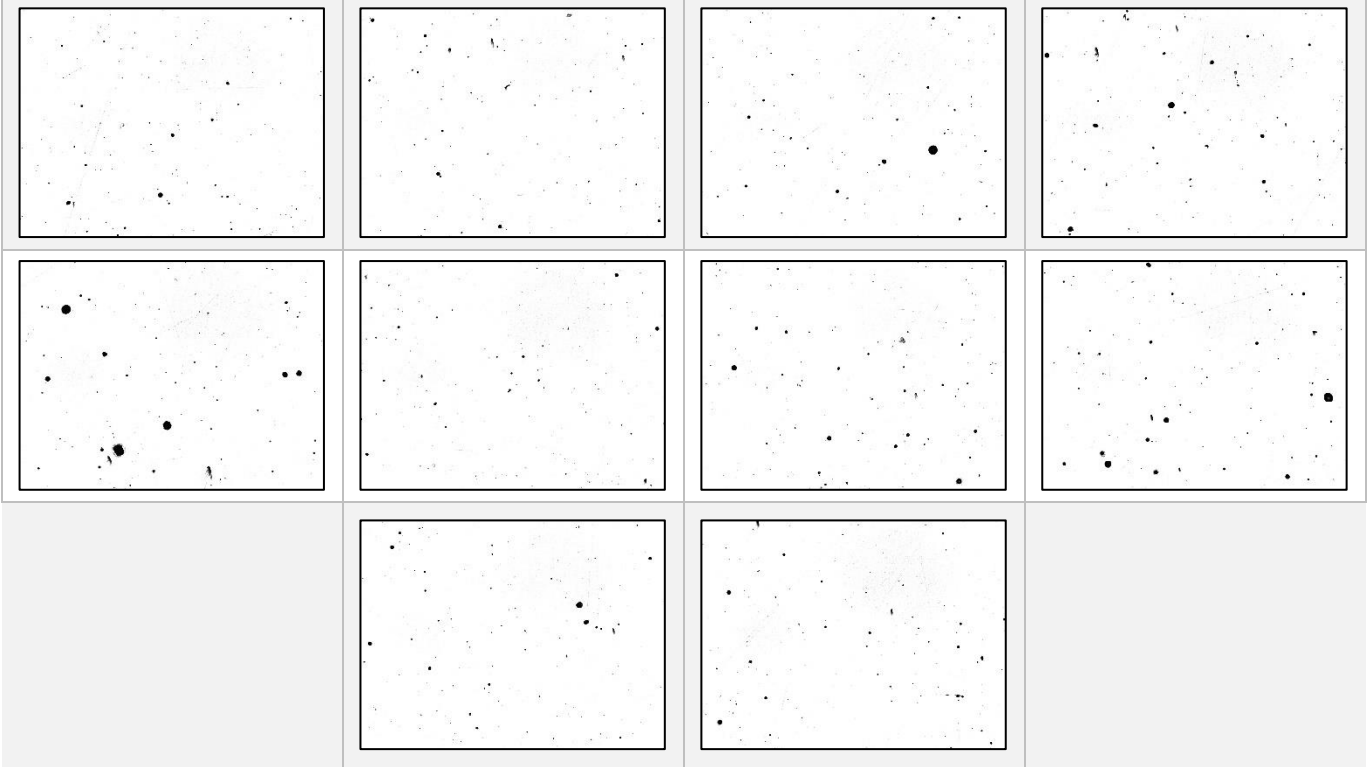
Sample 34



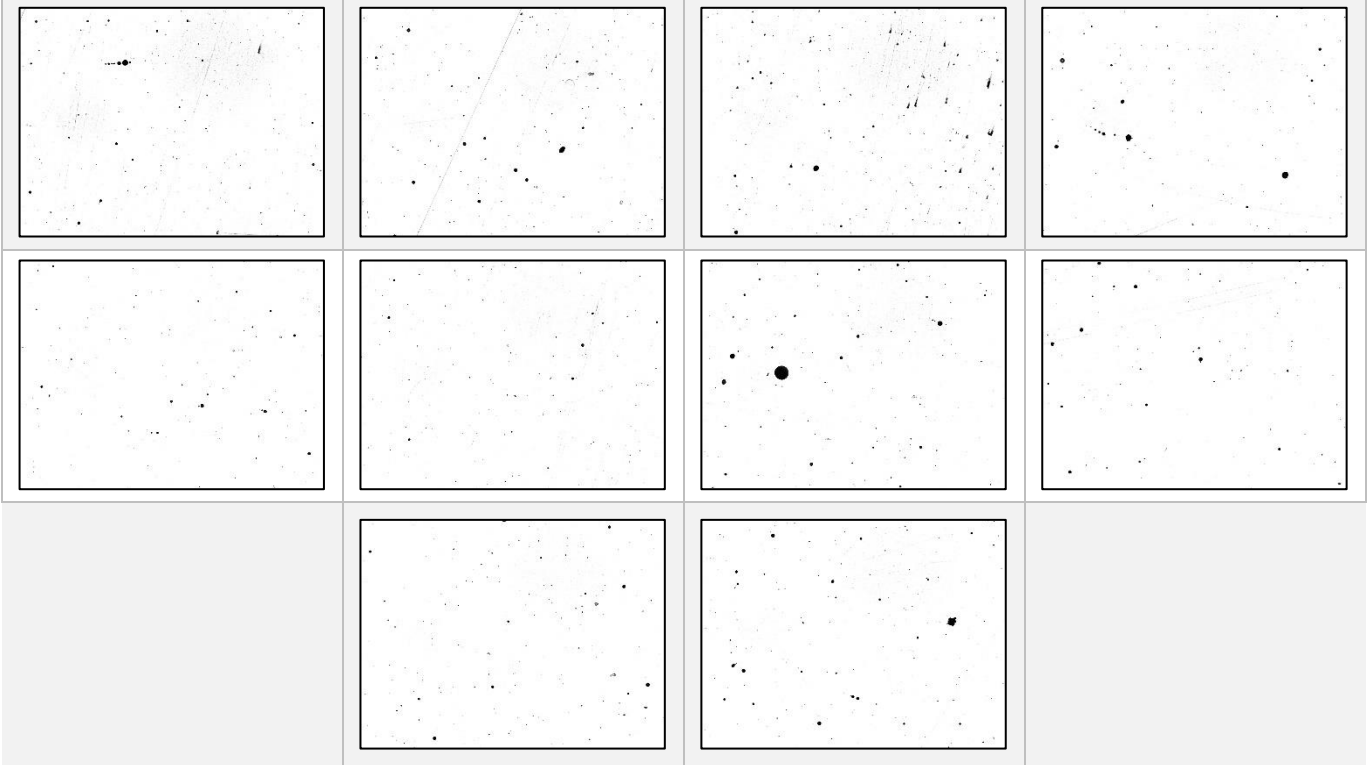
Sample 35



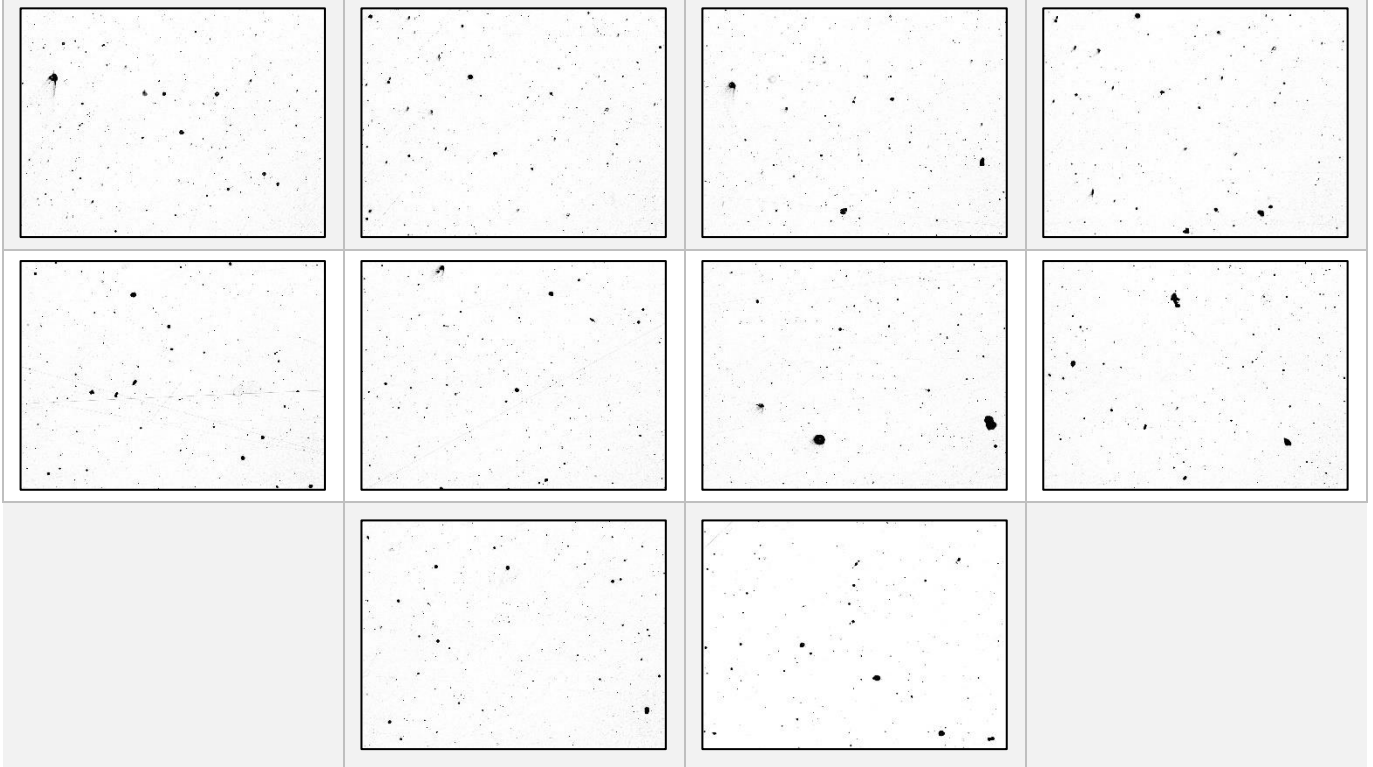
Sample 36



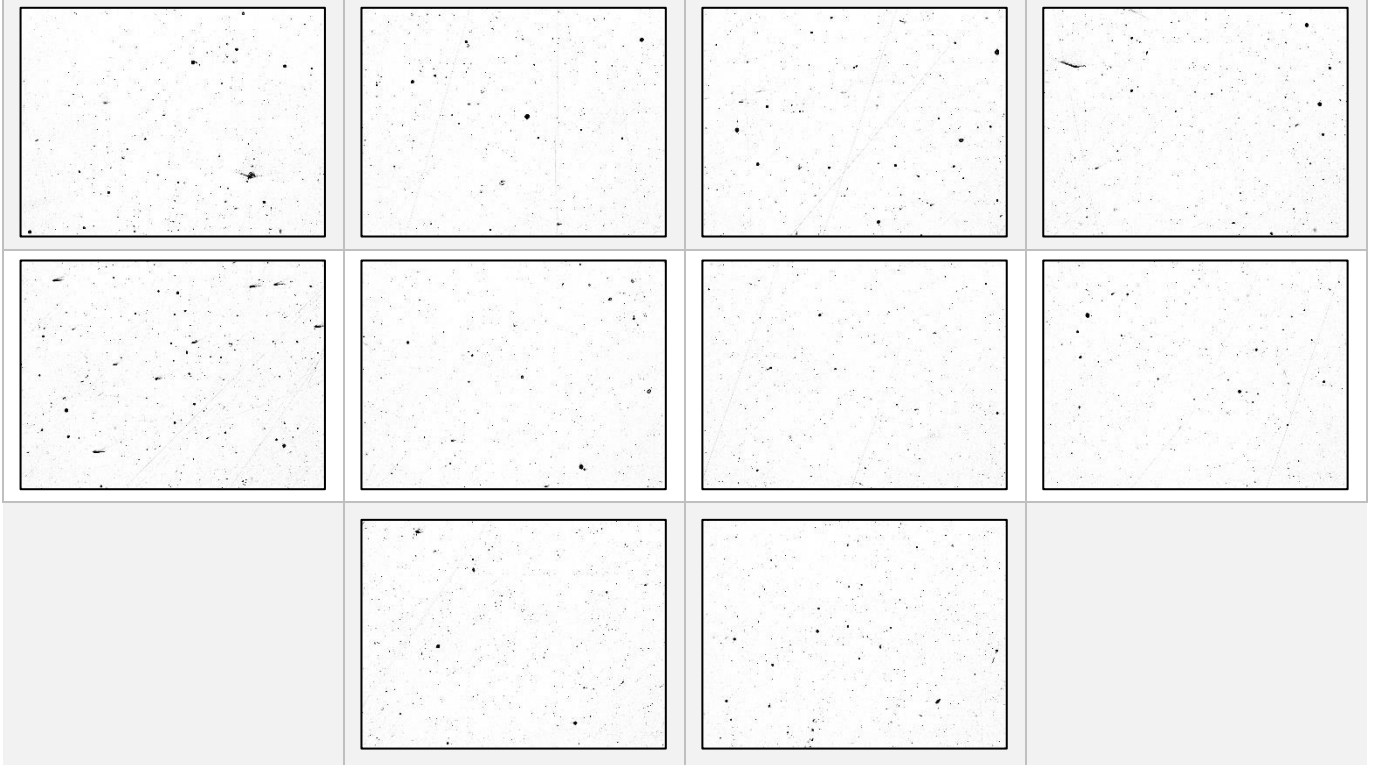
Sample 37



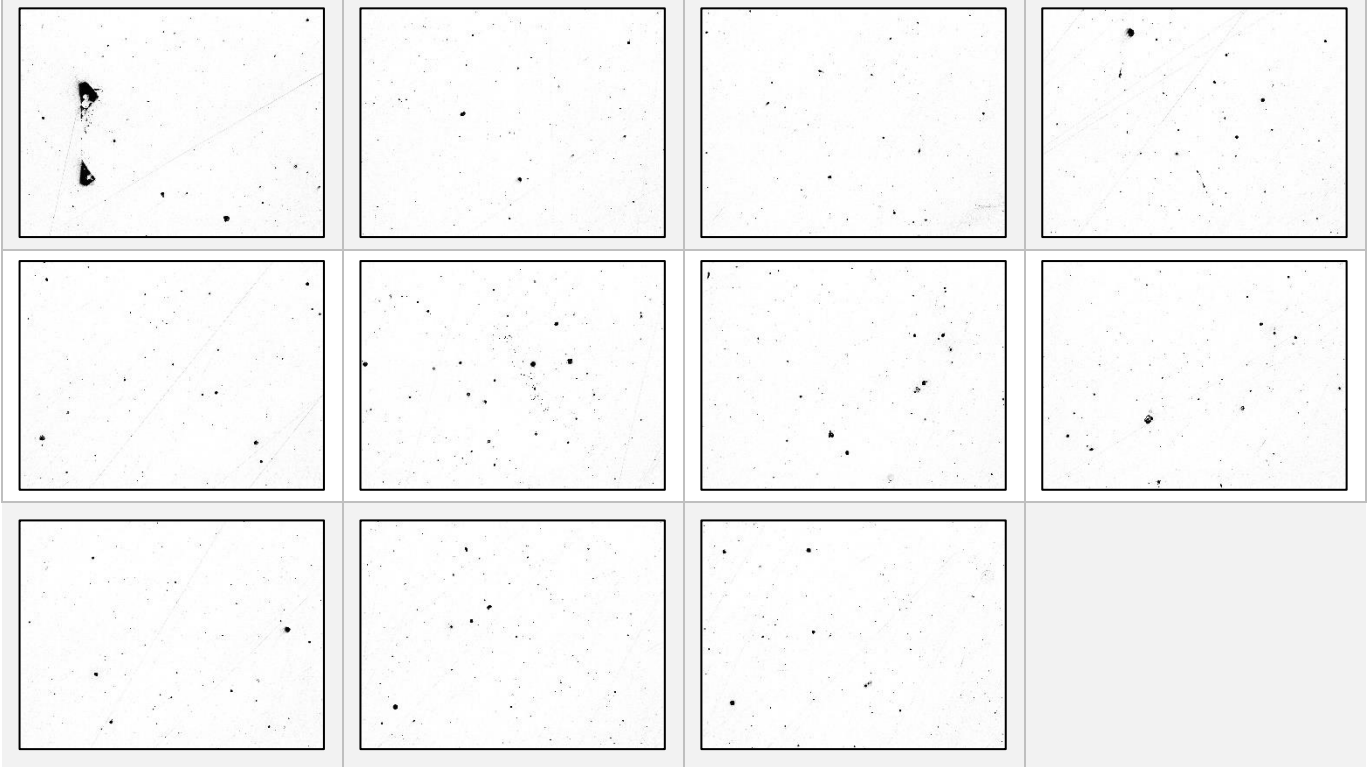
Sample 38



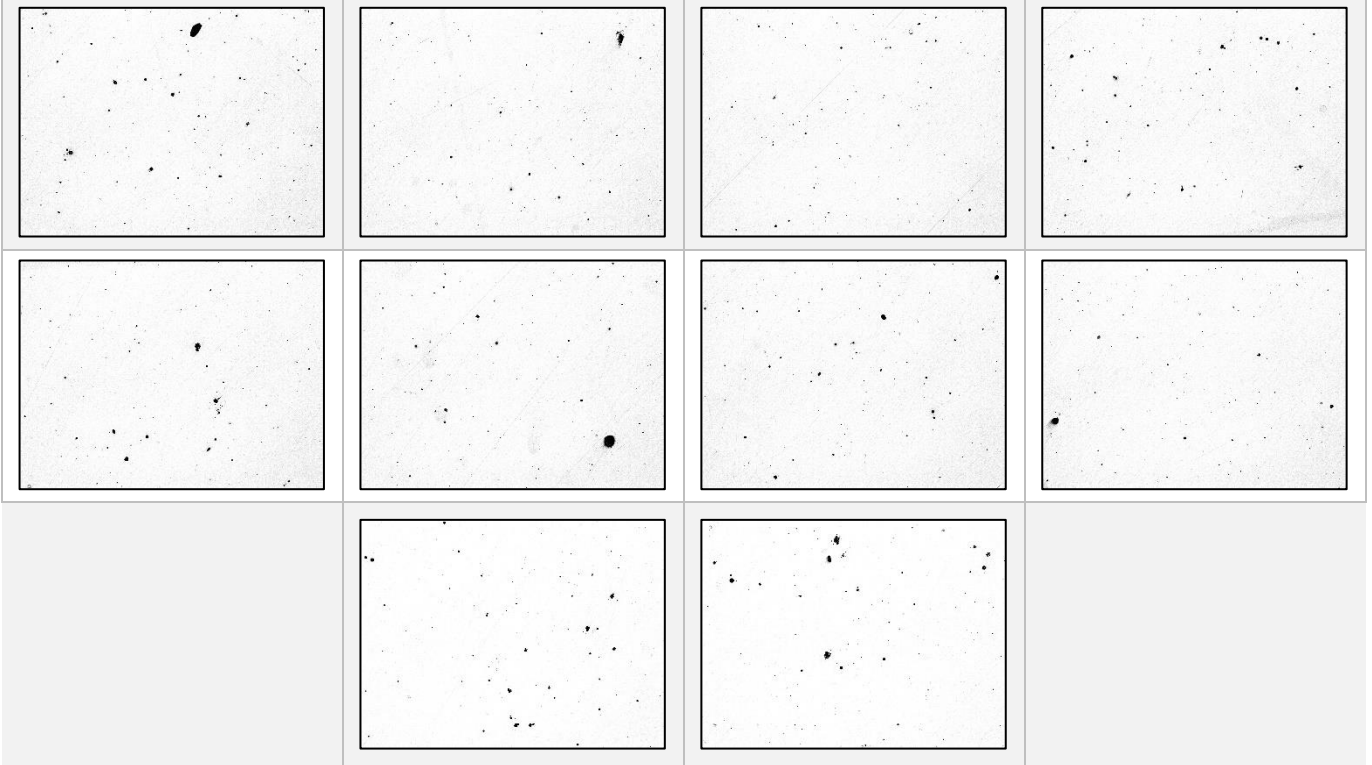
Sample 39



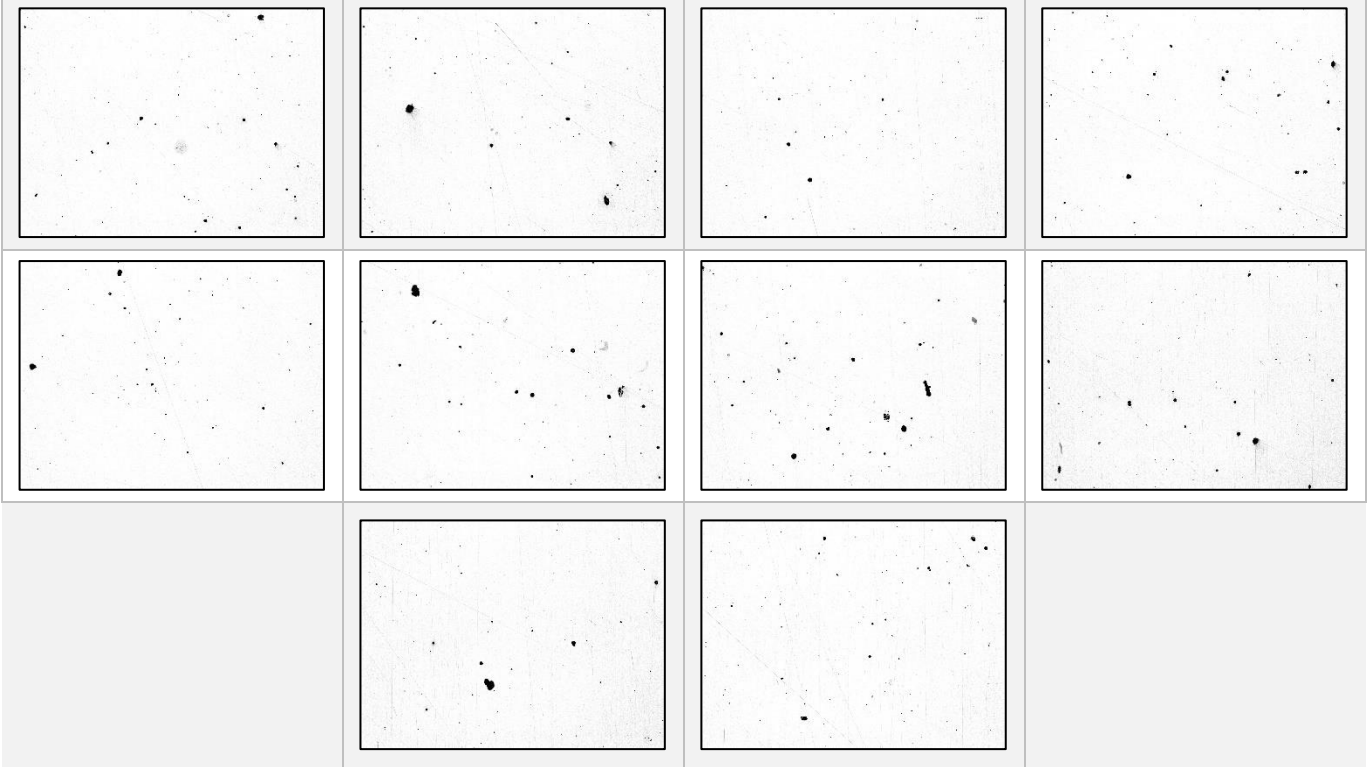
Sample 40



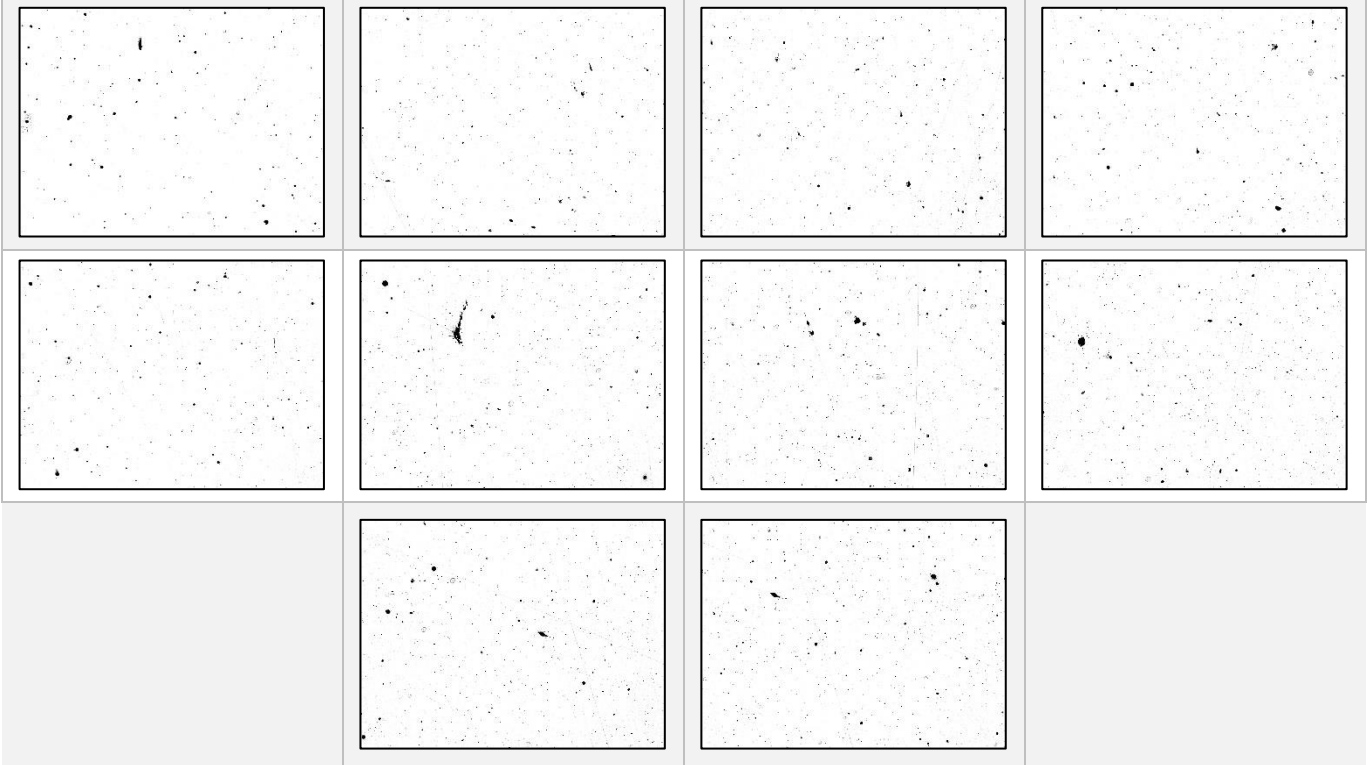
Sample 41



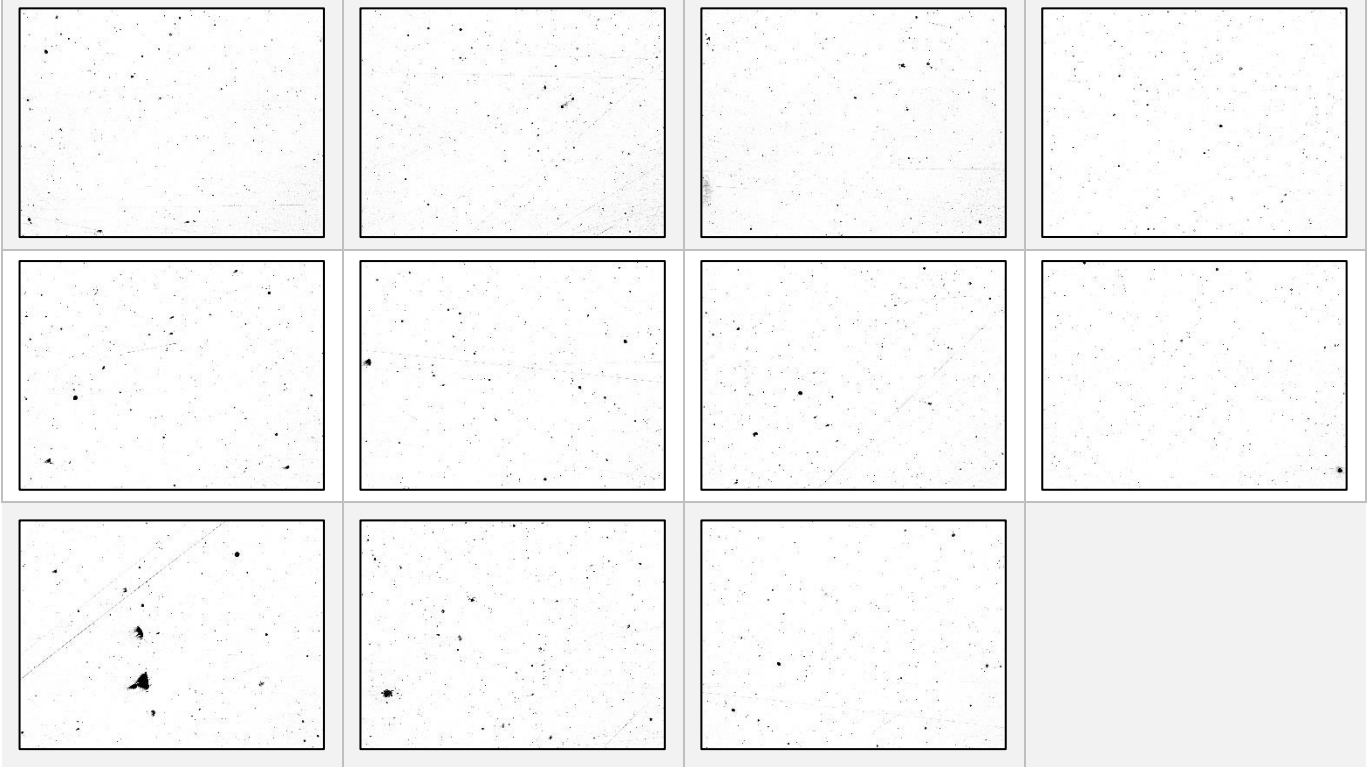
Sample 42



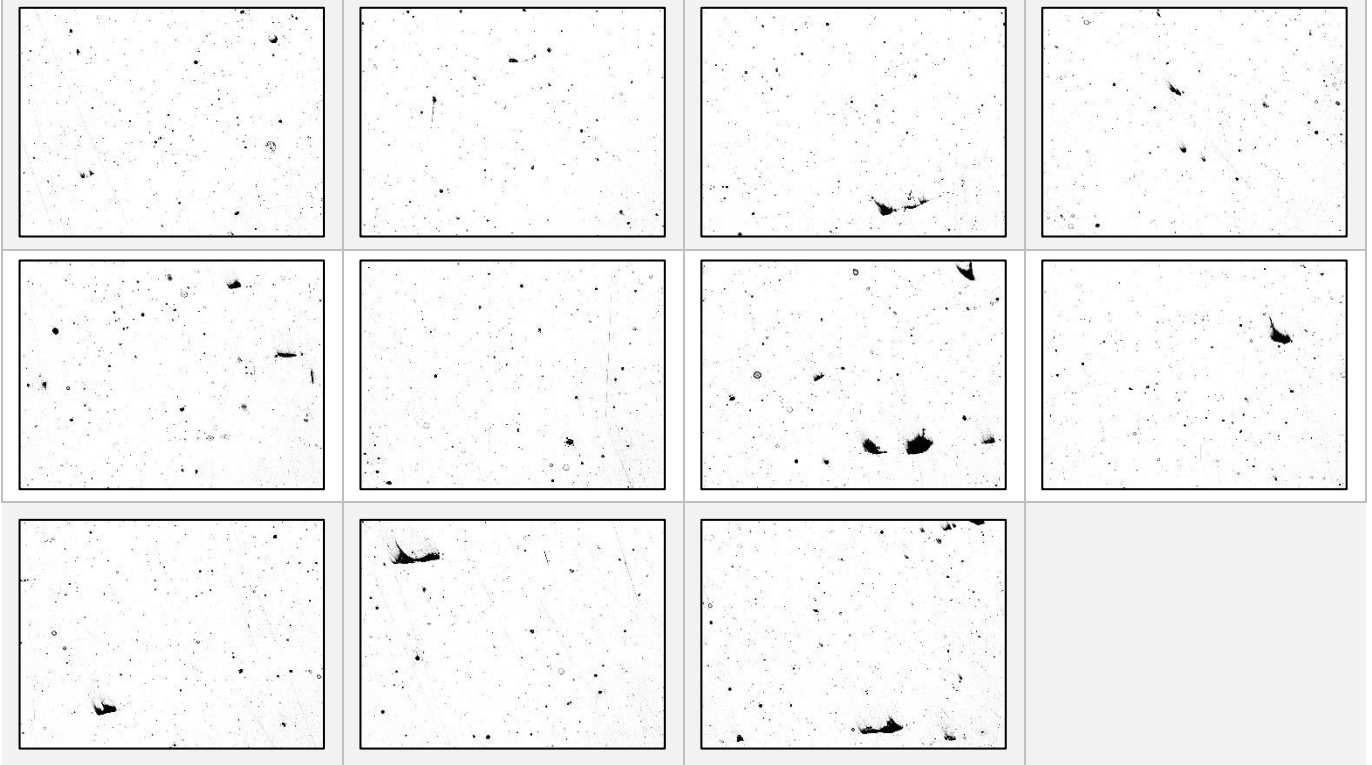
Sample 43



Sample 44



Sample 45



Sample 46

